Infrared Spectra of the *n*-Propyl and *i*-Propyl Radicals in Solid *para*-Hydrogen

Gregory T. Pullen, Peter R. Franke, Gary E. Douberly, Yuan-Pern Lee

June 23, 2017

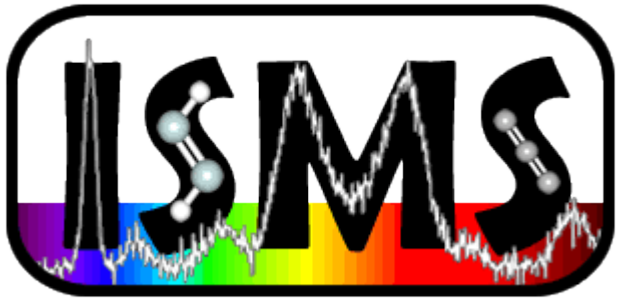

The QOOH radical is central to low temperature combustion chemistry

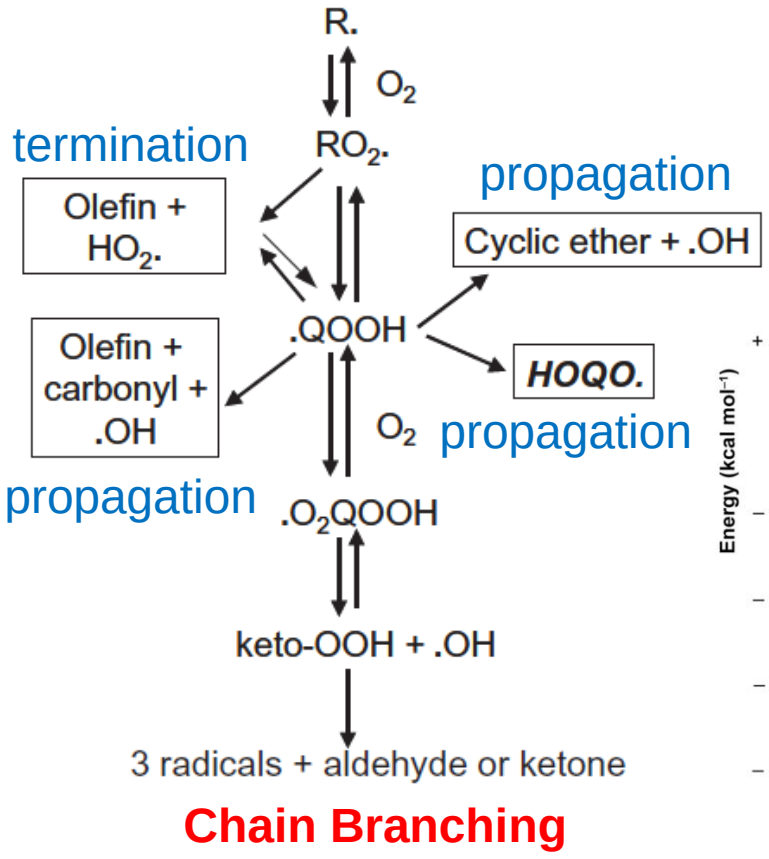

n-propyl oxidation

PES courtesy of W. D. Allen (UGA)

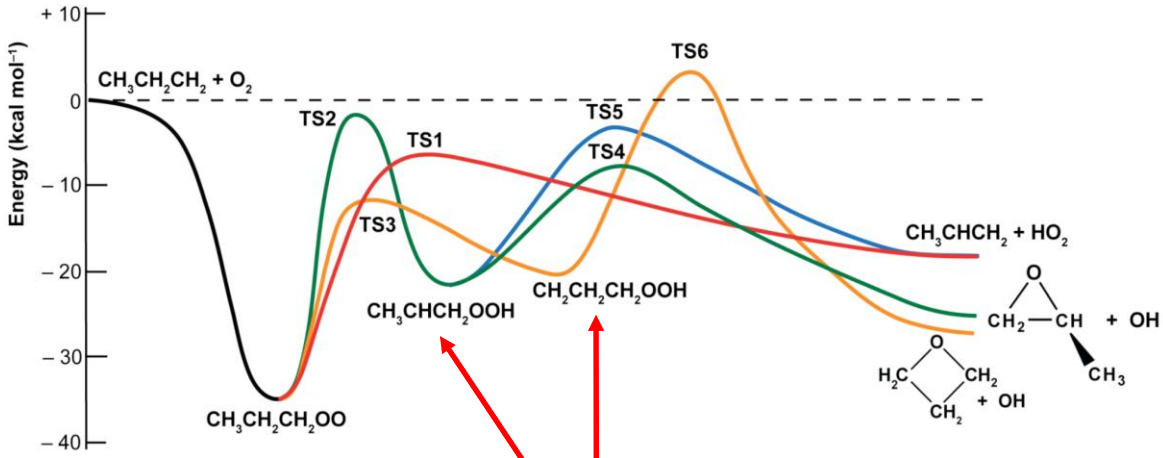

QOOH (hydroperoxypropyl radical)

$+ O_2$

O_2QOOH → Chain Branching

J. A. Miller, M. J. Pilling, and J. Troe, *Unraveling combustion mechanisms through a quantitative understanding of elementary reactions*, Proceedings of the Combustion Institute **s30**, 43-88 (2005).

The QOOH radical is central to low temperature combustion chemistry

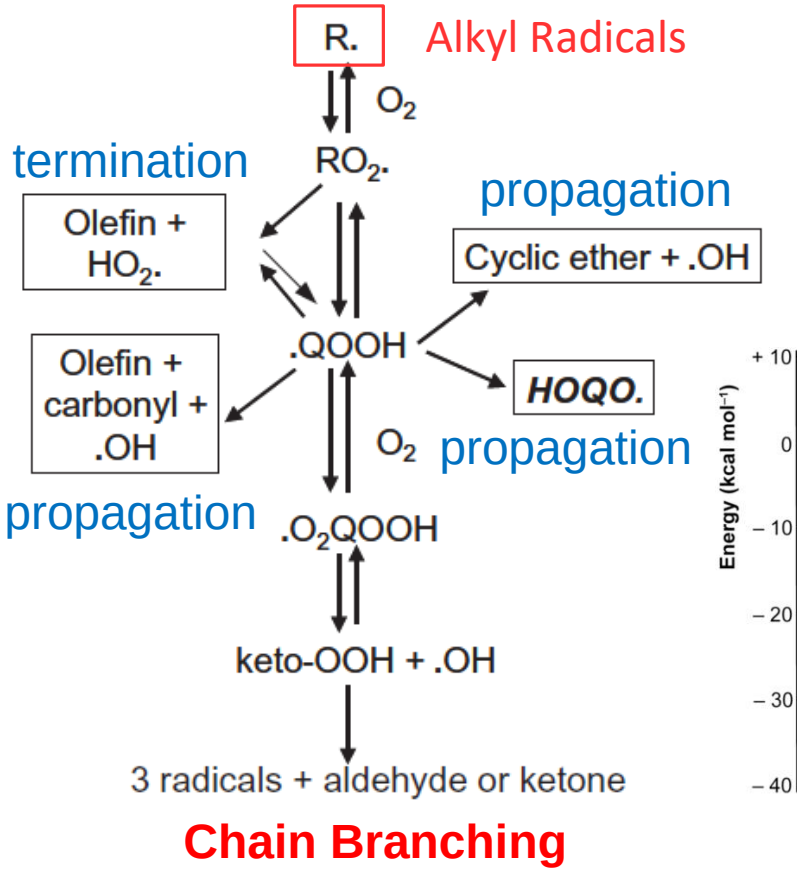

n-propyl oxidation

PES courtesy of W. D. Allen (UGA)

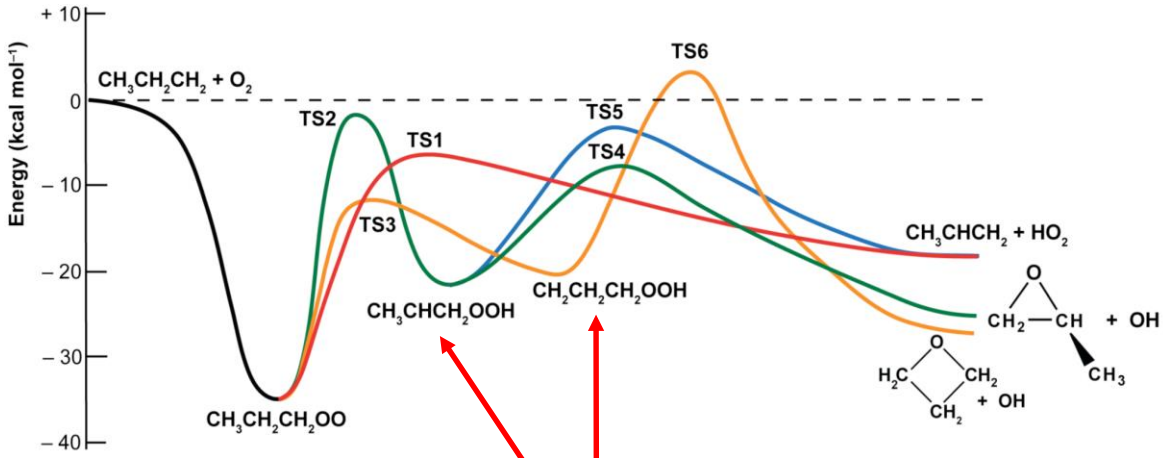

QOOH (hydroperoxypropyl radical)

$+ O_2$

O_2QOOH → Chain Branching

J. A. Miller, M. J. Pilling, and J. Troe, *Unraveling combustion mechanisms through a quantitative understanding of elementary reactions*, Proceedings of the Combustion Institute **s30**, 43-88 (2005).

Previous propyl radical spectroscopy

Infrared Matrix Isolation

- Pacansky, J. et al., *Journal of Physical Chemistry* **1977,** *81* (23), 2149-2154.
- Pacansky, J.; Coufal, H., *Journal of Molecular Structure* **1980,** *60* (JAN), 255-258.
- Pacansky, J.; Coufal, H., *Journal of Chemical Physics* **1980,** *72* (5), 3298-3303.
- Chettur, G.; Snelson, A., *Journal of Physical Chemistry* **1987,** *91* (4), 913-919.

Electron Paramagnetic Resonance

- Adrian, F. J. et al., *Journal of Chemical Physics* **1973,** *59* (8), 3946-3952.
- Shiga, T. et al., *Zeitschrift Fur Naturforschung Section a-a Journal of Physical Sciences* **1974,** *A 29* (4), 653-659.
- McDowell, C. A.; Shimokoshi, K., *Journal of Chemical Physics* **1974,** *60* (4), 1619-1623.
- Griller, D.; Preston, K. F., *Journal of the American Chemical Society* **1979,** *101* (8), 1975-1979.

UV Spectra

- Munk, J. et al., *Chemical Physics Letters* **1986,** *132* (4-5), 417-421.

Theory

- Pacansky, J.; Dupuis, M., *Journal of Chemical Physics* **1979,** *71* (5), 2095-2098.
- Pacansky, J.; Dupuis, M., *Journal of Chemical Physics* **1980,** *73* (4), 1867-1872.
- Pacansky, J.; Yoshimine, M., *Journal of Physical Chemistry* **1987,** *91* (5), 1024-1029.
- Claxton, T. A.; Graham, A. M., *Journal of the Chemical Society-Faraday Transactions Ii* **1988,** *84*, 121-134.
- Pacansky, J. et al., *Journal of the American Chemical Society* **1991,** *113* (1), 317-328.
- Pacansky, J. et al., *Journal of Physical Chemistry* **1993,** *97* (41), 10694-10701.
- Pacansky, J. et al., *Journal of Physical Chemistry* **1996,** *100* (42), 16828-16834.
- Li, C. Y. et al., *Journal of Physical Chemistry B* **2015,** *119* (3), 728-735.

Previous propyl radical spectroscopy

Infrared Matrix Isolation

- Pacansky, J. et al., *Journal of Physical Chemistry* **1977,** *81* (23), 2149-2154.
- Pacansky, J.; Coufal, H., *Journal of Molecular Structure* **1980,** *60* (JAN), 255-258.
- Pacansky, J.; Coufal, H., *Journal of Chemical Physics* **1980,** *72* (5), 3298-3303.
- Chettur, G.; Snelson, A., *Journal of Physical Chemistry* **1987,** *91* (4), 913-919.

Electron Paramagnetic Resonance

- Adrian, F. J. et al., *Journal of Chemical Physics* **1973,** *59* (8), 3946-3952.
- Shiga, T. et al., *Zeitschrift Fur Naturforschung Section a-a Journal of Physical Sciences* **1974,** *A 29* (4), 653-659.
- McDowell, C. A.; Shimokoshi, K., *Journal of Chemical Physics* **1974,** *60* (4), 1619-1623.
- Griller, D.; Preston, K. F., *Journal of the American Chemical Society* **1979,** *101* (8), 1975-1979.

UV Spectra

- Munk, J. et al., *Chemical Physics Letters* **1986,** *132* (4-5), 417-421.

Theory

- Pacansky, J.; Dupuis, M., *Journal of Chemical Physics* **1979,** *71* (5), 2095-2098.
- Pacansky, J.; Dupuis, M., *Journal of Chemical Physics* **1980,** *73* (4), 1867-1872.
- Pacansky, J.; Yoshimine, M., *Journal of Physical Chemistry* **1987,** *91* (5), 1024-1029.
- Claxton, T. A.; Graham, A. M., *Journal of the Chemical Society-Faraday Transactions Ii* **1988,** *84*, 121-134.
- Pacansky, J. et al., *Journal of the American Chemical Society* **1991,** *113* (1), 317-328.
- Pacansky, J. et al., *Journal of Physical Chemistry* **1993,** *97* (41), 10694-10701.
- Pacansky, J. et al., *Journal of Physical Chemistry* **1996,** *100* (42), 16828-16834.
- Li, C. Y. et al., *Journal of Physical Chemistry B* **2015,** *119* (3), 728-735.

Matrix Isolation Studies of Alkyl Radicals. The Characteristic Infrared Spectra of Primary Alkyl Radicals

J. Pacansky,* D. E. Horne, G. P. Gardini,† and J. Bargon

IBM Research Laboratory, San Jose, California 95193 (Received July 25, 1977)

Publication costs assisted by IBM Research Laboratory

Diacyl peroxide precursors
in Argon matrices

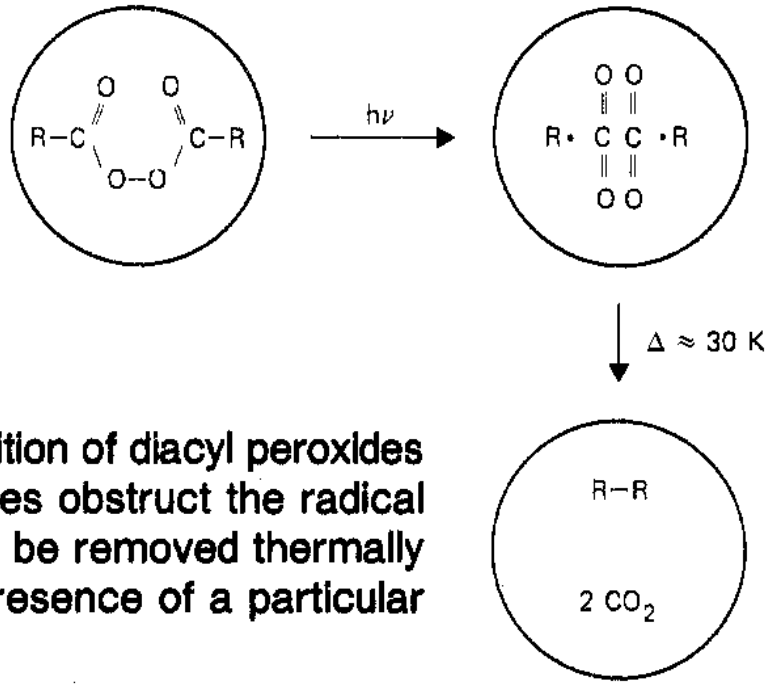

Figure 3. An illustration of the photodecomposition of diacyl peroxides isolated in a rare gas solid. The CO_2 molecules obstruct the radical recombination process. This obstruction may be removed thermally and thus provides direct information for the presence of a particular radical species.

Matrix Isolation Studies of Alkyl Radicals. The Characteristic Infrared Spectra of Primary Alkyl Radicals

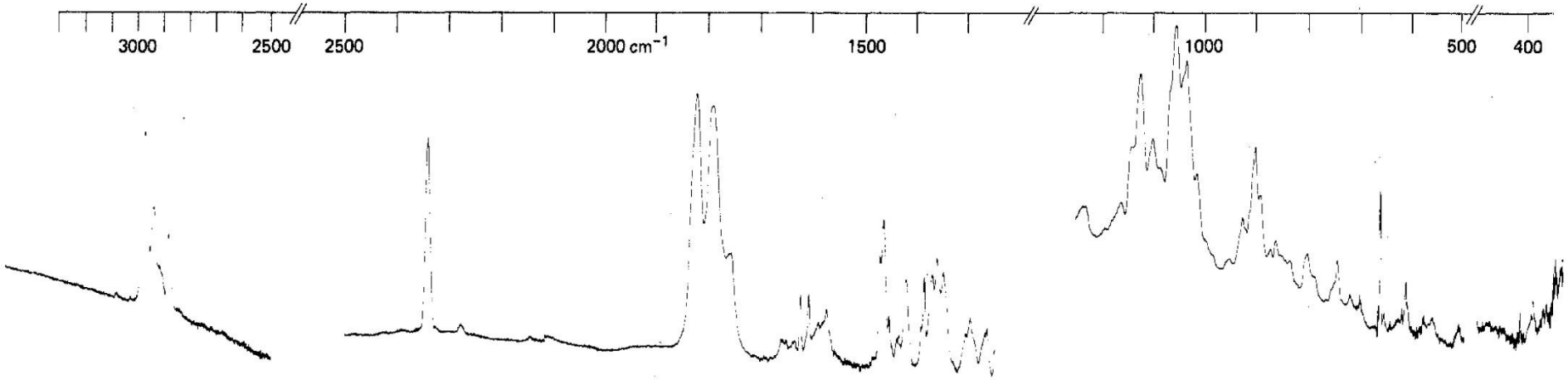

Figure 7. The infrared spectrum of dibutyryl peroxide isolated in an argon matrix (concentration: 1/500).

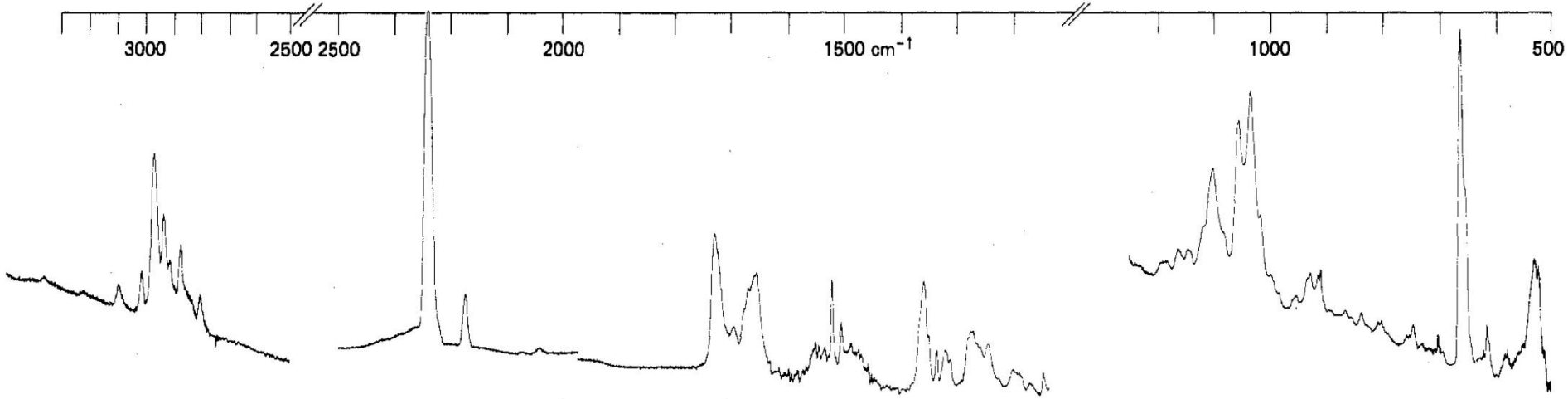

Figure 8. The infrared spectrum of butyryl peroxide in an argon matrix after irradiation with light $\lambda > 3000$ Å for $t = 1950$ min. The bands at 2340 cm^{-1} are due to CO_2. Those at ~ 1800 cm^{-1} are due to residual peroxide carbonyl absorption.

Matrix Isolation Studies of Alkyl Radicals. The Characteristic Infrared Spectra of Primary Alkyl Radicals

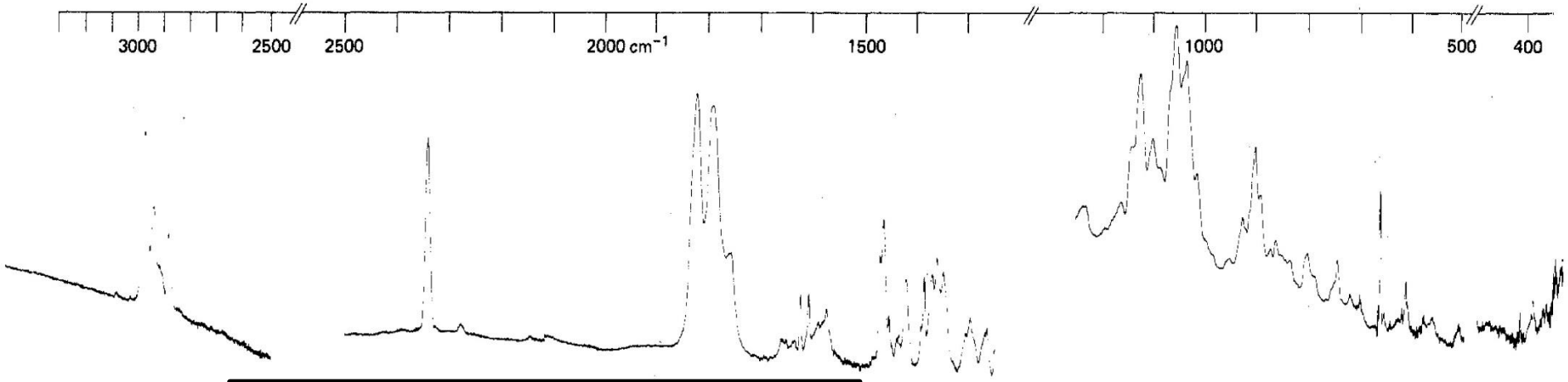

Figure 7. The infra … trix (concentration: 1/500).

TABLE 1: Experimental Vibrational Frequencies (cm^{-1}) Characteristic for Some *n*-Alkyl Radicals

ethyl	*n*-propyl	*n*-butyl	*n*-pentyl	vibrational mode
3112.5	3100	3105	3103	α-CH asymmetric stretch
3032.5	3017.5	3024	3025	α-CH symmetric stretch
2840	2850	2835	2838	β-CH_2 asymmetric stretch
	2812.5	2809	2802	β-CH_2 symmetric stretch
	1469	1463		$-CH_2-$ deformation
	1427	1425	1425	β-CH_2 deformation
		1183	1181	β-CH_2 deformation
541	530	520	519	pyramidal bend

Pacansky, J.; Waltman, R. J.; Barnes, L. A., *Journal of Physical Chemistry* **1996,** *100* (42), 16828-16834.

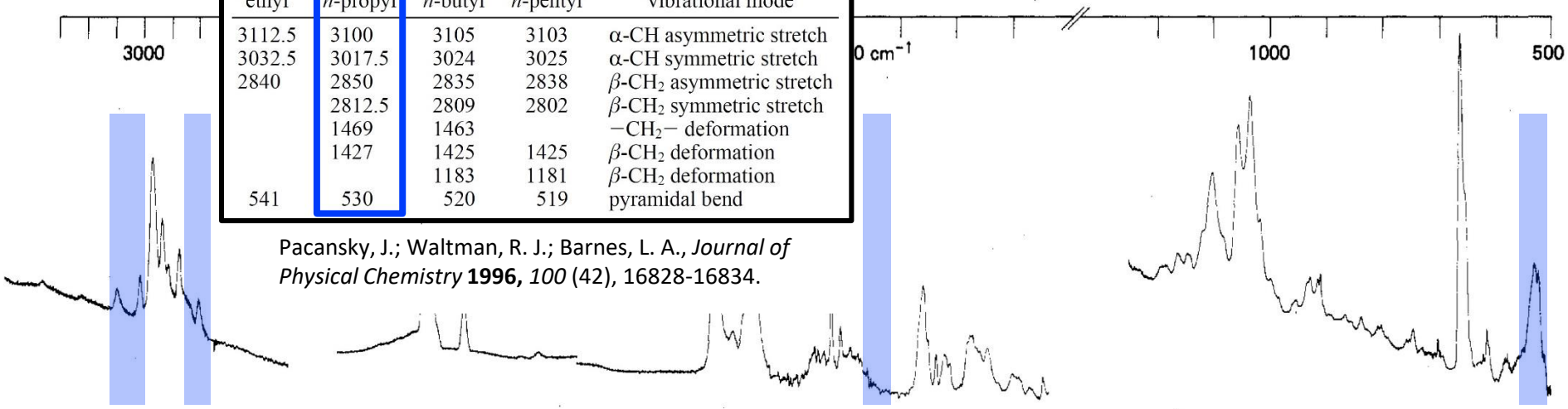

Figure 8. The infrared spectrum of butyryl peroxide in an argon matrix after irradiation with light λ >3000 Å for t = 1950 min. The bands at 2340 cm^{-1} are due to CO_2. Those at ~1800 cm^{-1} are due to residual peroxide carbonyl absorption.

THE JOURNAL OF CHEMICAL PHYSICS **145**, 224304 (2016)

Infrared laser spectroscopy of the *n*-propyl and *i*-propyl radicals: Stretch-bend Fermi coupling in the alkyl CH stretch region

Peter R. Franke,[1] Daniel P. Tabor,[2] Christopher P. Moradi,[1] Gary E. Douberly,[1,a)]
Jay Agarwal,[1,3] Henry F. Schaefer III,[3] and Edwin L. Sibert III[2,a)]
[1]*Department of Chemistry, University of Georgia, Athens, Georgia 30602, USA*
[2]*Department of Chemistry and Theoretical Chemistry Institute, University of Wisconsin-Madison, Madison, Wisconsin 53706, USA*
[3]*Center for Computational Quantum Chemistry, University of Georgia, Athens, Georgia 30602, USA*

(Received 20 September 2016; accepted 17 November 2016; published online 13 December 2016)

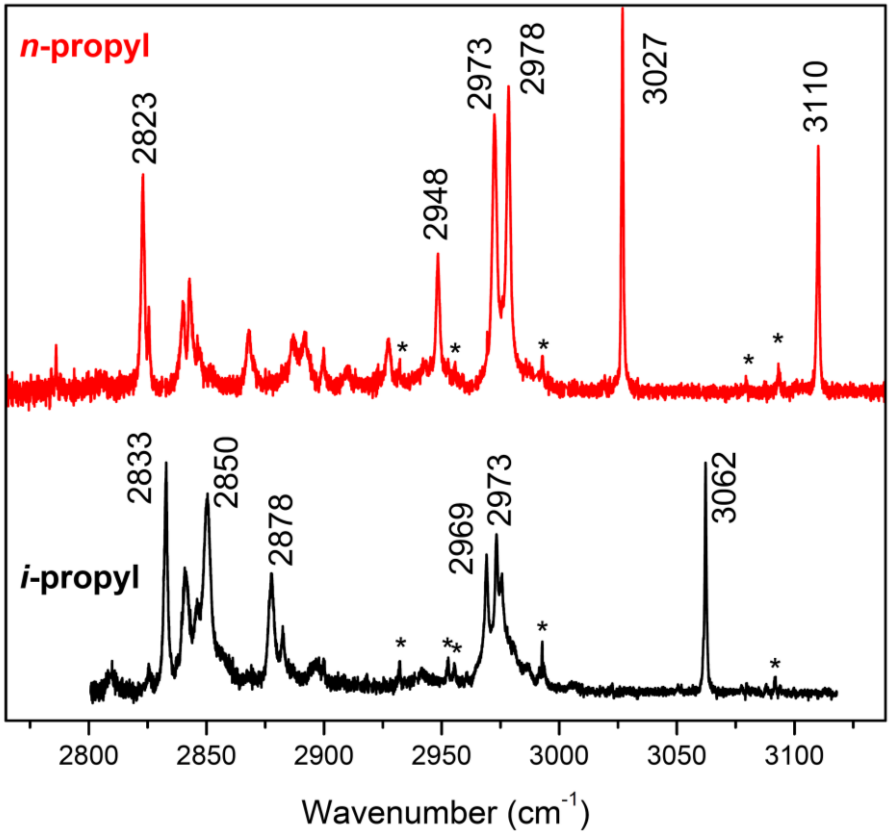

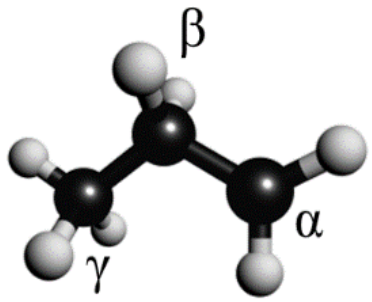

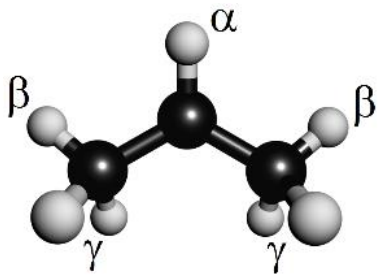

* = propene

Infrared laser spectroscopy of the *n*-propyl and *i*-propyl radicals: Stretch-bend Fermi coupling in the alkyl CH stretch region

n-propyl

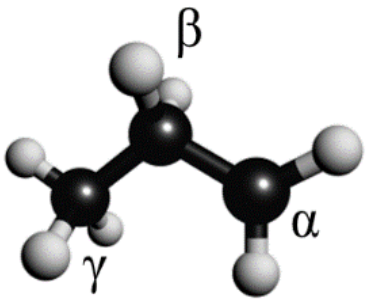

VPT2+K

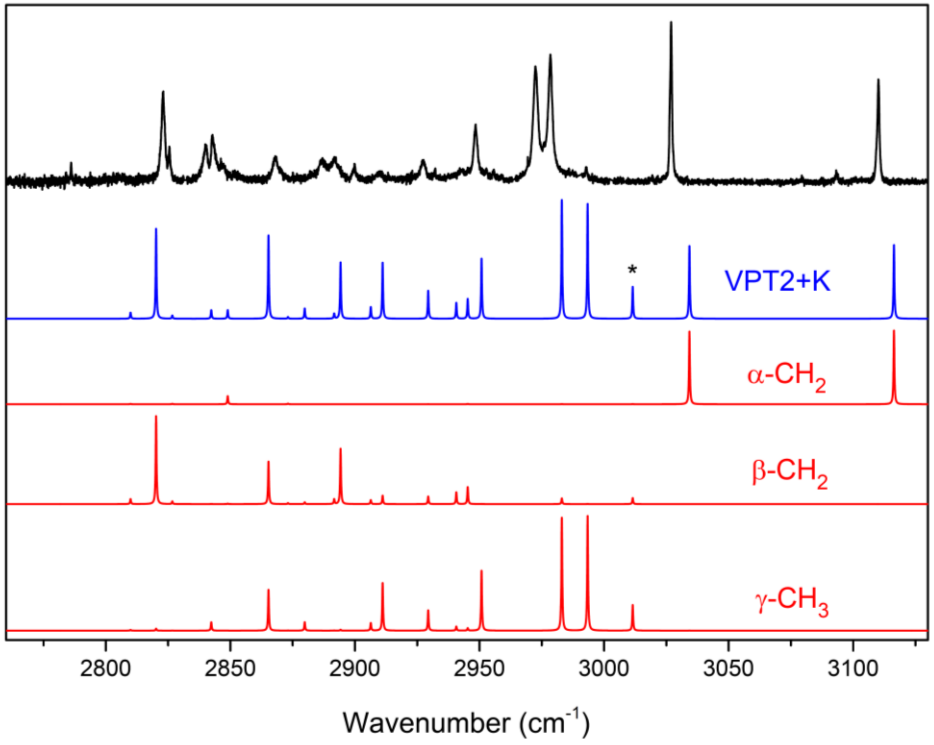

Local Mode Model

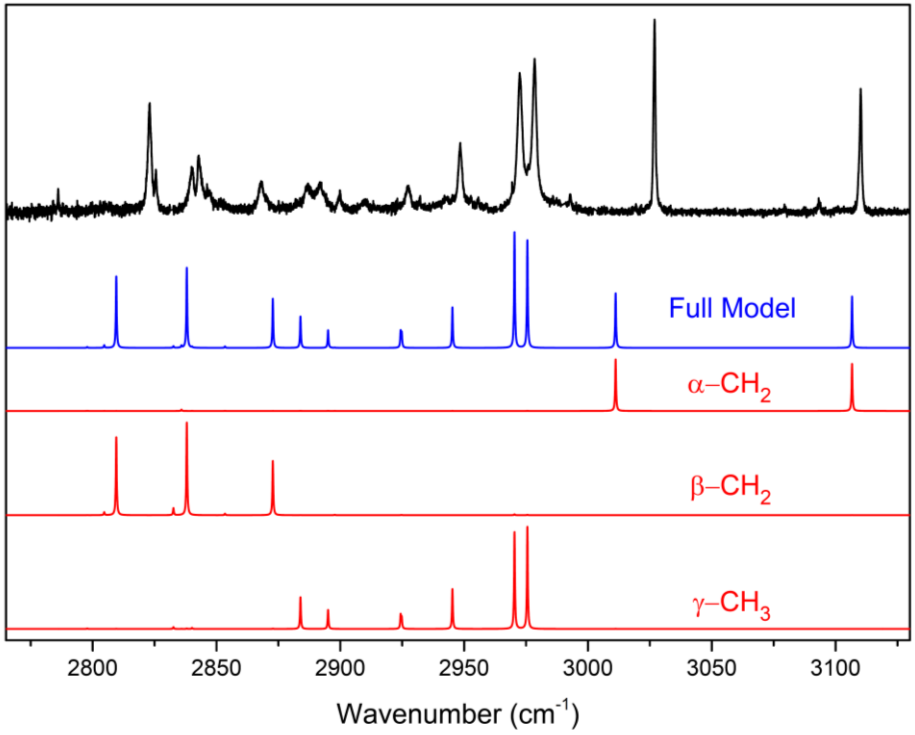

Infrared laser spectroscopy of the *n*-propyl and *i*-propyl radicals: Stretch-bend Fermi coupling in the alkyl CH stretch region

i-propyl

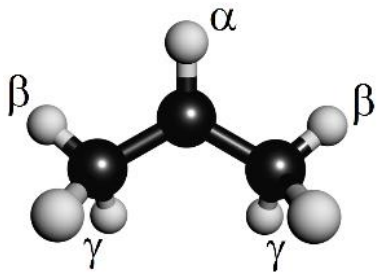

VPT2+K

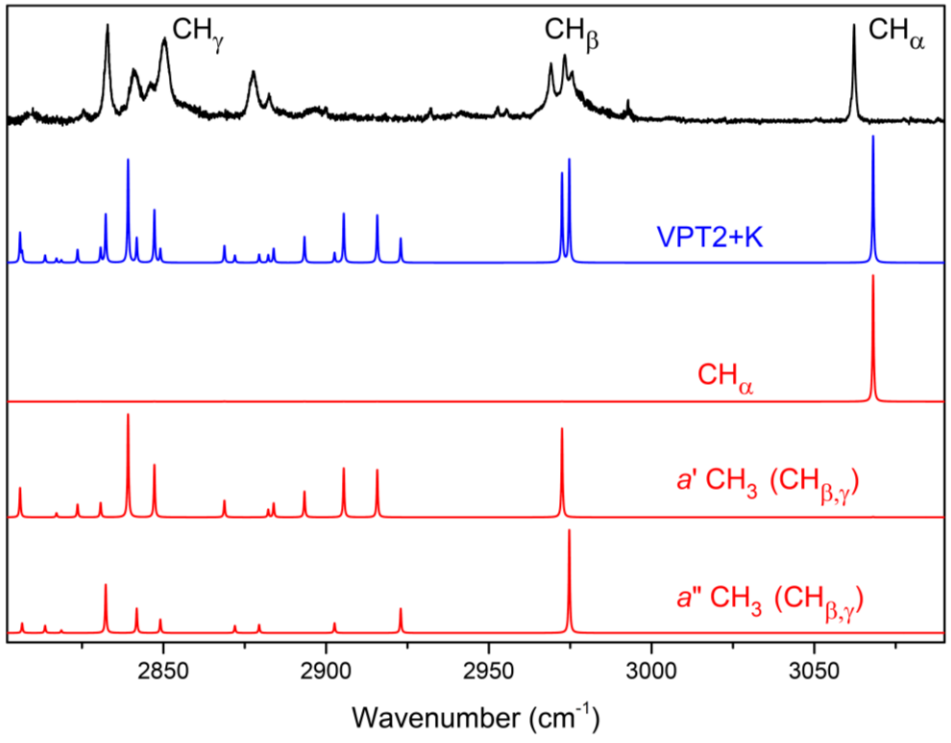

Local Mode Model

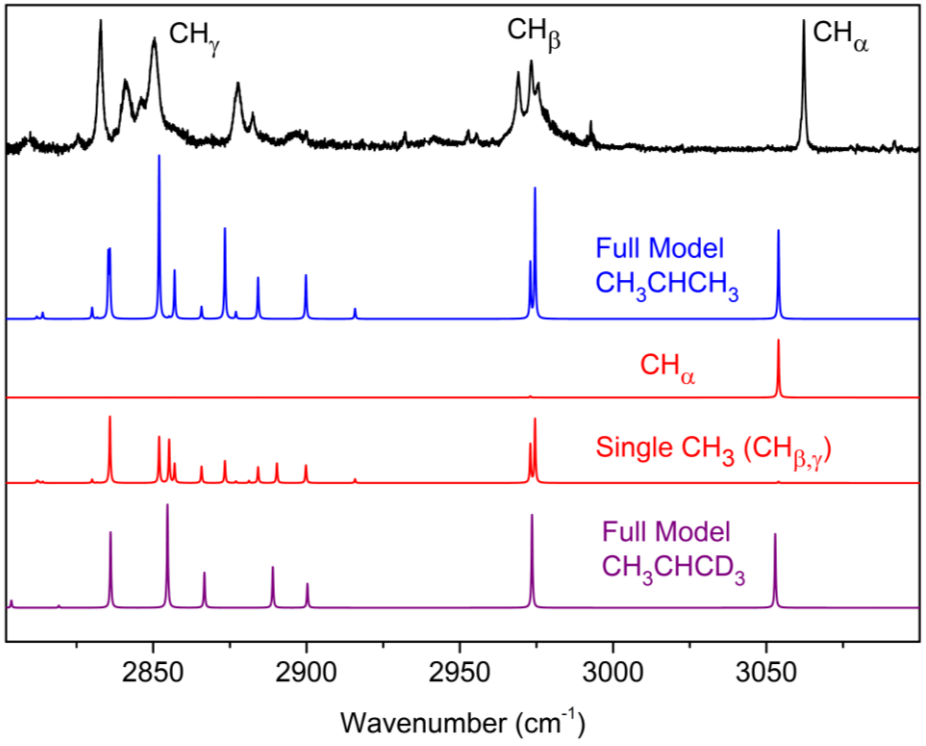

Solid *para*-Hydrogen (p-H_2) Matrix Isolation

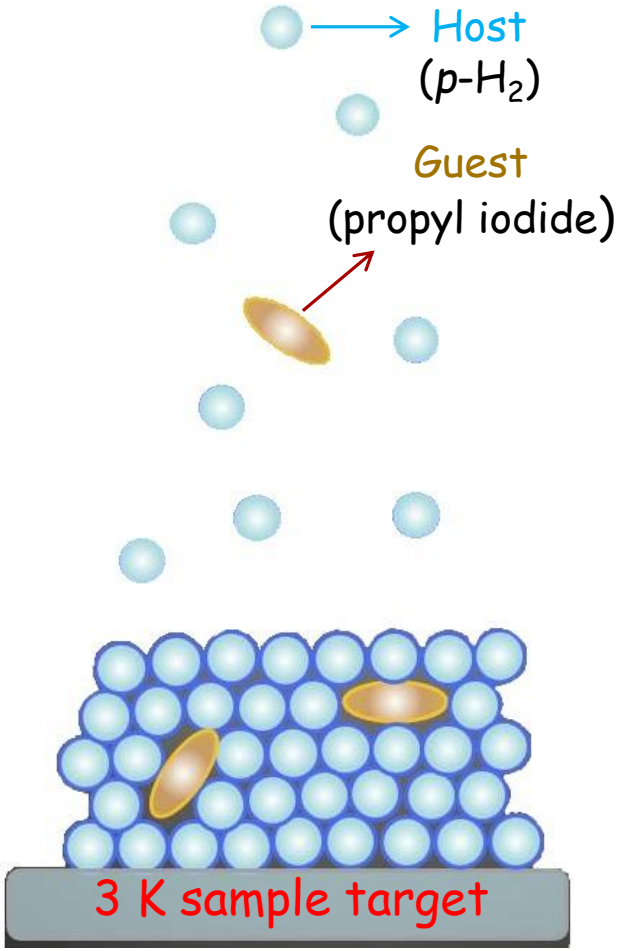

Experimental Details

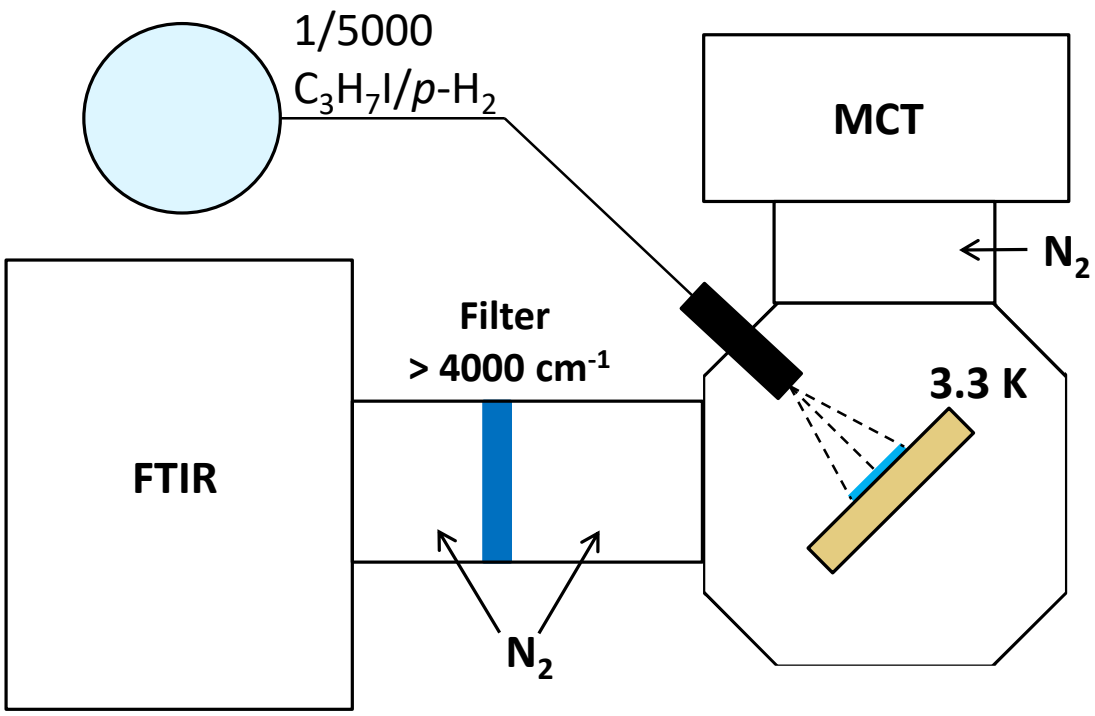

Deposition time: 10 hr

Experimental Details

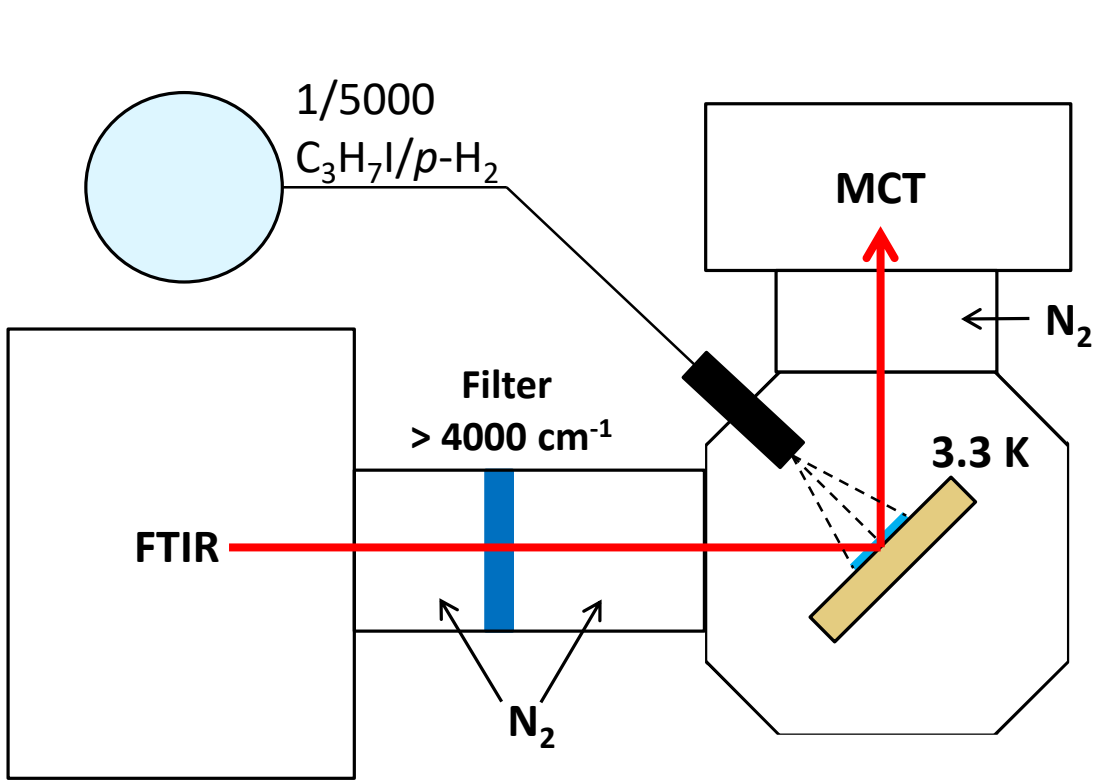

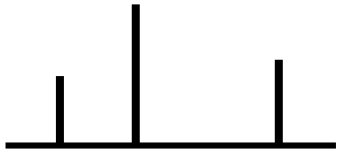

precursor

Deposition time: 10 hr
Range: 400 – 4000 cm^{-1}
Resolution: 0.25 cm^{-1}

Experimental Details

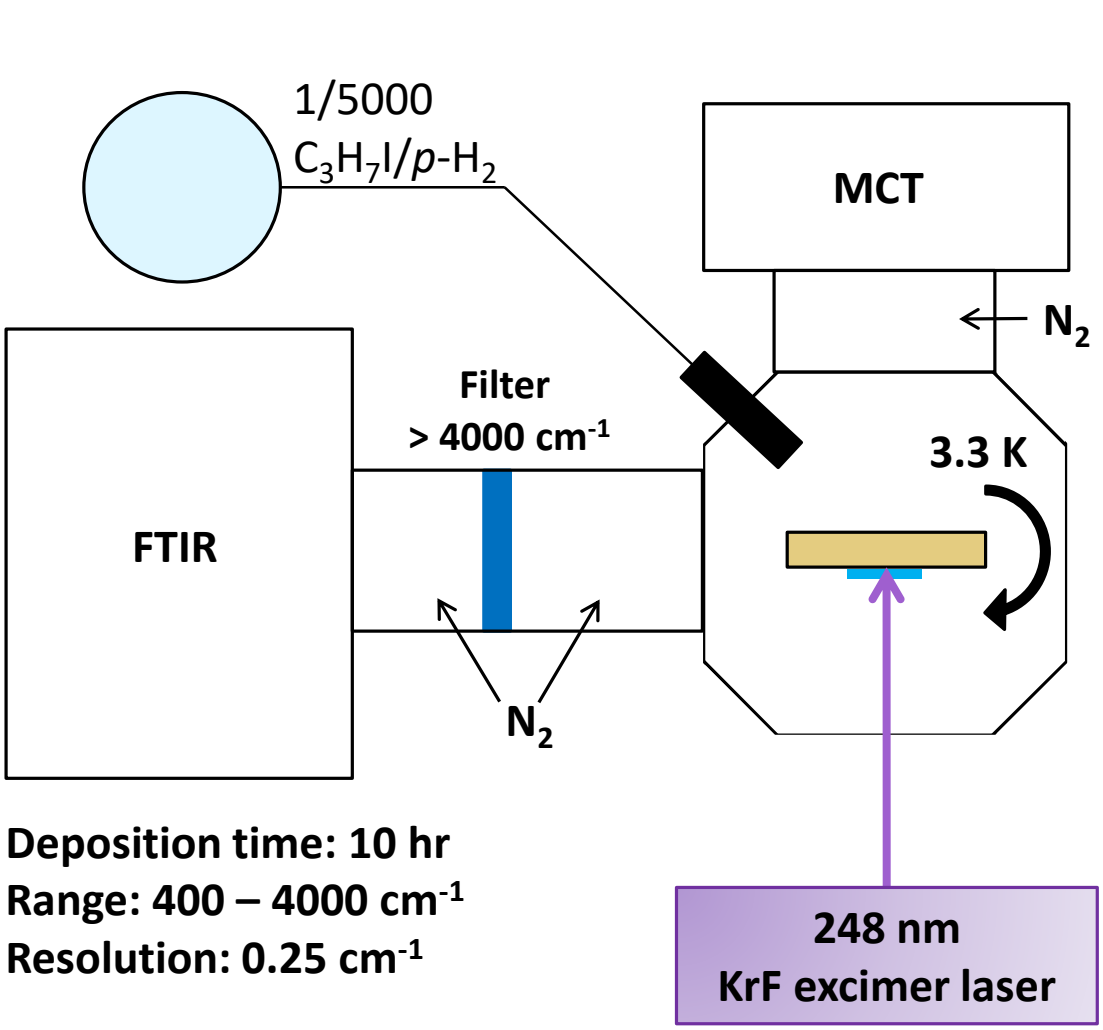

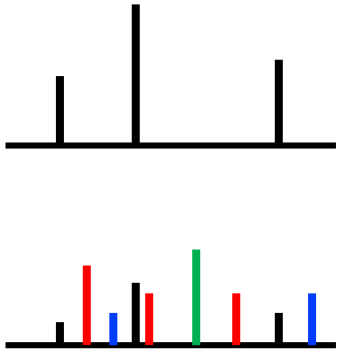

precursor

radical
side product 1
side product 2

Deposition time: 10 hr
Range: 400 – 4000 cm^{-1}
Resolution: 0.25 cm^{-1}

Experimental Details

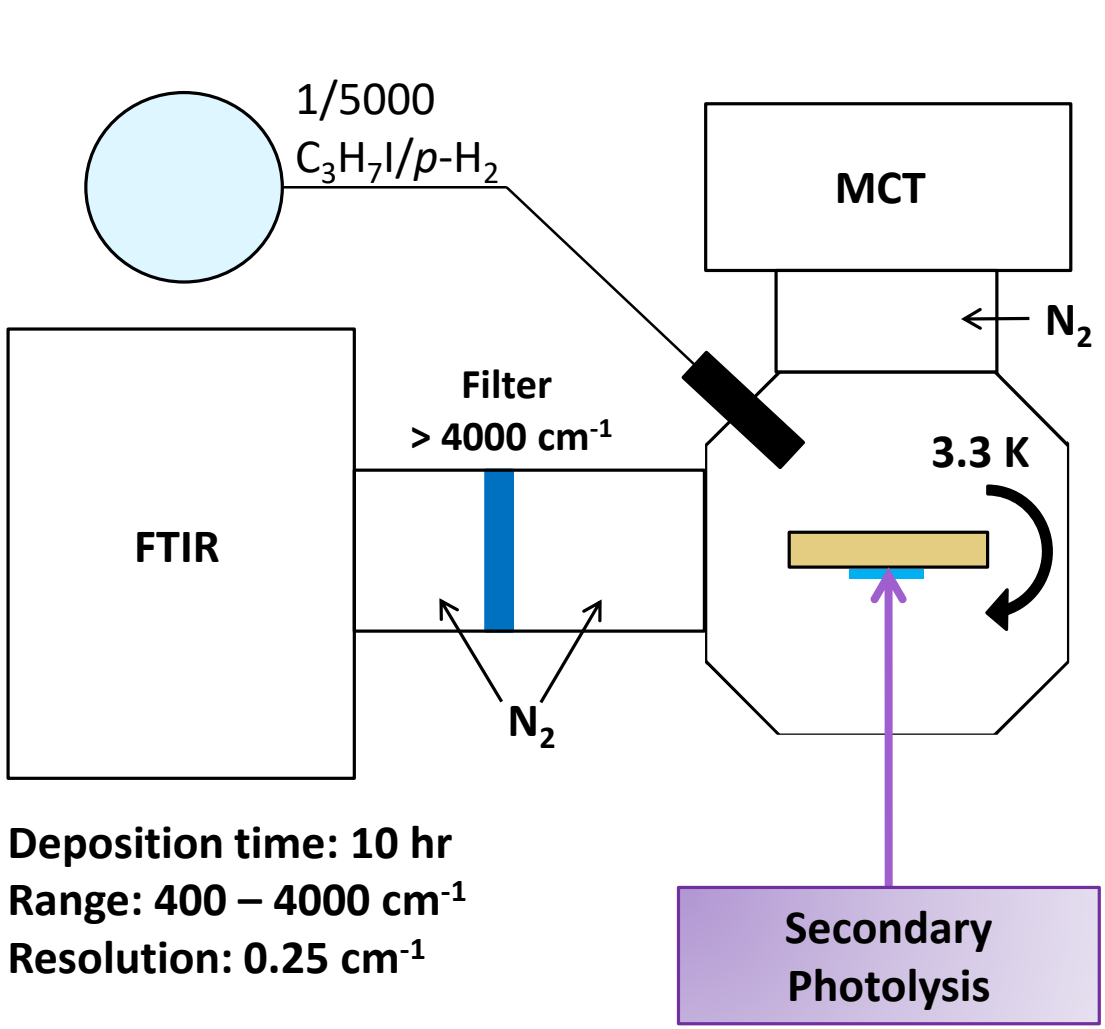

Deposition time: 10 hr
Range: 400 – 4000 cm^{-1}
Resolution: 0.25 cm^{-1}

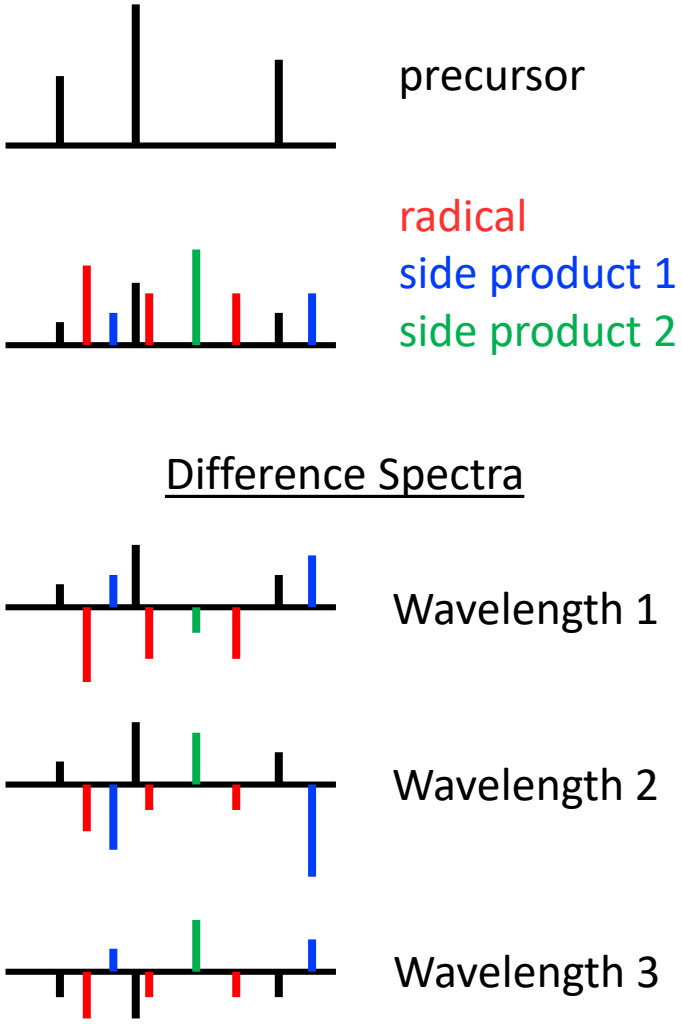

n-Propyl Secondary Photolysis Difference Spectra

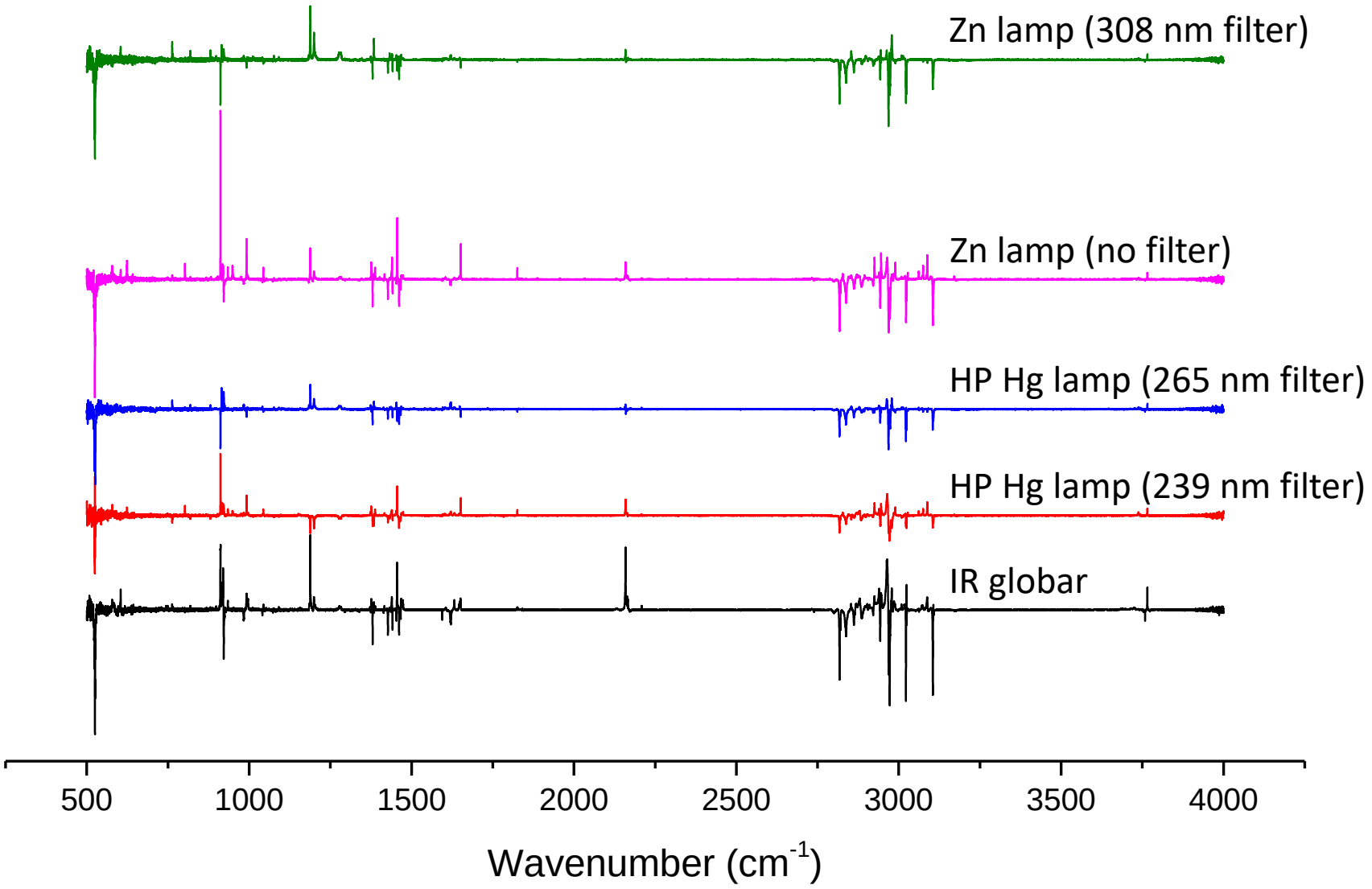

Solid *p*-H_2 spectrum of the *n*-propyl radical

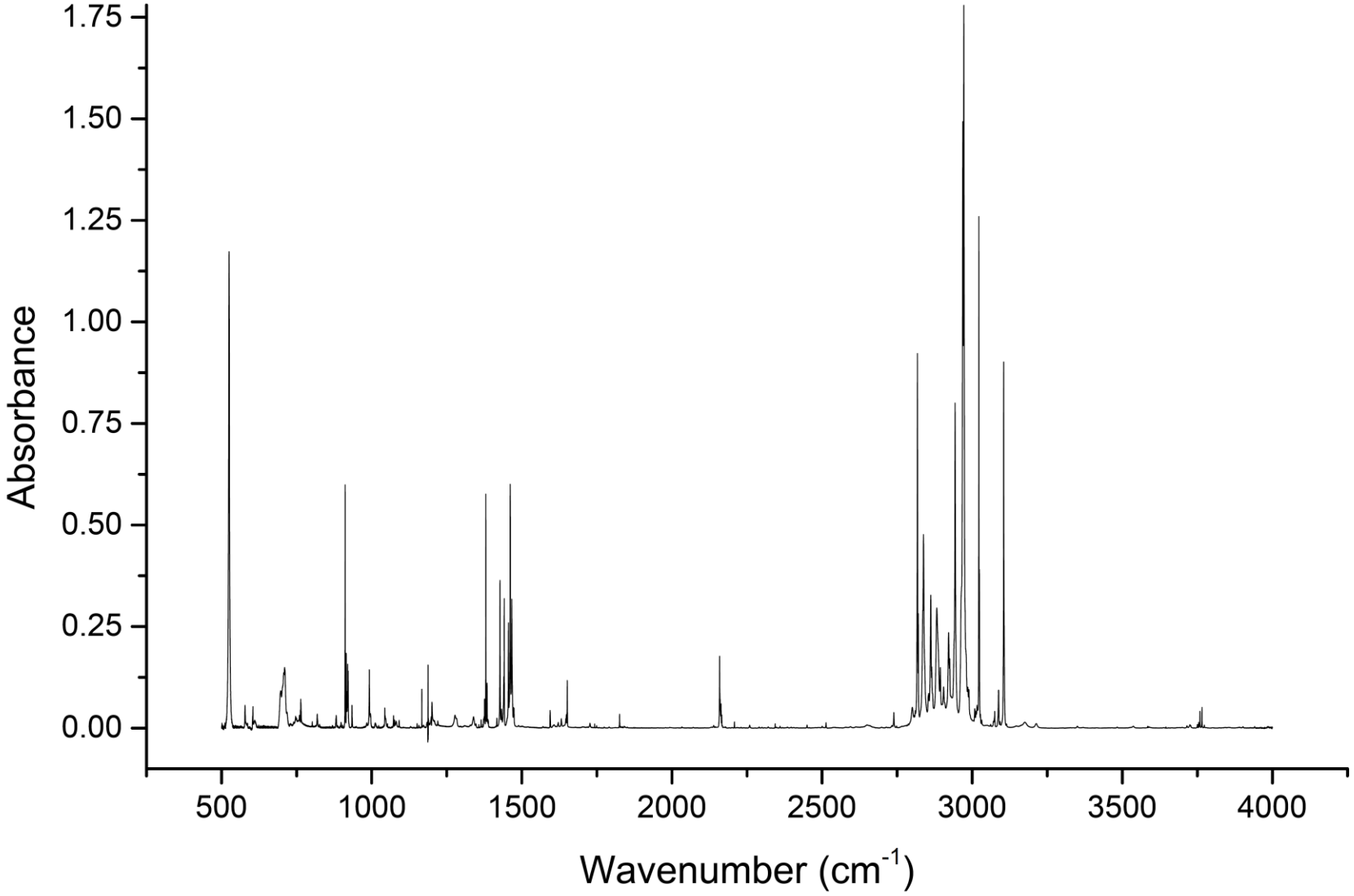

Solid *p*-H_2 spectrum of the *n*-propyl radical

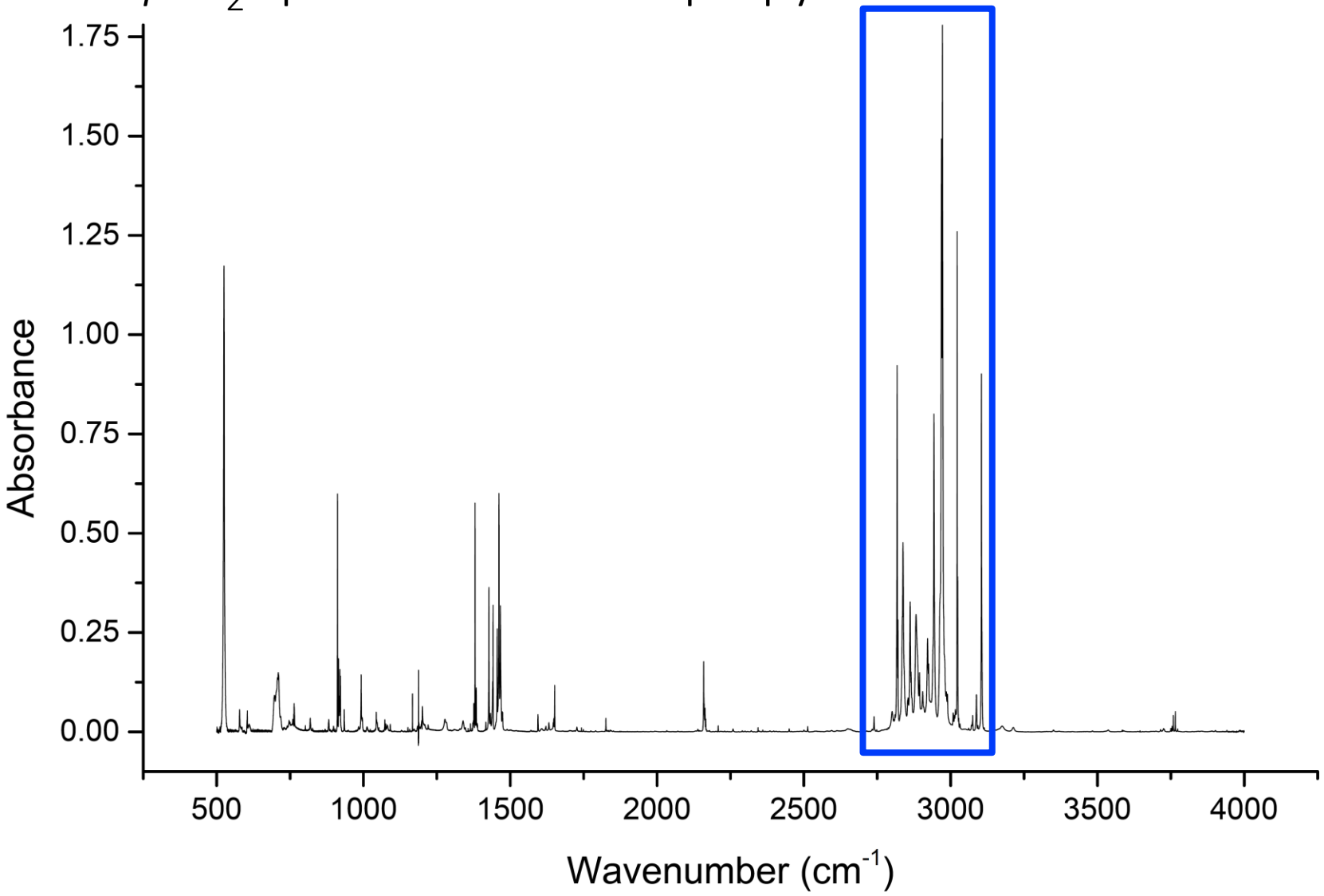

Comparison of *n*-propyl in *p*-H_2 and HENDI

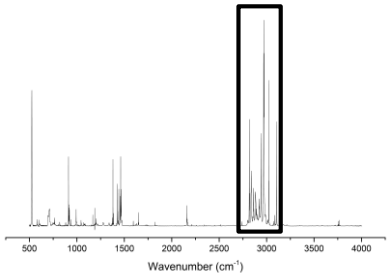

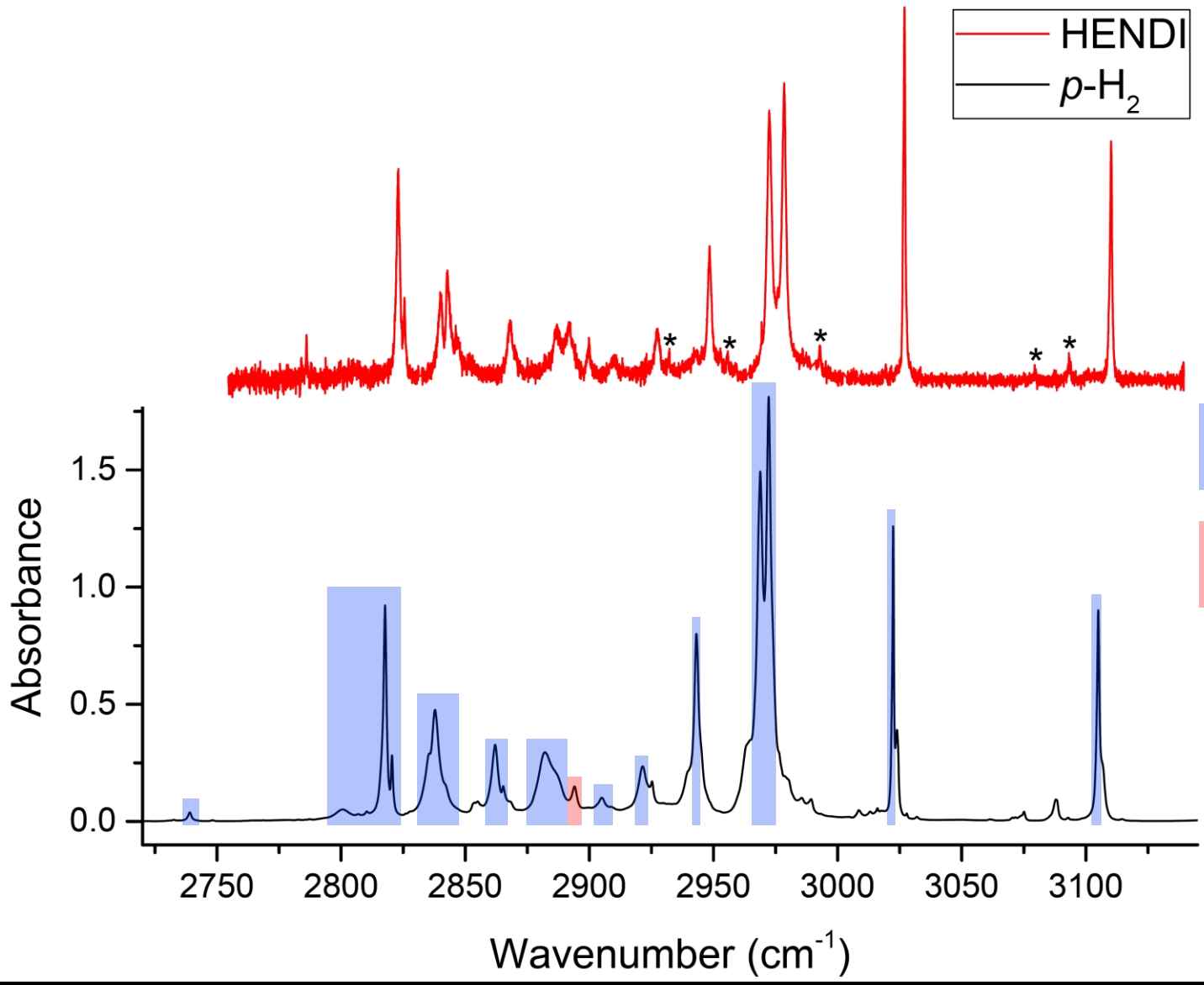

* = propene

= *n*-propyl radical

= overlapping peaks

Comparison of *n*-propyl in *p*-H_2 and VPT2+K

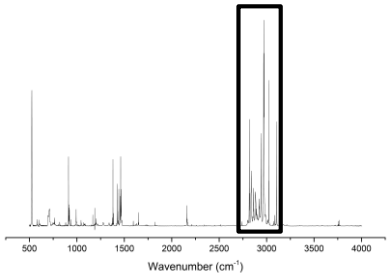

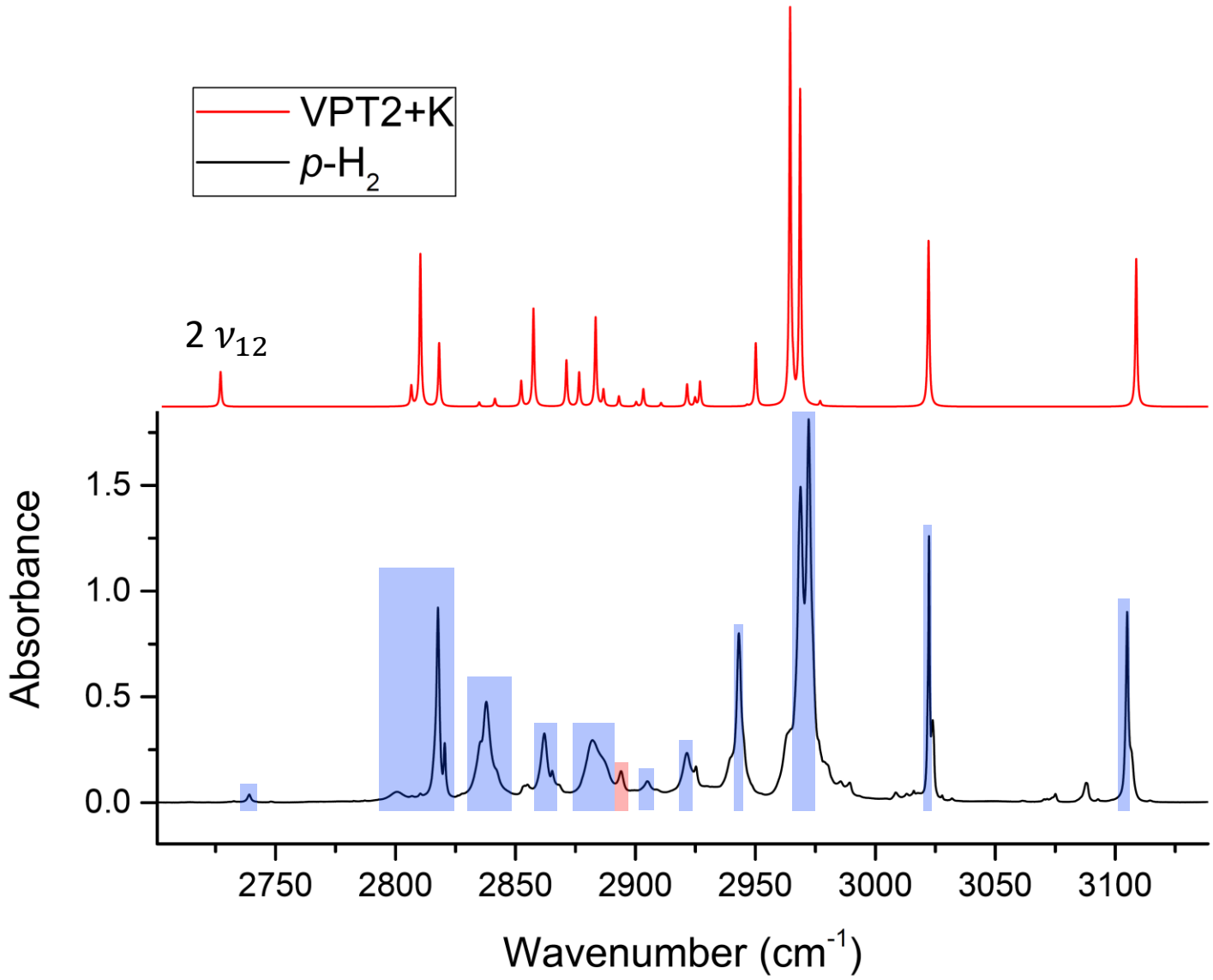

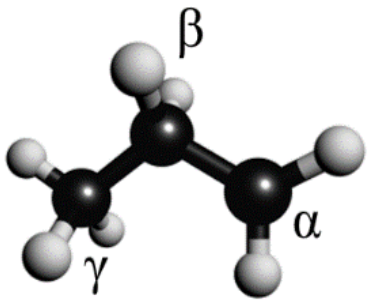

= *n*-propyl radical

= overlapping peaks

$\nu_{12}: \delta_s(\gamma - CH_3)$

Previously unreported *n*-propyl peaks above 2000 cm^{-1}

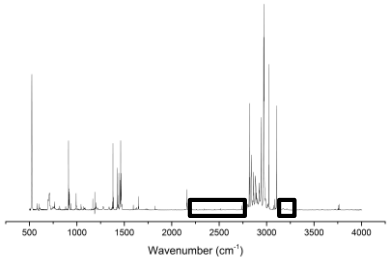

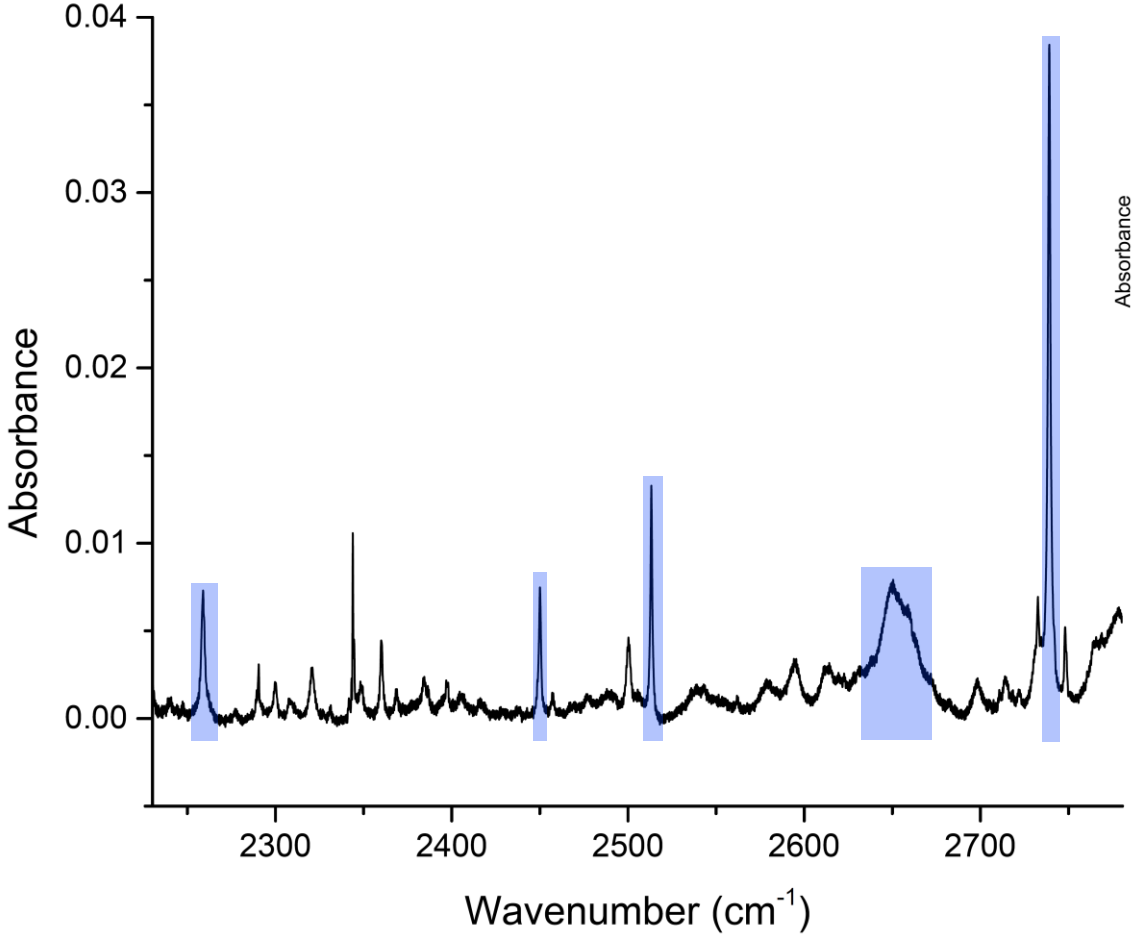

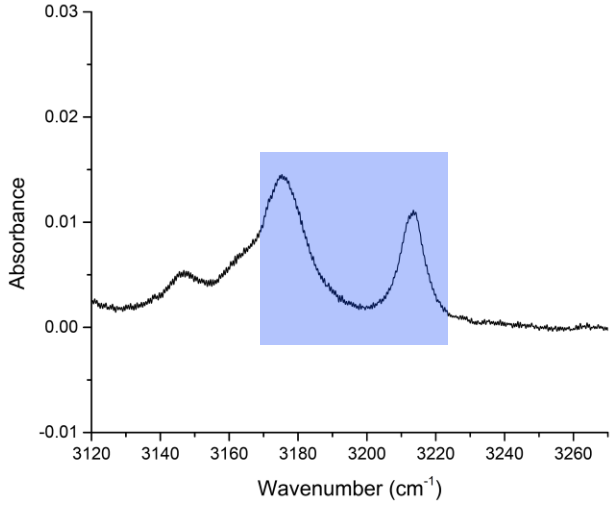

= *n*-propyl radical

n-Propyl C-H bending region

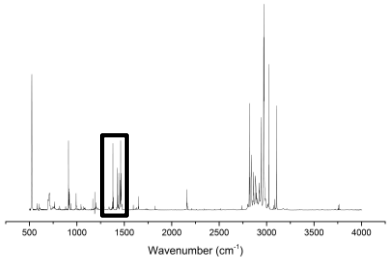

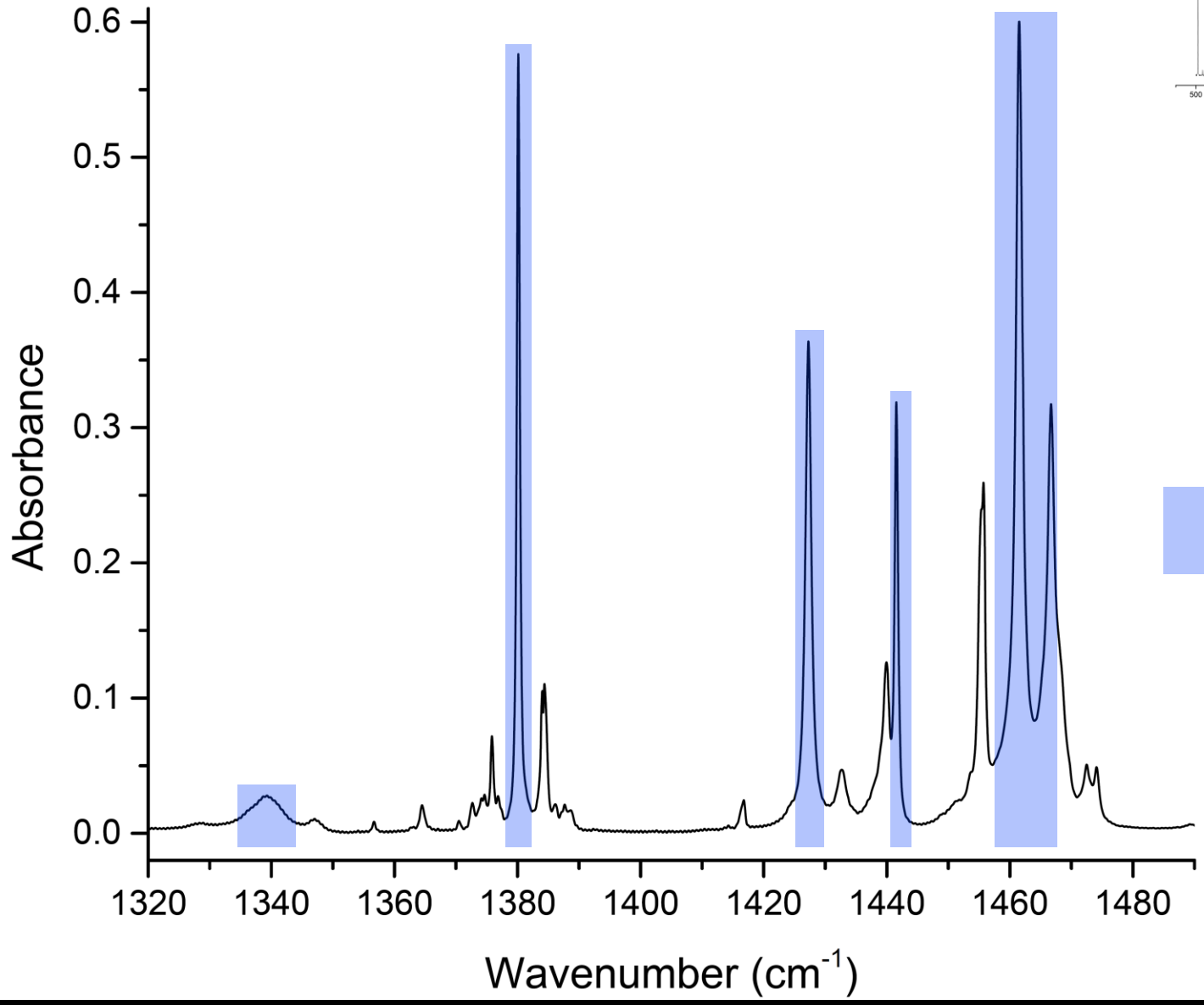

= *n*-propyl radical

Comparison of *n*-propyl in *p*-H_2 and VPT2+K

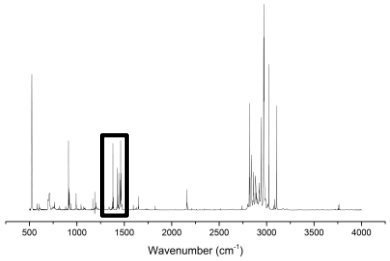

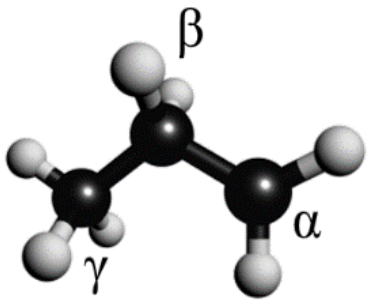

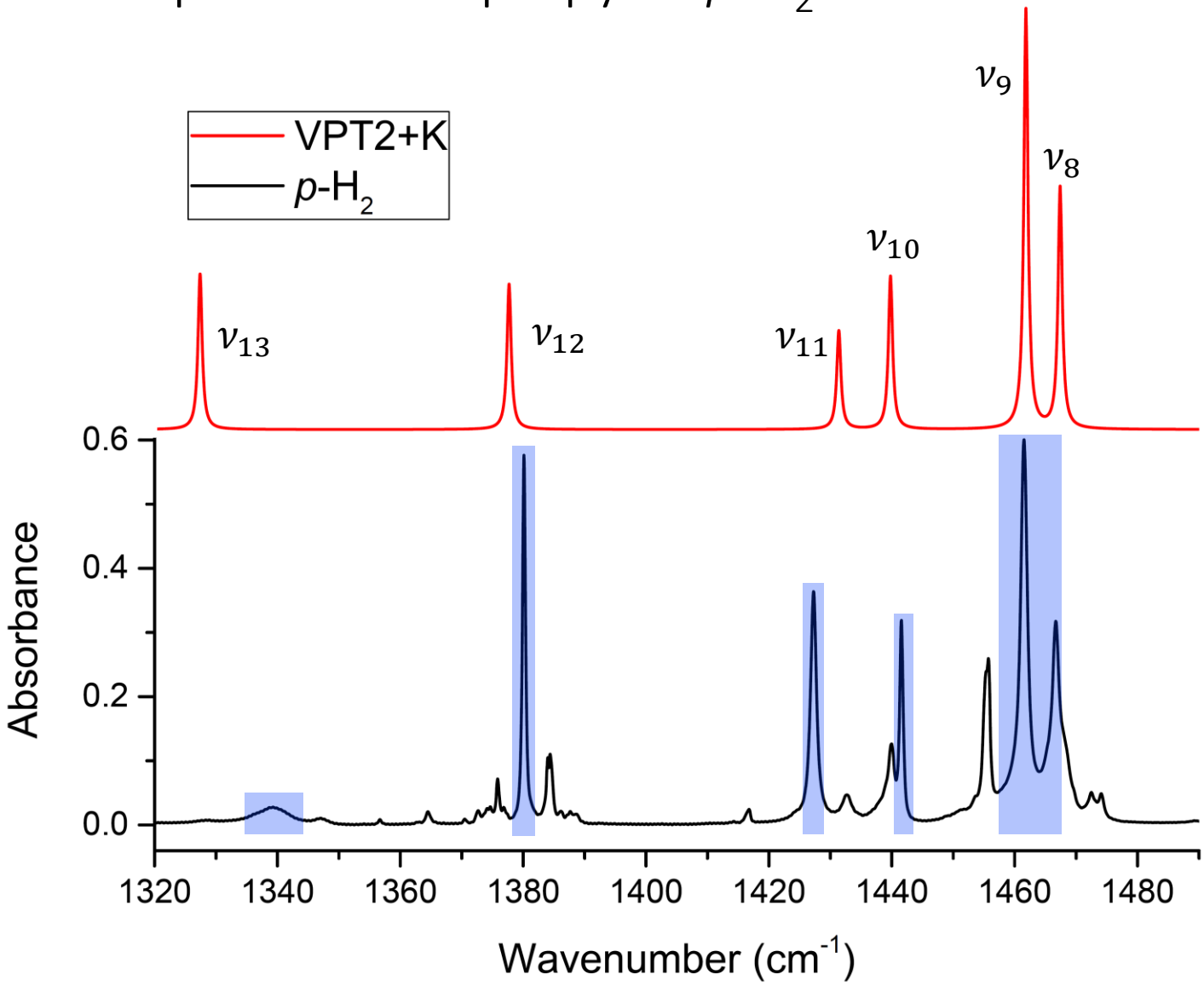

= *n*-propyl radical

$\nu_{13}: \rho_w(\beta - CH_2)$

$\nu_{12}: \delta_s(\gamma - CH_3)$

$\nu_{11}: \delta(\alpha - CH_2)$

$\nu_{10}: \delta(\beta - CH_2)$

$\nu_9: \delta_{as}^{a''}(\gamma - CH_3)$

$\nu_8: \delta_{as}^{a'}(\gamma - CH_3)$

Comparison of *n*-propyl in *p*-H_2 and VPT2+K

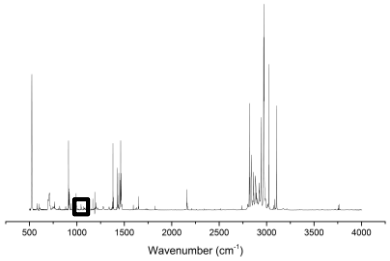

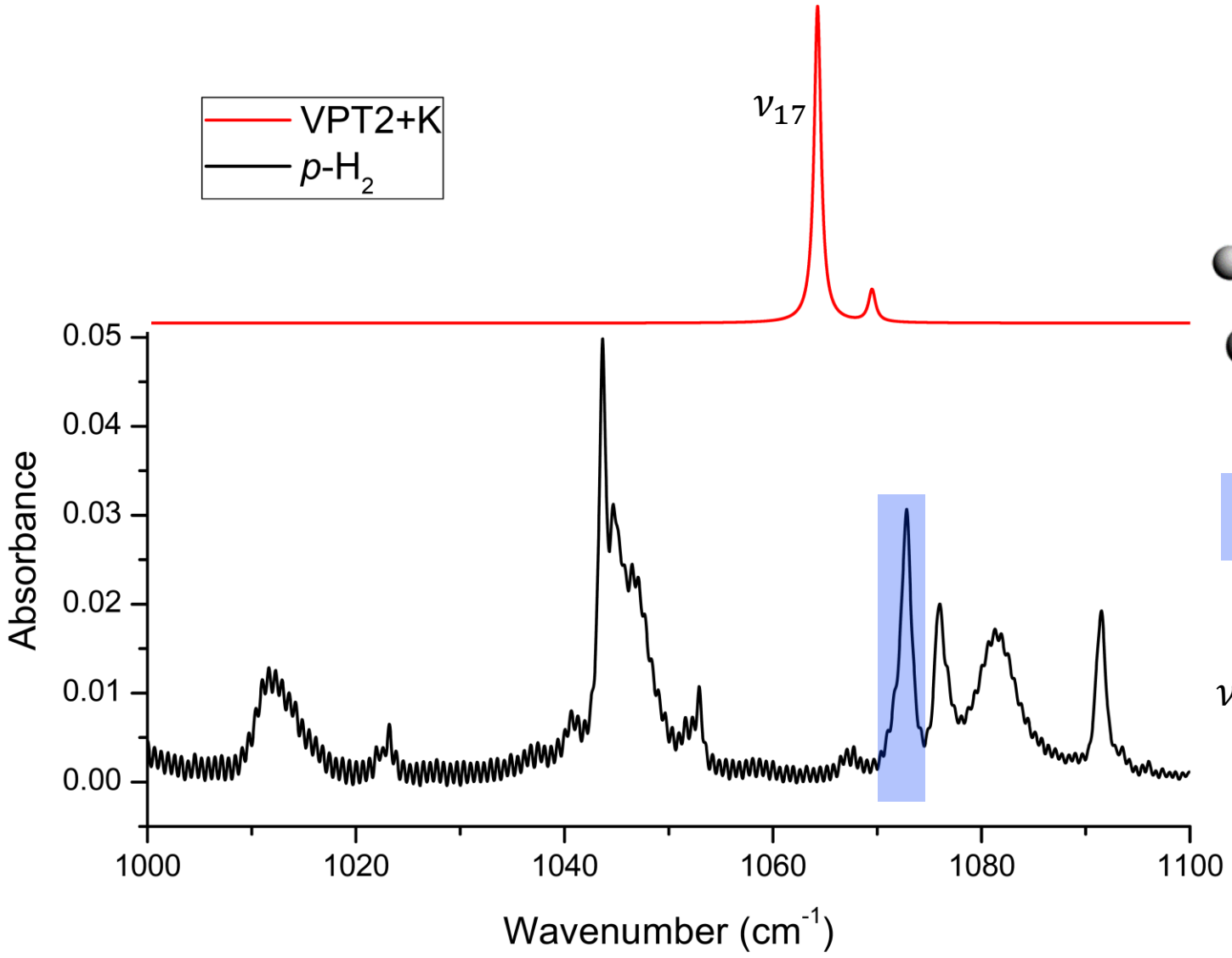

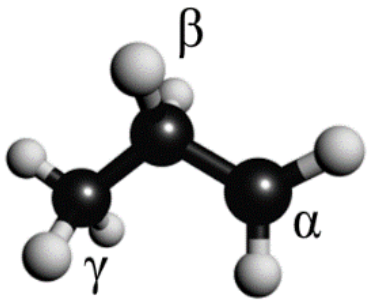

= *n*-propyl radical

$\nu_{17}: \rho_t(\beta - \mathrm{CH_2})$

Comparison of *n*-propyl in *p*-H_2 and VPT2+K

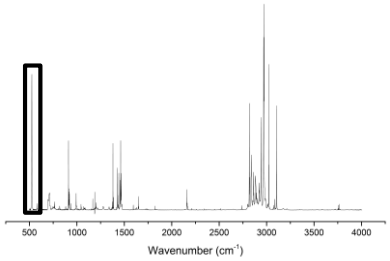

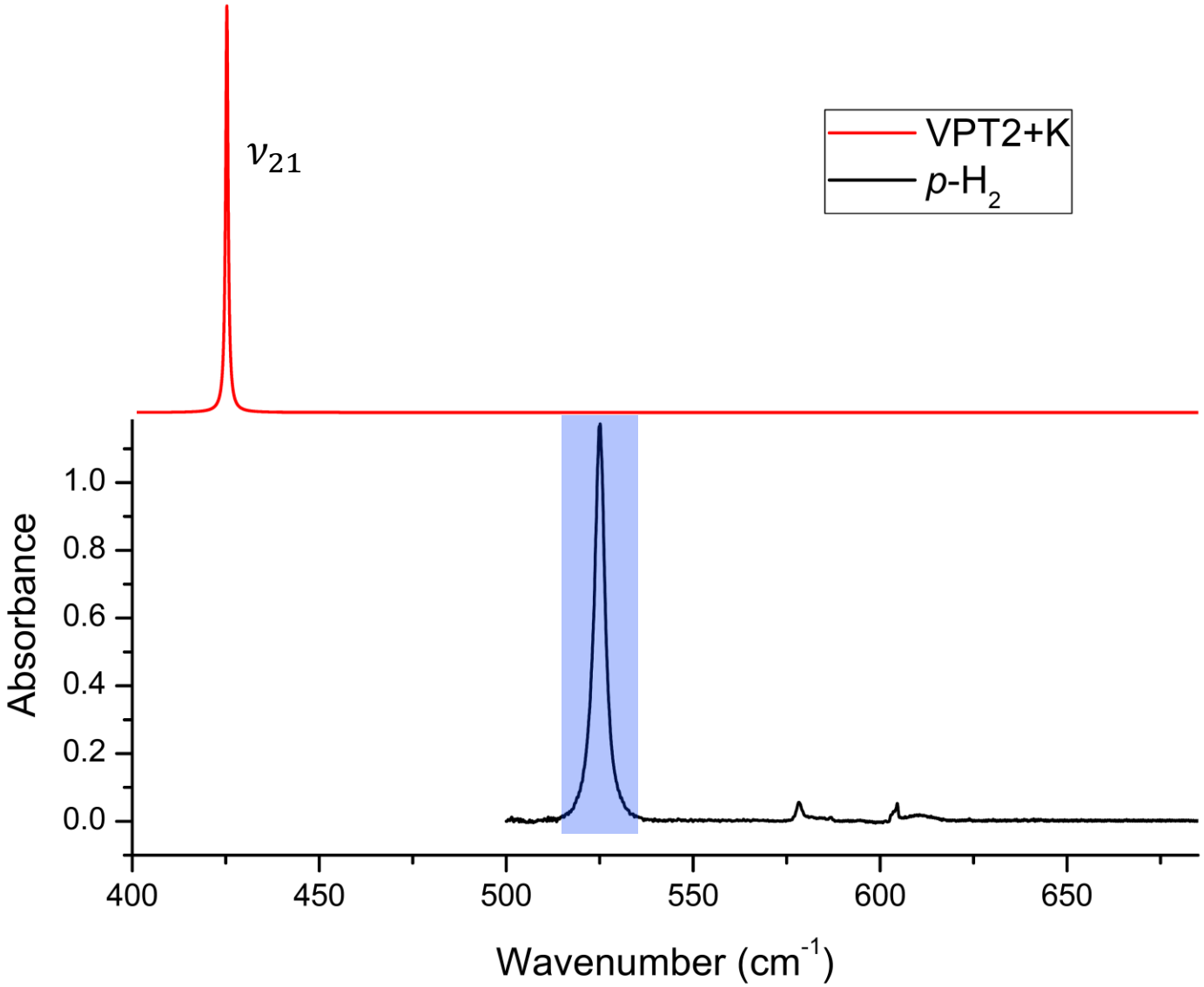

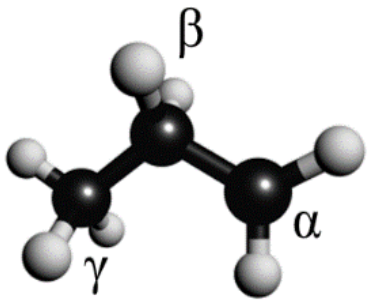

= *n*-propyl radical

ν_{21}: $\rho_w(\alpha - CH_2)$

Solid *p*-H_2 spectrum of the *i*-propyl radical

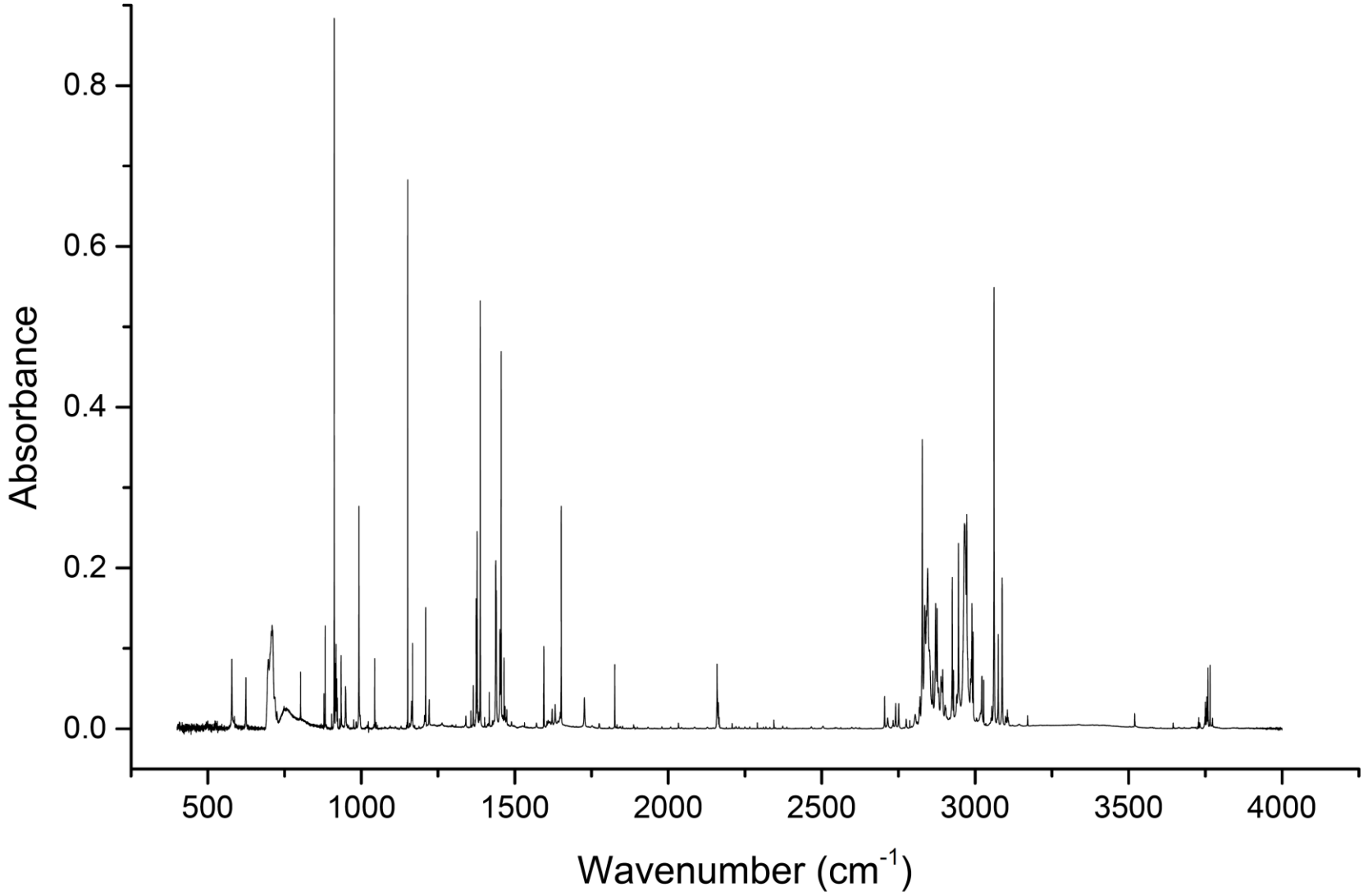

Solid *p*-H_2 spectrum of the *i*-propyl radical

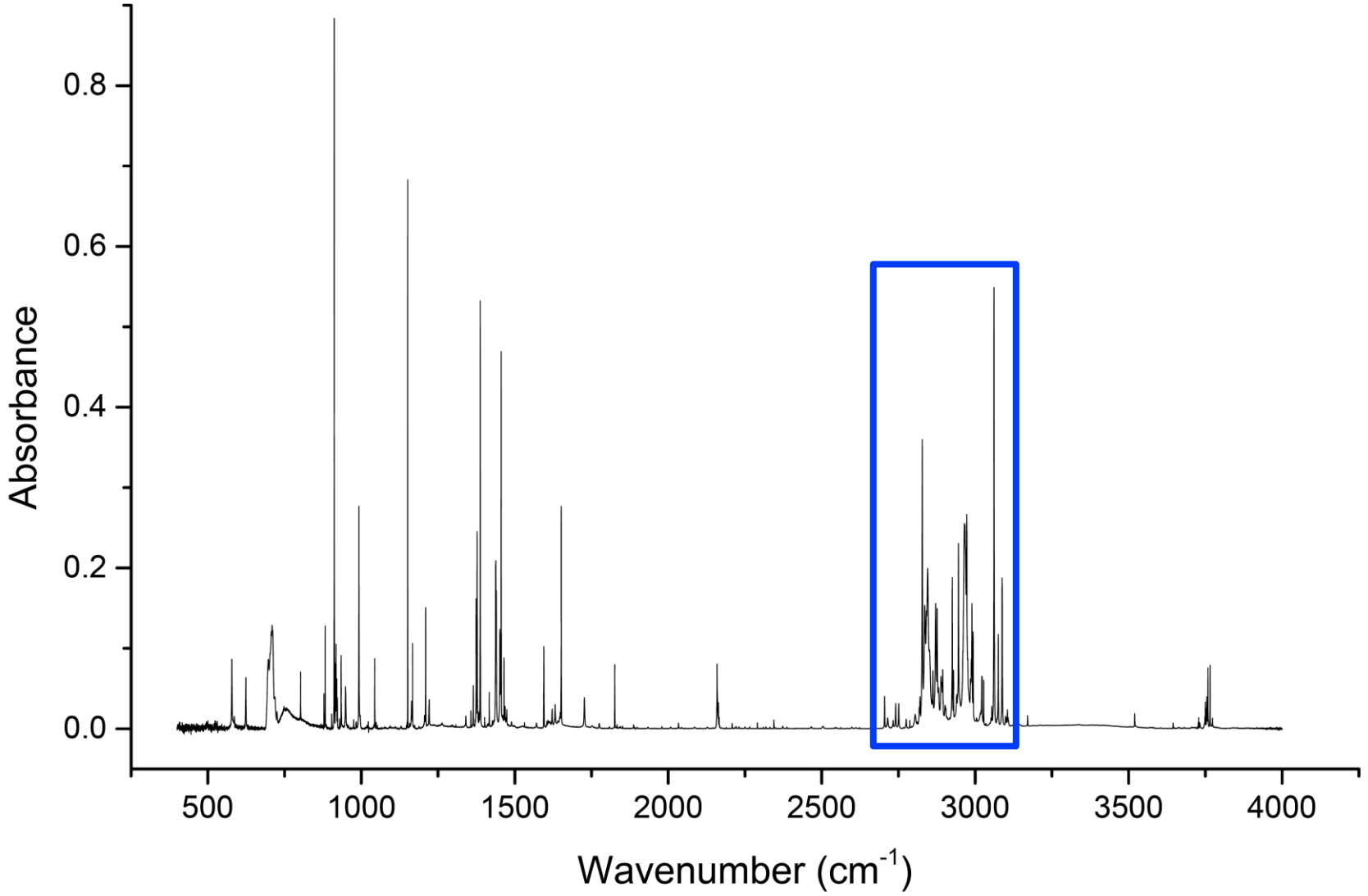

Comparison of *i*-propyl in *p*-H_2 and HENDI

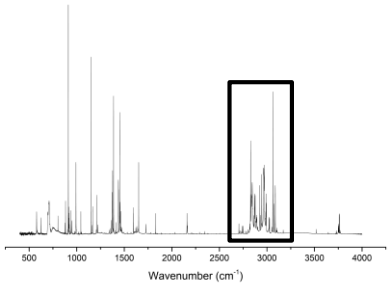

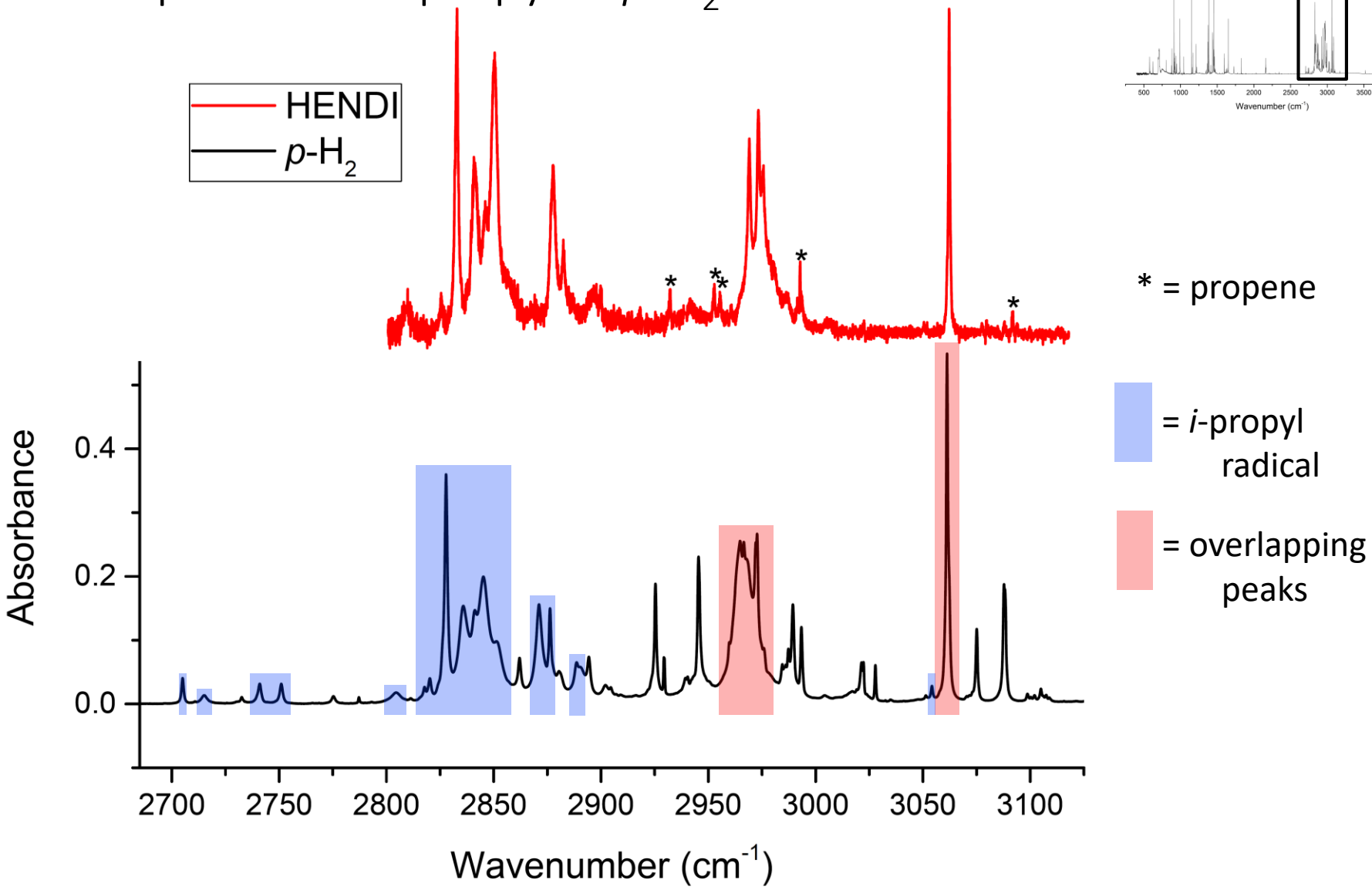

* = propene

= *i*-propyl radical

= overlapping peaks

Comparison of *i*-propyl in *p*-H_2 and VPT2+K

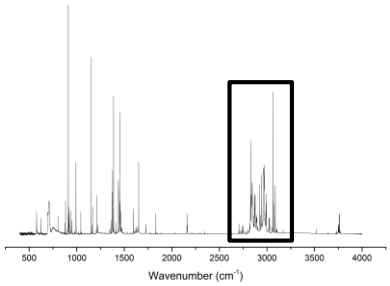

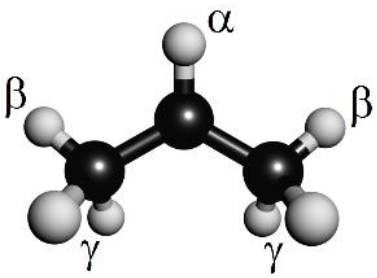

= *i*-propyl radical

= overlapping peaks

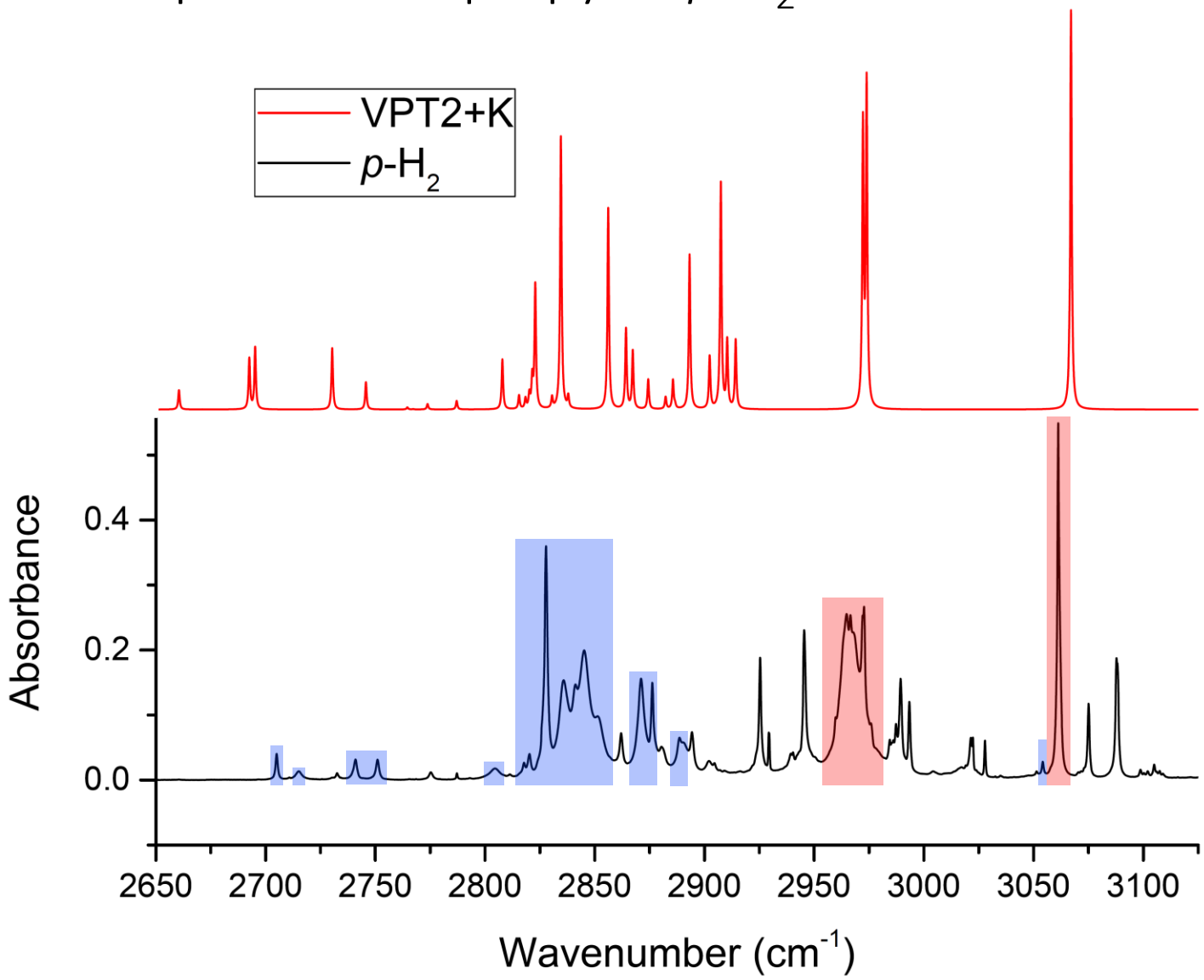

Comparison of *i*-propyl in *p*-H_2 and VPT2+K

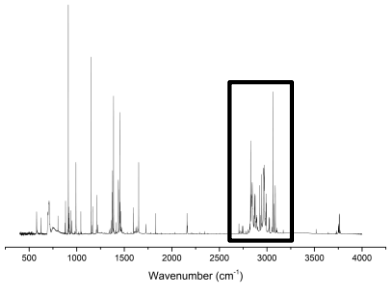

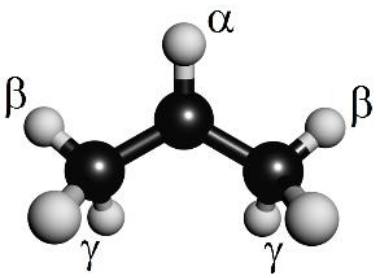

= *i*-propyl radical

= overlapping peaks

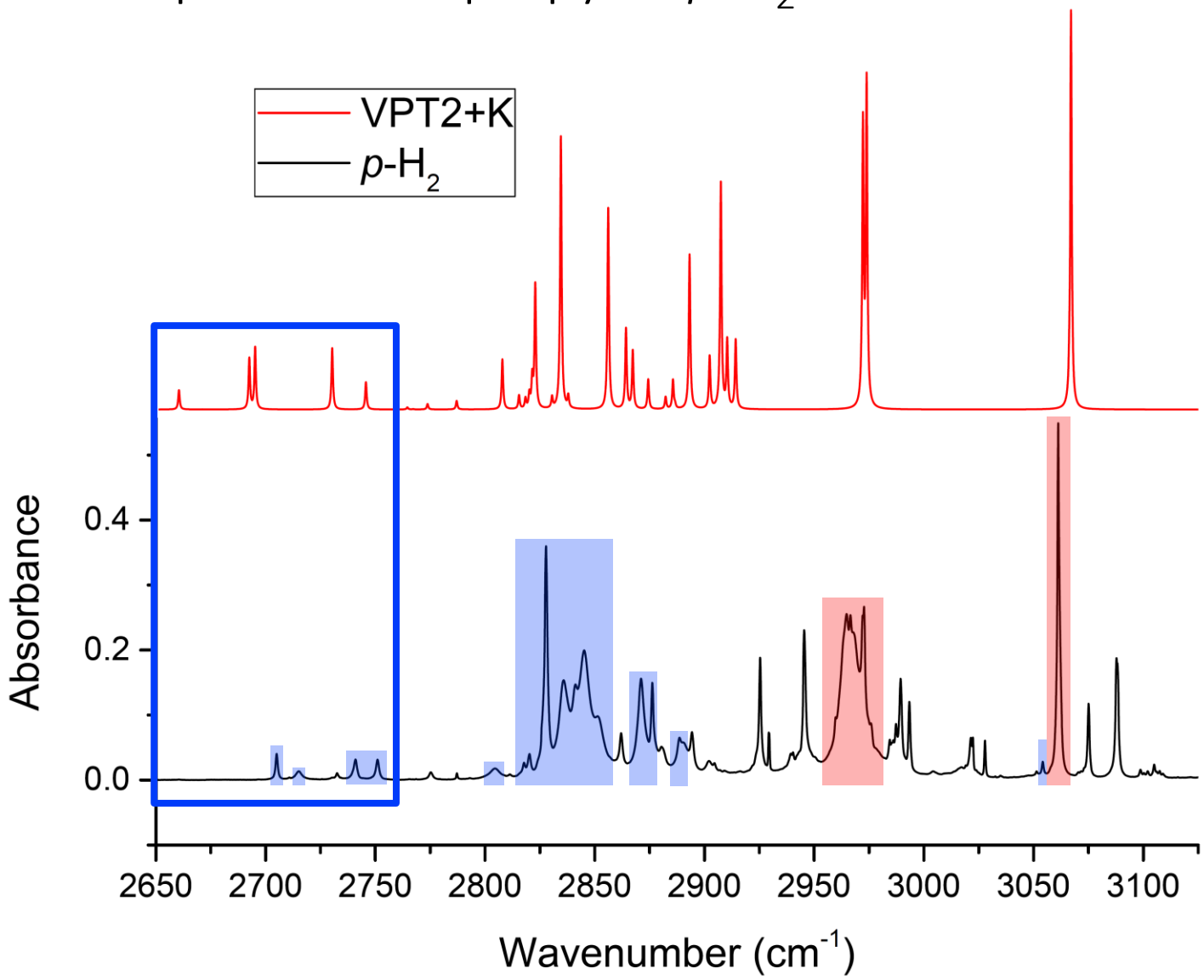

Comparison of *i*-propyl in *p*-H_2 and VPT2+K

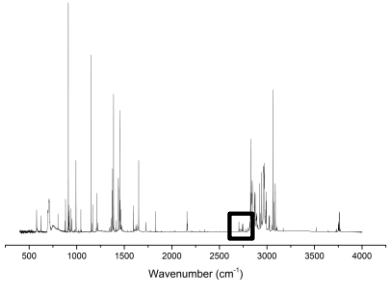

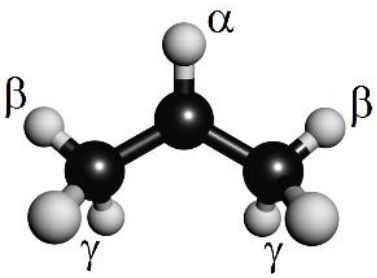

= *i*-propyl radical

ν_{20}: $\rho_w(\alpha - \mathrm{CH})$

ν_7: $\delta_s^{a'}(\beta/\gamma - \mathrm{CH_3})$

ν_{19}: $\delta_s^{a''}(\beta/\gamma - \mathrm{CH_3})$

VPT2+K

p-H_2

90% $2\,\nu_{20}$

70% $\nu_{20} + \nu_7$

70% $\nu_{20} + \nu_{19}$

30% $\nu_{20} + \nu_7$
60% $\nu_7 + \nu_{19}$

20% $\nu_{20} + \nu_{19}$
30% $2\,\nu_7$
30% $2\,\nu_{19}$

Absorbance

0.04
0.02
0.00

2660
2680
2700
2720
2740
2760

Wavenumber (cm^{-1})

Comparison of *i*-propyl in *p*-H_2 and VPT2+K

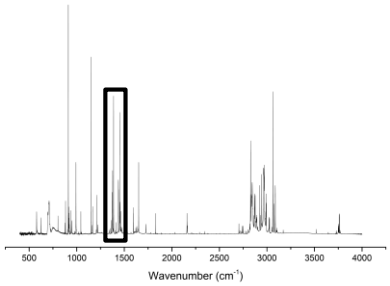

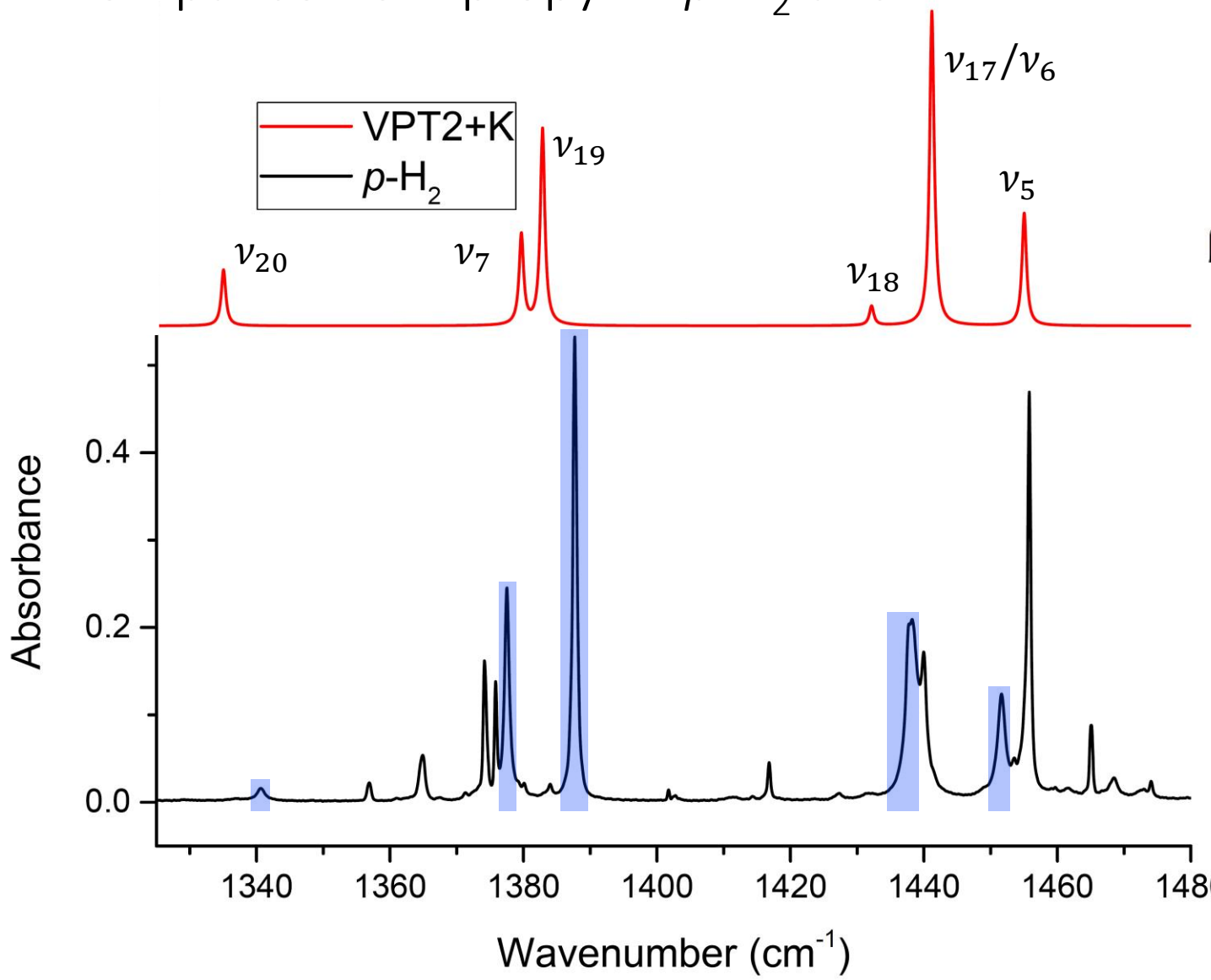

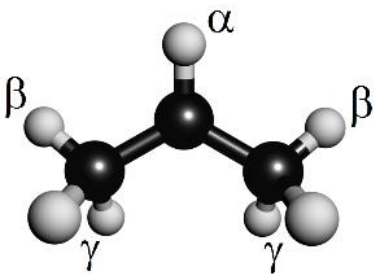

= *i*-propyl radical

ν_{20}: $\rho_w(\alpha - \mathrm{CH})$

ν_7: $\delta_s^{a'}(\beta/\gamma - \mathrm{CH_3})$

ν_{19}: $\delta_s^{a''}(\beta/\gamma - \mathrm{CH_3})$

ν_{18}: $\delta_{as}^{a''}(\beta/\gamma - \mathrm{CH_3})$

ν_{17}: $\delta_{as}^{a''}(\beta/\gamma - \mathrm{CH_3})$

ν_6: $\delta_{as}^{a'}(\beta - \mathrm{CH_3})$

ν_5: $\delta_{as}^{a'}(\gamma - \mathrm{CH_3})$

Comparison of *i*-propyl in *p*-H_2 and VPT2+K

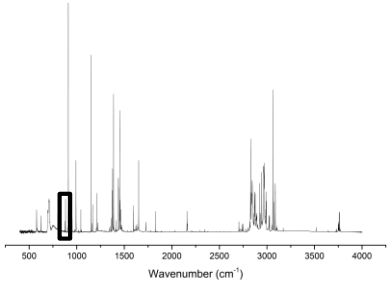

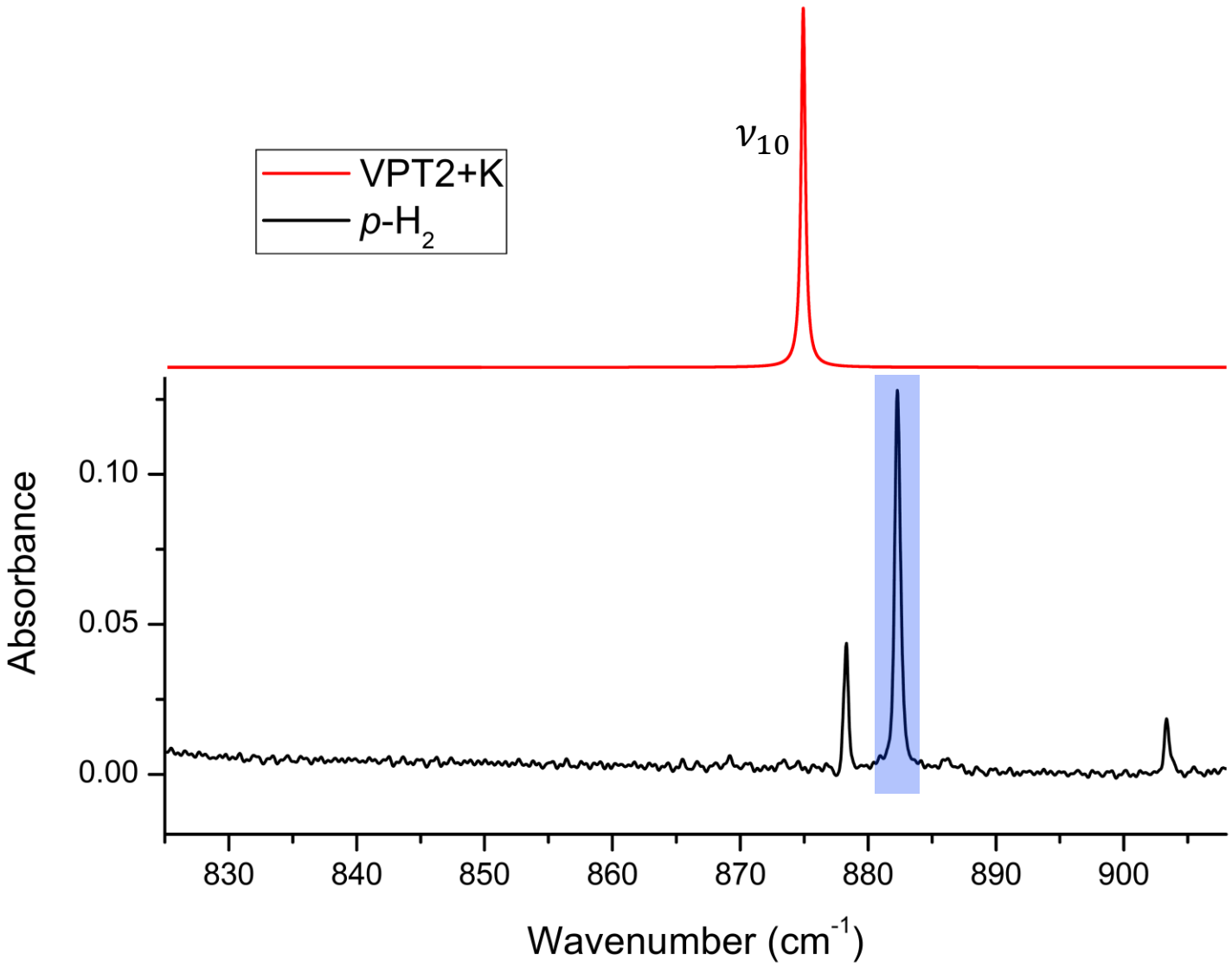

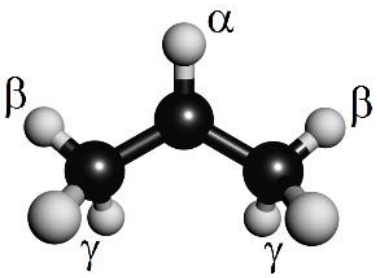

= *i*-propyl radical

ν_{10}: ν_s(C − C)

Comparison of results to previous work for *n*-propyl

p-H_2	HENDI	Pacansky	Chettur/Snelson
525		530	523
1073			1035
1380			
1427		1427	
1442			
1462			
1467		1469	
2259			
2450			
2513			
2650			
2739			
	2786		
2801	2805		
2807			
2810			
2818	2823	2812.5	

p-H_2	HENDI	Pacansky	Chettur/Snelson
2820	2826		
2835	2840		
2838	2843		
2842	2846		
2862	2868	2850	
2882	2887		
2886	2892		
	2900		
2905	2910		
2921	2927		
2943	2948		
2969	2972		
2972	2978		
3022	3027	3017.5	3028
3105	3110	3100	3118
3175			
3213			

Comparison of results to previous work for *i*-propyl

p-H_2	HENDI	Pacansky	Chettur/Snelson
		369	364
882			879
1164 (?)			1165
1341			
1378		1378	
1388		1388	
1438			
1452		1468	
2705			
2715			
2741			
2751			
2805	2809		
2818			
2820	2825		
2828	2833	2830	

p-H_2	HENDI	Pacansky	Chettur/Snelson
2836	2841		
2841	2846		
2845	2850		
2851			
2871	2878		
2876	2882		
2889			
2890	2896	2920	
	2941		
	2969		
2968	2973		
	2976		
2978	2980		
3054			
3061	3062	3069	3052

Funding

U.S. DEPARTMENT OF ENERGY

Office of International Education
UNIVERSITY OF GEORGIA

Graduate School
UNIVERSITY OF GEORGIA

科 技 部

Ministry of Science and Technology

國立交通大學
National Chiao Tung University

Support:

U.S. Department of Energy, Office of Science (BES-GPCP)
The University of Georgia, Office of International Education
The University of Georgia, Graduate School
The Ministry of Science and Technology of Taiwan
The Ministry of Education of Taiwan
National Chiao Tung University

Acknowledgements

Dr. Yuan-Pern Lee

Dr. Karolina Haupa
Dr. Jay Amicangelo
Kelly Tseng
Peter Chen
The rest of the Lee group

Dr. Gary Douberly

Peter Franke
Joseph Brice
Alaina Brown
The rest of the Douberly group

Thank you for your attention

Summary

- The infrared spectra of the *n*-propyl and *i*-propyl radicals have been measured from 400 – 4000 cm^{-1} in solid *para*-hydrogen matrices
- These spectra were compared against the infrared spectra of the *n*-propyl and *i*-propyl radicals in helium nanodroplets, with excellent agreement
- Many previously unreported peaks were measured and compared against *ab initio* VPT2+K anharmonic frequency calculations using a CCSD(T)/ANO1//CCSD(T)/ANO0 hybrid force field (*n*-propyl) and a CCSD(T)/ANO1 force field (*i*-propyl), with very good agreement
- Analysis of butyl radical spectra and corresponding alkyl peroxy radical spectra (propyl peroxy and butyl peroxy radicals) is underway

Structure of the *n*-propyl radical

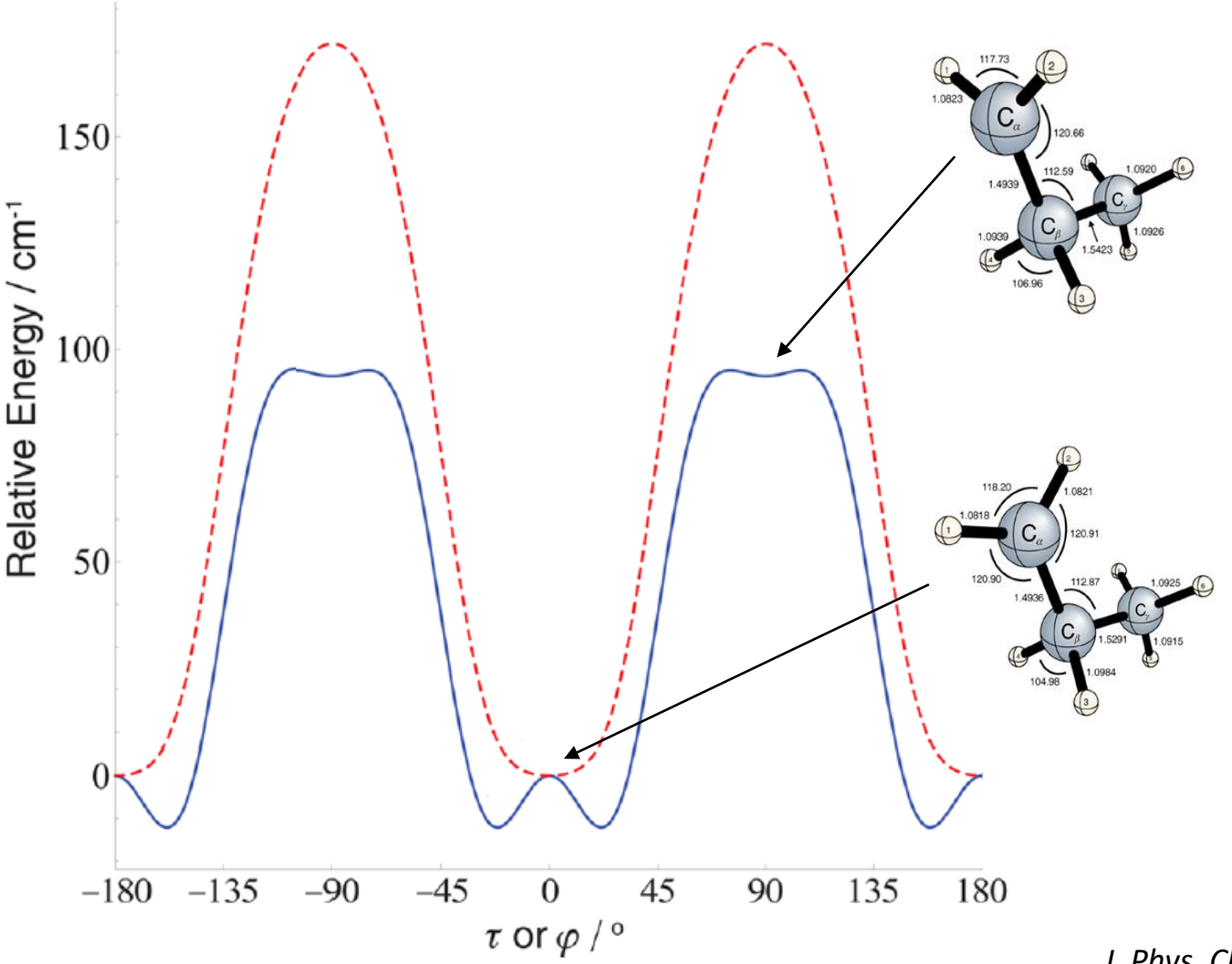

The electronic minimum is predicted to have C_1 symmetry. A shallow transition state with C_s symmetry separates the equivalent C_1 minima on the methylene torsional potential (blue). After ZPVE-correction, only a single well remains (red). These DRC curves were computed at the CCSD(T)/cc-pVQZ// MP2/cc-pVTZ level of theory by Schaefer and co-workers.

J. Phys. Chem. B., 2015, 119, 728-735

Structure of the *i*-propyl radical

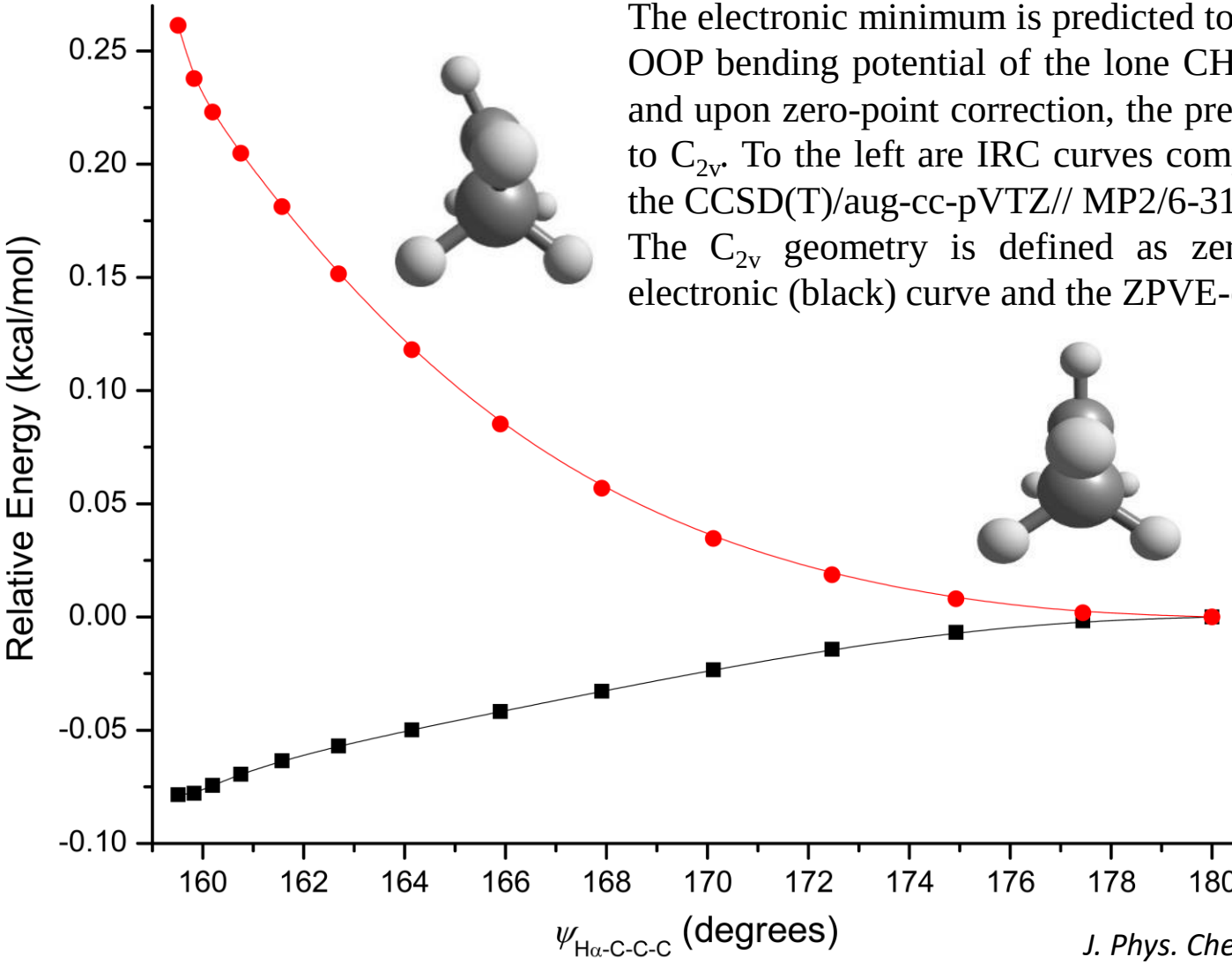

The electronic minimum is predicted to have C_s symmetry. The OOP bending potential of the lone CH is rather flat, however, and upon zero-point correction, the preferred structure changes to C_{2v}. To the left are IRC curves computed in Gaussian 09 at the CCSD(T)/aug-cc-pVTZ// MP2/6-311++G** level of theory. The C_{2v} geometry is defined as zero energy on both the electronic (black) curve and the ZPVE-corrected (red) curve.

J. Phys. Chem. B., 2015, 119, 728-735

Basic quantum physics of solid *p*-H_2

Fermion (^{1}H Nuclear spin I = $\frac{1}{2}$) ➡ ψ_{total}: anti-symmetric

$$\psi_{total} = \psi_e \, \psi_v \, \psi_r \, \psi_n$$

ψ_r	ψ_n
Odd J Anti-symmetric Ground State: $J = 1$	Symmetric ***ortho*-H_2**
Even J Symmetric Ground State: $J = 0$	Anti-symmetric ***para*-H_2**

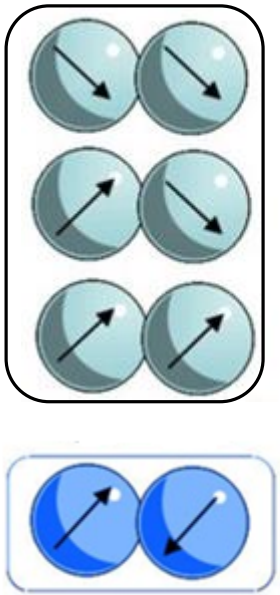

The ratio of *o*-H_2:*p*-H_2 is 3:1 @ R.T. and 0:1 @ 0 K

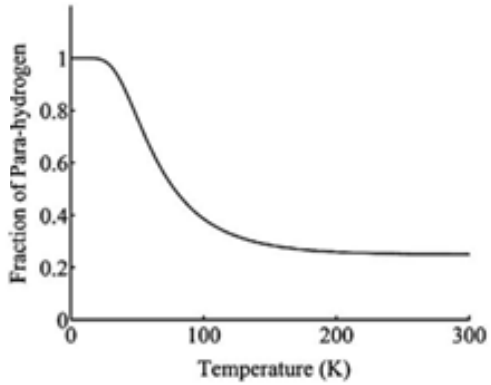

1. Equilibrium fraction of para-hydrogen as a function of temperature.

Benefits of *p*-H_2 as Matrix Host

No dipole moment

J = 0 rotational state is occupied
spherically symmetric charge distribution

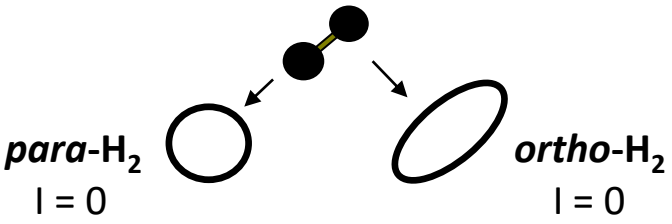

Ar and Ne have fcc and hcp crystal structures

p-H_2 only has an hcp crystal structure

The host-guest interaction in *p*-H_2 is weaker than in rare gas matrices

	***p*-H_2**	**Ne**	**Ar**
Lattice Constant (Å)	3.78	4.47	5.31
Zero-Point Amplitude Motion	18%	9%	5%
Zero-Point Lattice Vibration (Å)	0.68	0.42	0.27

p-H_2 has a high thermal conductivity

	***p*-H_2**	**Fe**	**Ar**
Thermal Conductivity (W cm^{-1} K^{-1})	0.72	0.68	0.04

Benefits of large ZP vibrational motion in *p*-H_2

	***p*-H_2**	**Ne**	**Ar**
Lattice Constant (Å)	3.78	4.47	5.31
Zero-Point Amplitude Motion	18%	9%	5%
Zero-Point Lattice Vibration (Å)	0.68	0.42	0.27

The amplitude of the zero-point lattice vibrations of *p*-H_2 is a substantial fraction of the spacing between nearest H_2 molecules.

The matrix is considered to be ***'soft'***.

Crystal defects around guest species are expected to be repaired automatically.

Brings homogeneity to *p*-H_2 matrix.

Reduces the possibility of having *multiple trapping sites* and leads to reduced *inhomogeneous broadening of lines* of the guest molecules.

Benefits of large ZP vibrational motion in *p*-H_2

	***p*-H_2**	**Ne**	**Ar**
Lattice Constant (Å)	3.78	4.47	5.31
Zero-Point Amplitude Motion	18%	9%	5%
Zero-Point Lattice Vibration (Å)	0.68	0.42	0.27

Some guest molecule rotation possible

CO, CH_4, H_2O, and HCl:
slightly hindered rotation in solid *p*-H_2

Larger species:

Some internal rotation (torsion) feasible: CH_3OH

Some rotation about a single axis: CH_3F

Such rotations not observed in noble-gas matrices

Matrix cage effect

Inert-gas matrices

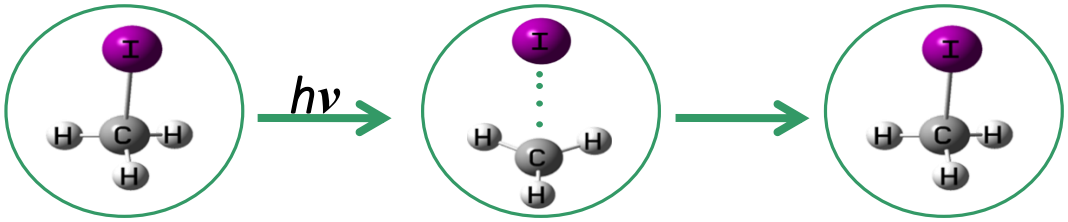

Diminished cage effect

p-H_2 matrix

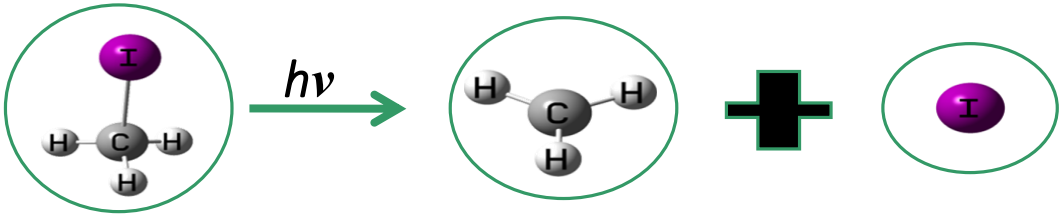

p-H_2 Matrix Isolation Experimental Details

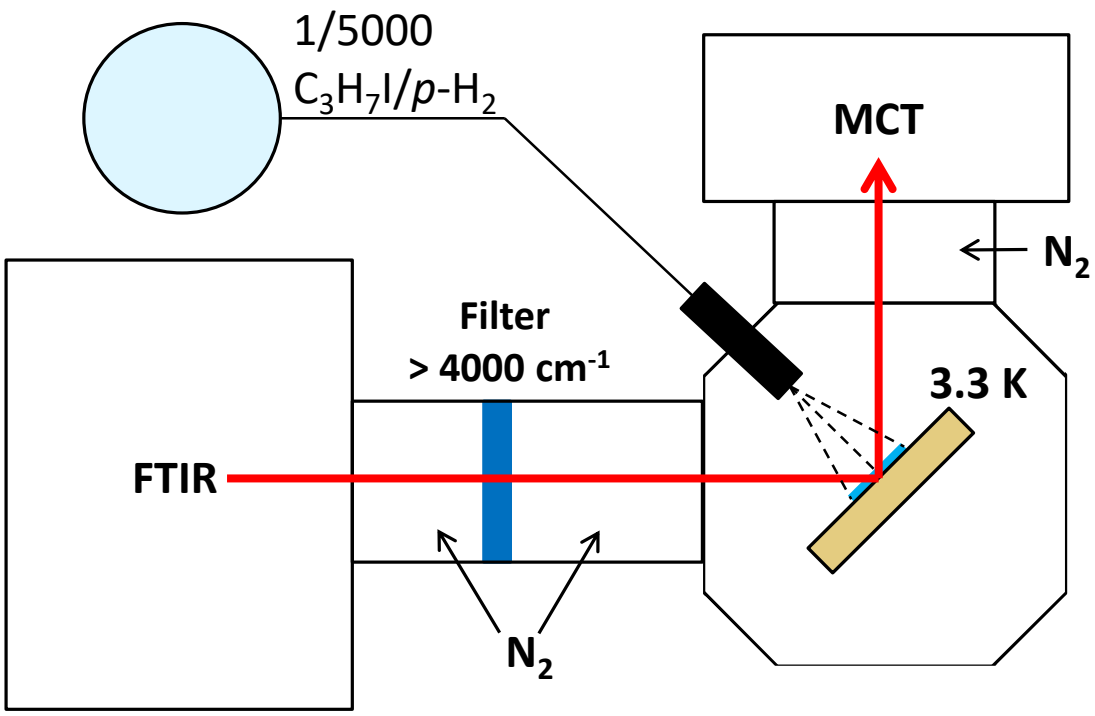

Bruker Vertex 80v FTIR
KBr Beamsplitter
Range: 4000 – 400 cm^{-1}
Resolution: 0.25 cm^{-1}
200 scans

IR filter: Spectrogon LP-2500
cut-off wavelength ~2.4 µm
(~4200 cm^{-1})

L-N_2 cooled MCT detector

Precursor: propyl iodide
Matrix mirror: 1 in diameter
gold coated copper plate
Deposition time: 10 hr
Gas flow rate: ~4 sccm
(~11 mmol/hr)

<u>Spectral mixing ratios</u>
***n*-propyl: ~250 ppm**
***i*-propyl: ~210 ppm**

<u>Matrix Thickness</u>
***n*-propyl: ~1.1 mm**
***i*-propyl: ~1.2 mm**

p-H_2 Matrix Isolation Photolysis Details

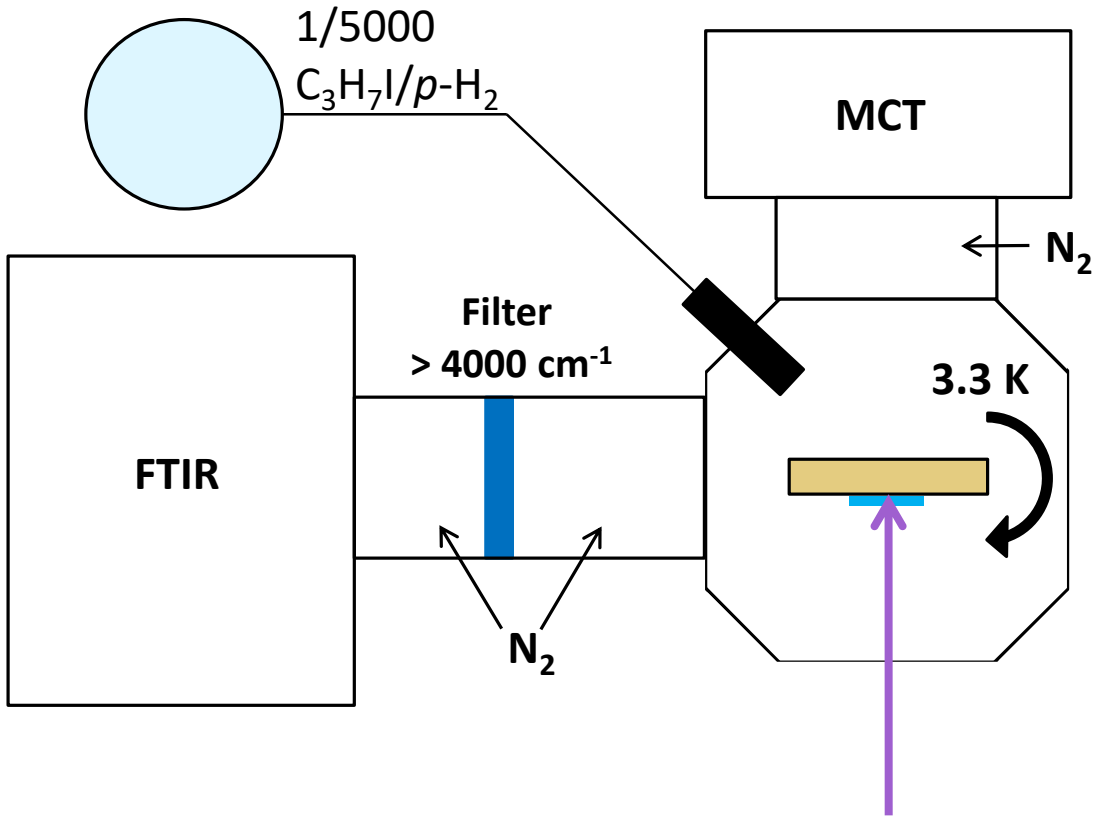

Primary Photolysis

248 nm KrF excimer laser

Intensity: ~400 – 500 µJ/pulse on a 1 in diameter mirror

Repetition Rate: 1 Hz

Duration of irradiation:

- ***n*-propyl: 140 min**
- ***i*-propyl: 120 min**

Secondary Photolysis

1. **Zn lamp (308 nm filter)**
2. **Zn lamp (no filter)**
3. **High Pressure Hg lamp (265 nm filter)**
4. **High Pressure Hg lamp (239 nm filter)**
5. **IR globar**

1 hour each

Production of *p*-H_2 Details

Fe_2O_3 catalyst
Temperature: 12.9 $\pm$ 0.5 K
Final concentration of *o*-H_2:
$\sim$400 – 600 ppm

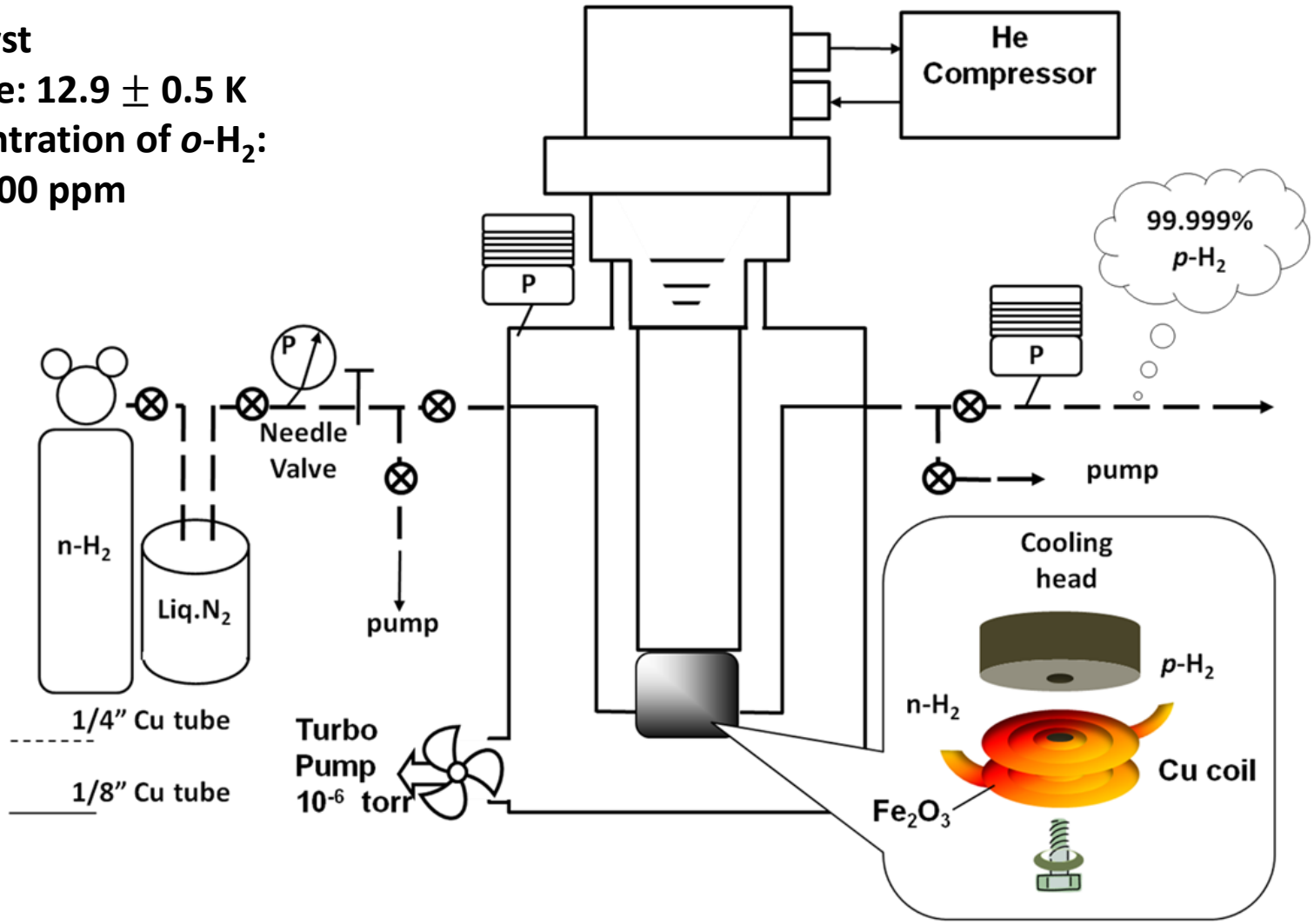

p-H_2 Matrix Experimental Details

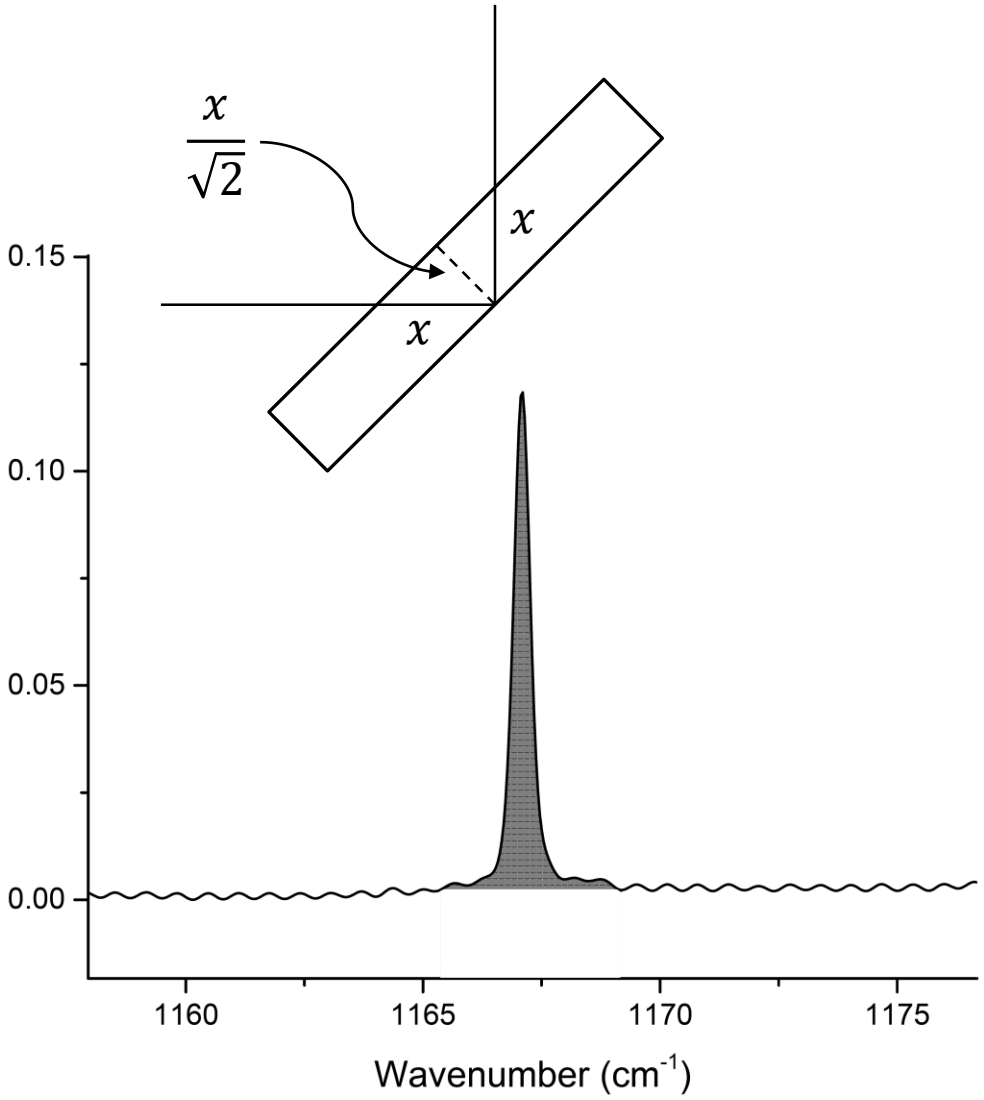

Matrix Thickness

Integration of peak at 1167.1 cm^{-1}:

Optical Path Length (OPL)

n-propyl: ~3.2 mm

i-propyl: ~3.4 mm

Thickness $= \frac{\mathrm{OPL}}{2\sqrt{2}}$

***n*-propyl: ~1.1 mm**

***i*-propyl: ~1.2 mm**

i-propyl layering:

top: ~0.2 mm – pure p-H_2

middle: ~0.9 mm – mixture

bottom: ~0.1 mm – pure p-H_2

p-H_2 Matrix Experimental Details

Sample Concentration

$$c\ (\text{ppm}) = \frac{\ln(10) \int \log_{10}\left(\frac{I}{I_o}\right) dv}{\varepsilon\ l} V_o \times 10^6$$

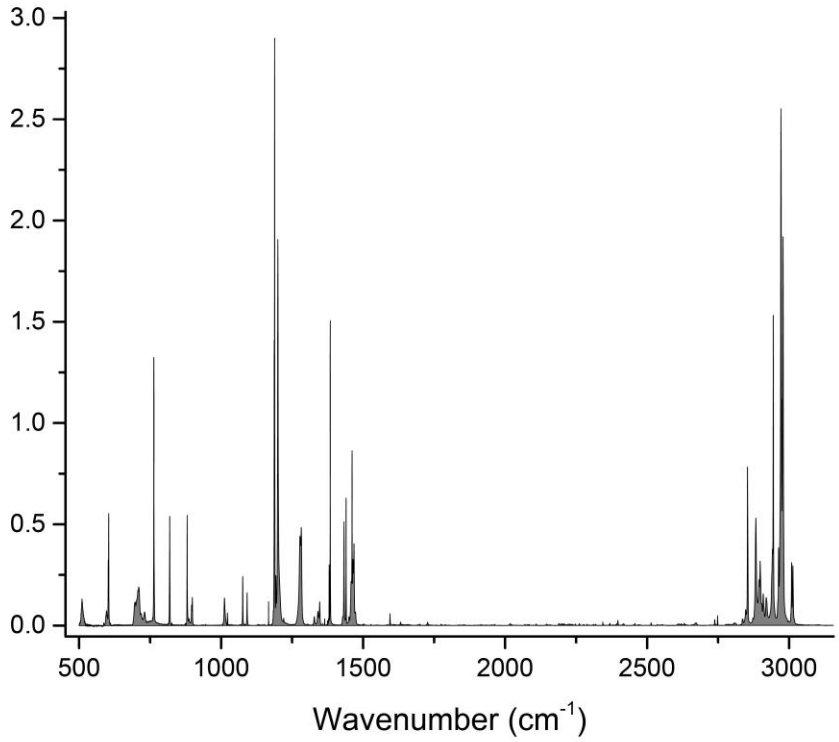

ε: absorption coefficient (in cm/mol)
l: optical path length (in cm)
V_o: molar volume of solid p-H_2 (23.16 cm^3/mol)

absorption coefficient from frequency calculation:

B3LYP with aug-cc-pVTZ for C and H, and LANL2DZ(dp) ECP for I

***n*-propyl: ~250 ppm**
***i*-propyl: ~210 ppm**

Intended 1/5000, or 200 ppm

p-H_2 Matrix Experimental Details

n-Propyl Iodide Conformers

trans

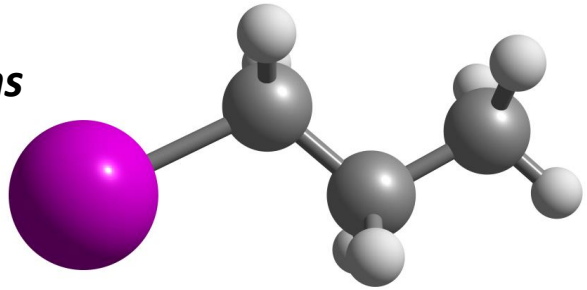

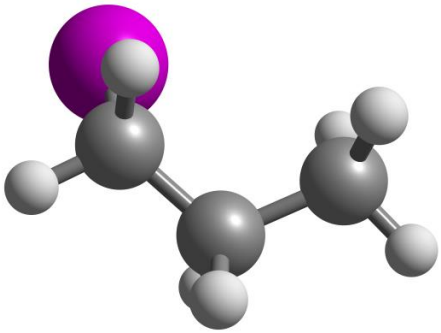

gauche

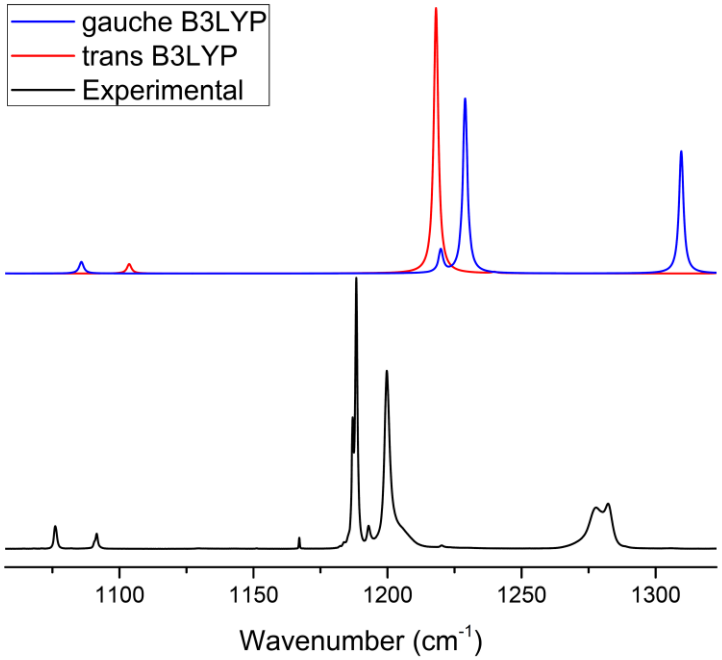

B3LYP with aug-cc-pVTZ for C and H,
and LANL2DZ(dp) ECP for I

trans lower in energy by:
0.000563 Hartrees
(~1.5 kJ/mol, ~0.35 kcal/mol,
~120 cm^{-1}, ~178 K)

Room temperature Boltzmann Population:
~48/52 *trans/gauche*

Experimental Details

precursor
radical
side product 1
side product 2

Scale the Precursor Spectrum

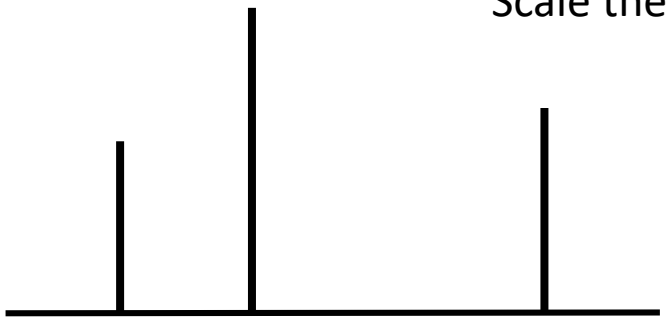

$\times 0.3 =$

Photolysis

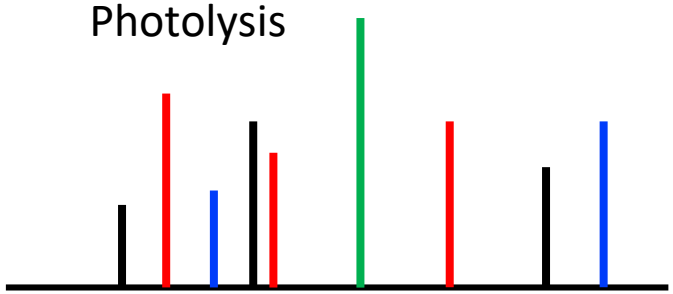

$-$

Scaled Precursor

$=$

Final Spectrum

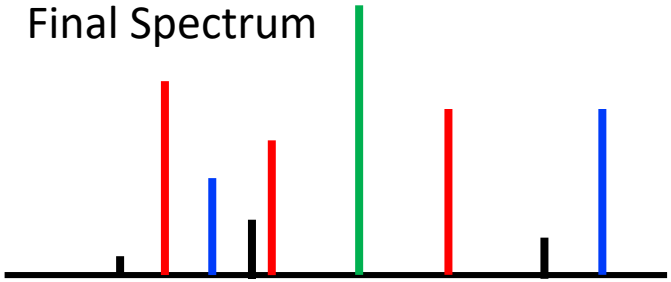

Solid *p*-H_2 spectrum of the *n*-propyl radical

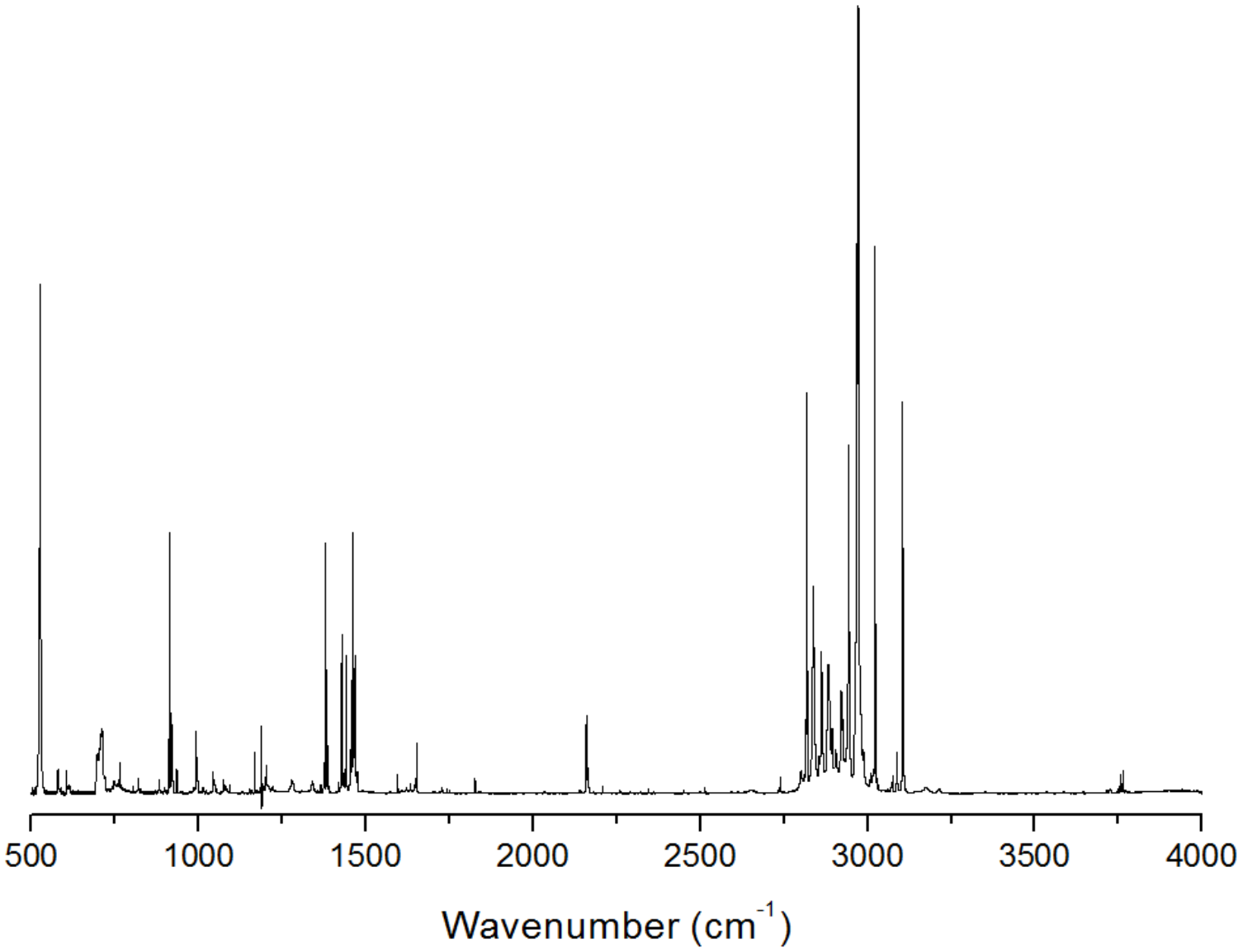

Solid *p*-H_2 spectrum of the *n*-propyl radical (stripped peak-by-peak)

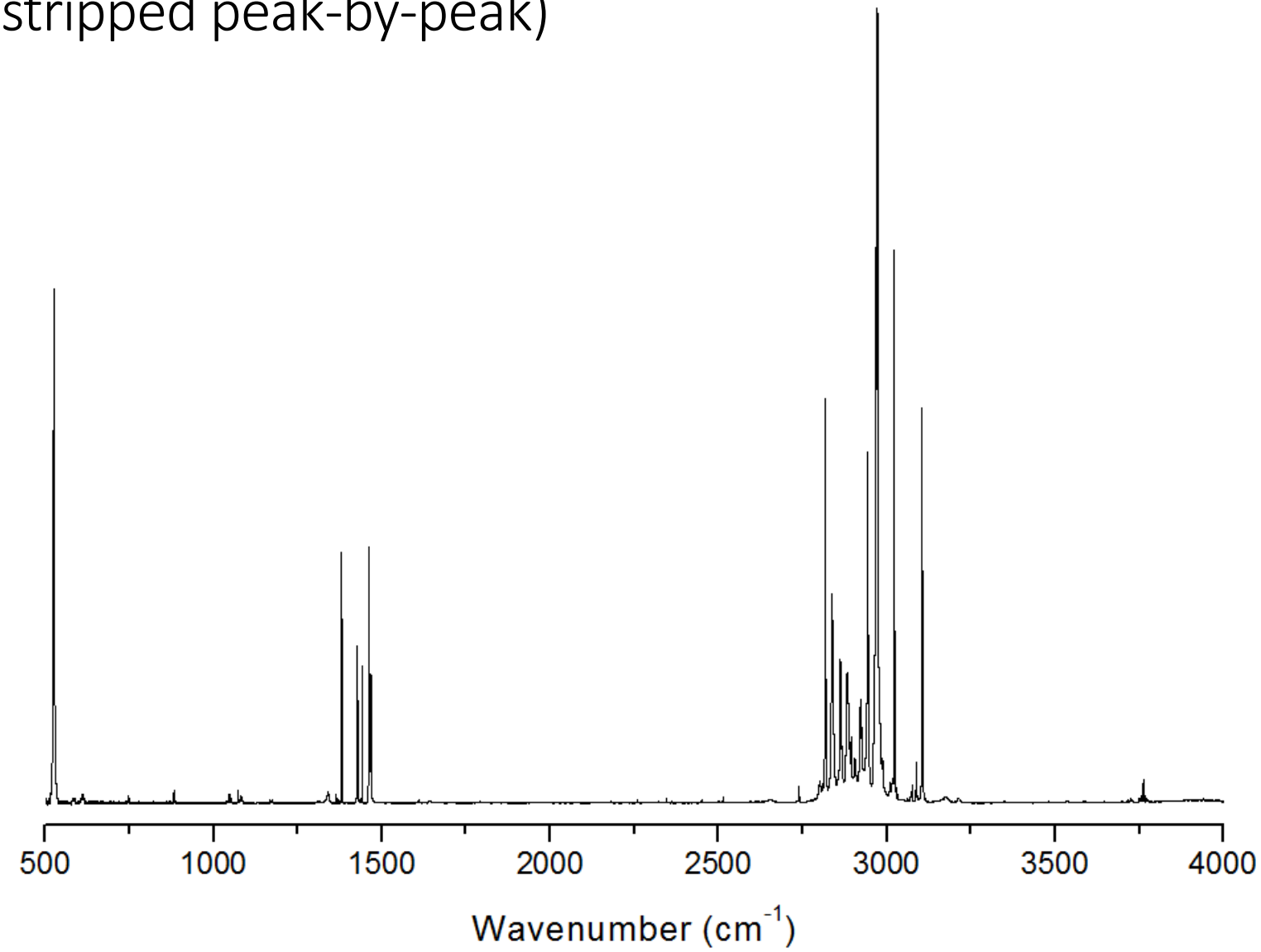

The butyl radicals

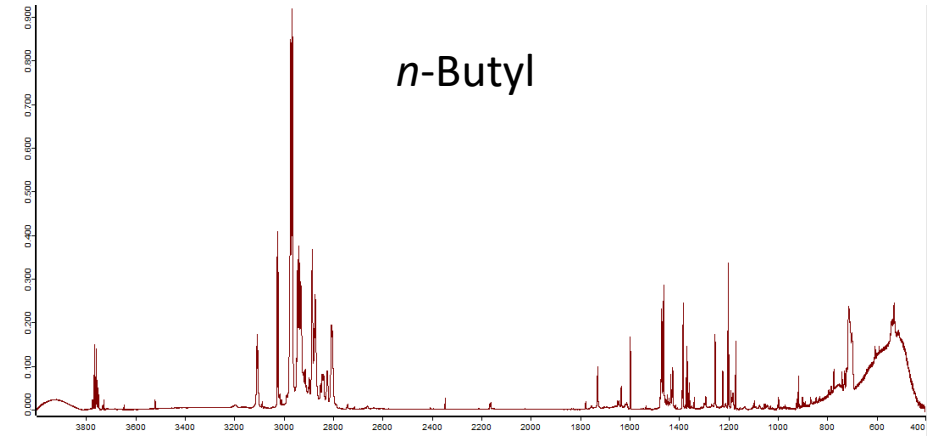

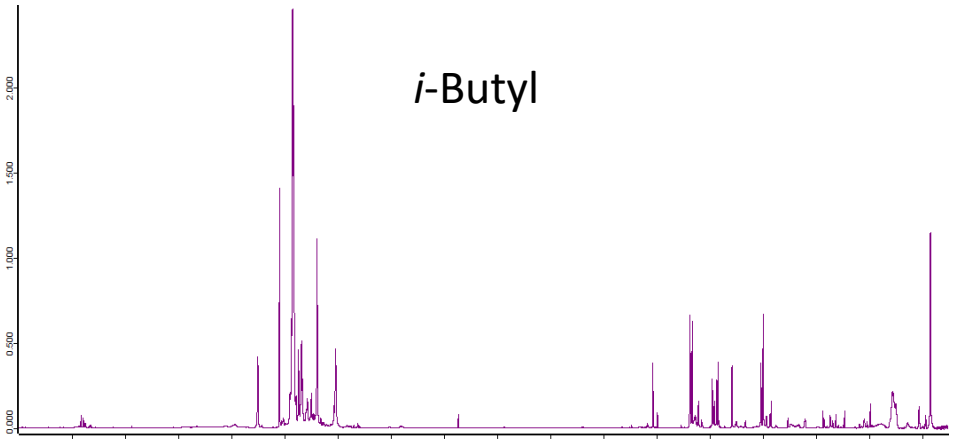

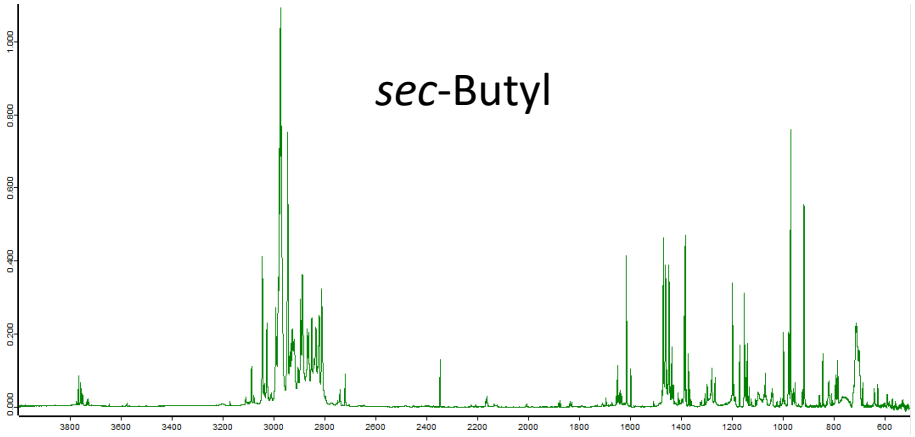

The propyl and butyl peroxy radicals

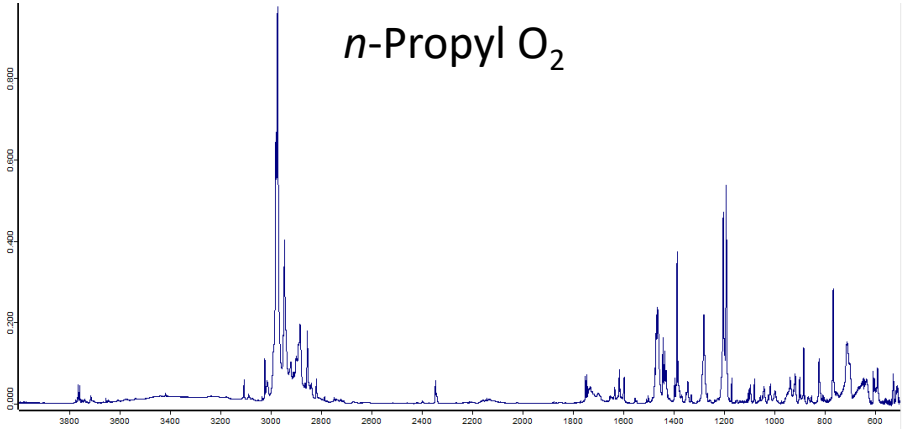

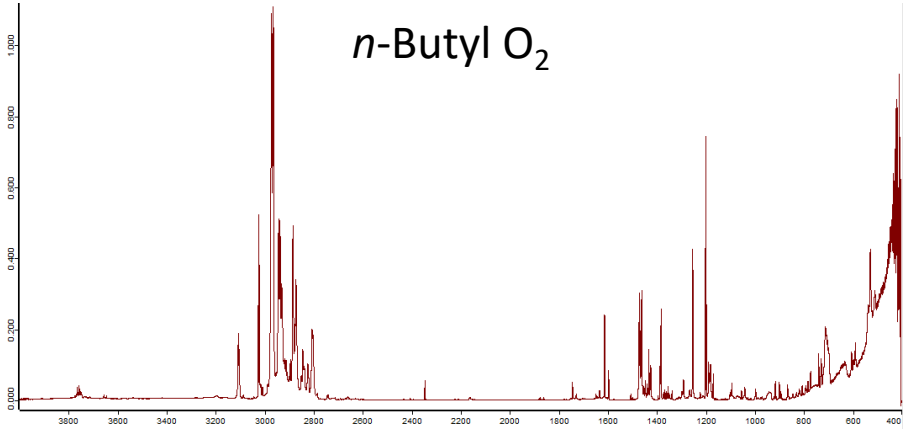

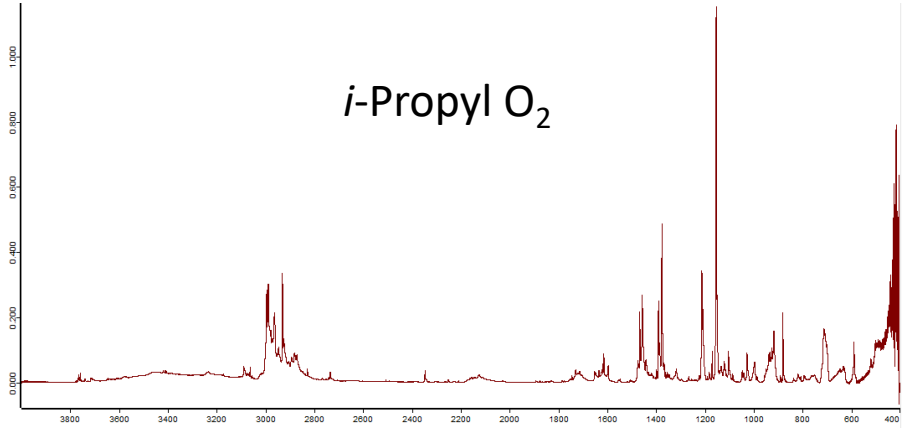

i-Butyl O_2

sec-Butyl O_2

Solid *p*-H_2 spectrum of the *n*-propyl radical

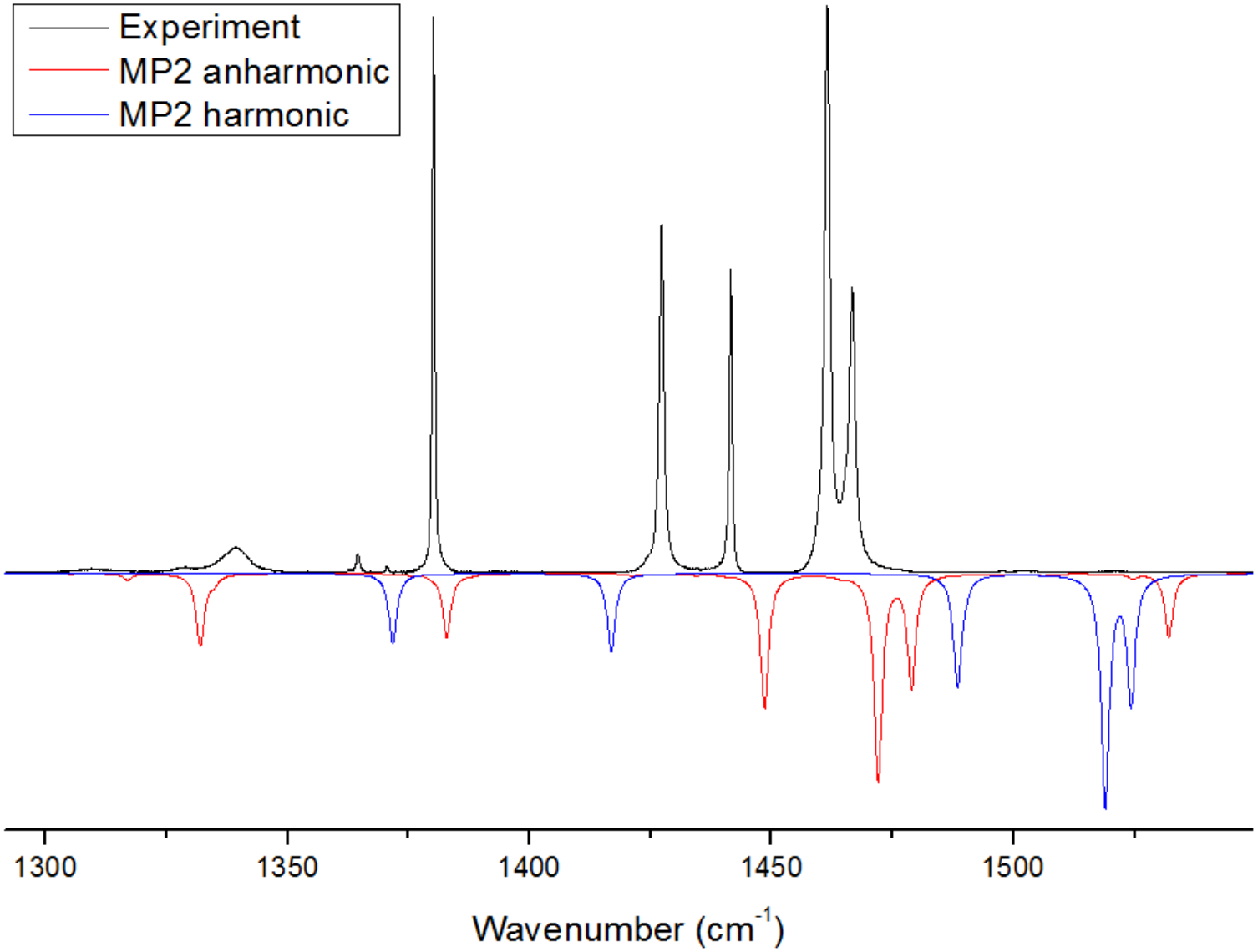

Introduction to VPT2+K

VTP2 with explicit treatment of Fermi and Darling-Dennison Resonances

$$\begin{pmatrix} \Omega_{10_2} & \frac{\phi_{10,10,7}}{4} & \frac{1}{2\sqrt{2}}K_{10,10;11,8} & D_{10,10;10,8} \\ \frac{\phi_{10,10,7}}{4} & \Omega_{7} & \frac{\phi_{11,8,7}}{2\sqrt{2}} & \frac{\phi_{10,8,7}}{2\sqrt{2}} \\ \frac{1}{2\sqrt{2}}K_{10,10;11,8} & \frac{\phi_{11,8,7}}{2\sqrt{2}} & \Omega_{11_18_1} & D_{11,8;10,8} \\ D_{10,10;10,8} & \frac{\phi_{10,8,7}}{2\sqrt{2}} & D_{11,8;10,8} & \Omega_{10_18_1} \end{pmatrix}$$

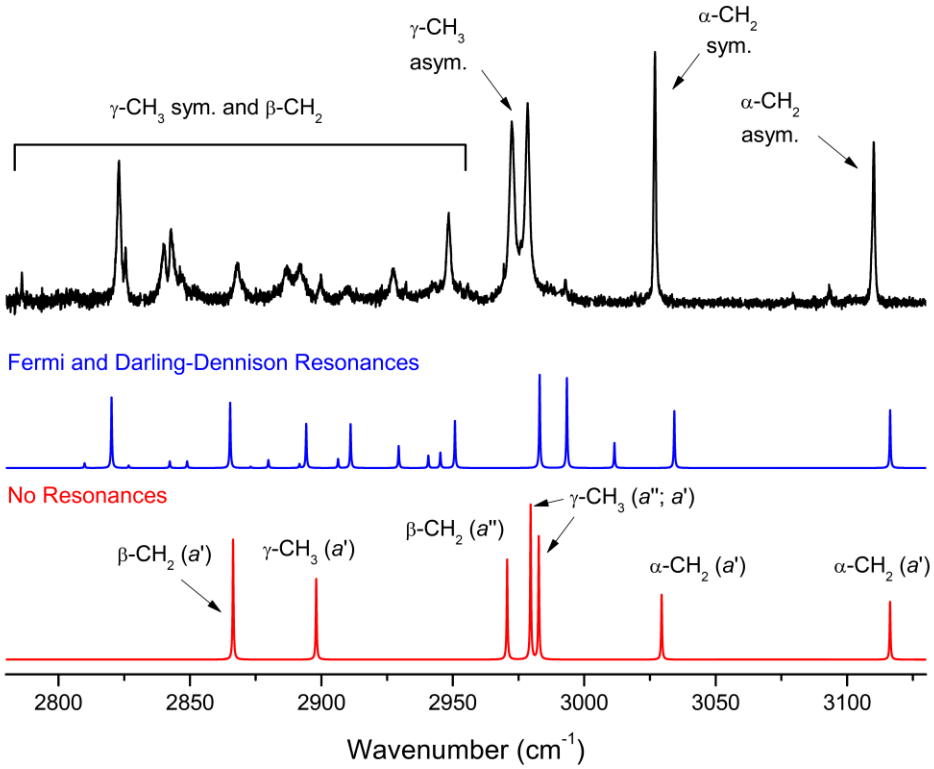

The VPT2+K method was applied using "semi-diagonal" quartic force fields computed at the CCSD(T) level of theory with the ANO1 (*i*-propyl) and ANO0/ANO1 (*n*-propyl) basis sets, using the CFOUR package. Our implementation of VPT2+K entails a full treatment of the vibrational problem with VPT2 (red trace) followed by deperturbation of the strong interactions between CH stretch fundamentals and CH bend overtones/combinations. The strong interactions are then treated explicitly via diagonalization of an effective Hamiltonian (small example provided above), yielding a theoretical spectrum that accounts for both Fermi and Darling-Dennison type resonance interactions (blue trace). The *i*-propyl effective Hamiltonian contained 28 vibrational states, and *n*-propyl's contained 22; care was taken to select states (in normal coordinates) that were related to the local vibrational states chosen in the local mode model. Electrical harmonicity was assumed (i.e. the harmonic intensities of the bright CH stretch fundamentals was distributed into the dark states proportional to the squares of their eigenvector coefficients).

Introduction to Local Mode Model Hamiltonian

Daniel Tabor and Ned Sibert, Univ. Wisconsin

B3LYP Force Constant Matrix in Dimensionless Normal Coordinates

$$\begin{pmatrix}
3233.6 & & & & & & \\
0.0 & 3132.4 & & & & & \\
0.0 & 0.0 & 3089.4 & & & & \\
0.0 & 0.0 & 0.0 & 3083.5 & & & \\
0.0 & 0.0 & 0.0 & 0.0 & 3023.1 & & \\
0.0 & 0.0 & 0.0 & 0.0 & 0.0 & 2956.0 & \\
0.0 & 0.0 & 0.0 & 0.0 & 0.0 & 0.0 & 2953.3
\end{pmatrix}$$

Scaled Normal Mode Hamiltonian

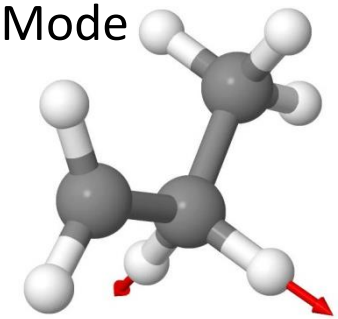

$$\begin{pmatrix}
3110.1 & & & & & & \\
0.0 & 3012.8 & & & & & \\
0.0 & 0.0 & 2971.4 & & & & \\
0.0 & 0.0 & 0.0 & 2965.7 & & & \\
0.0 & 0.0 & 0.0 & 0.0 & 2907.6 & & \\
0.0 & 0.0 & 0.0 & 0.0 & 0.0 & 2843.1 & \\
0.0 & 0.0 & 0.0 & 0.0 & 0.0 & 0.0 & 2840.5
\end{pmatrix}$$

Local Mode Hamiltonian

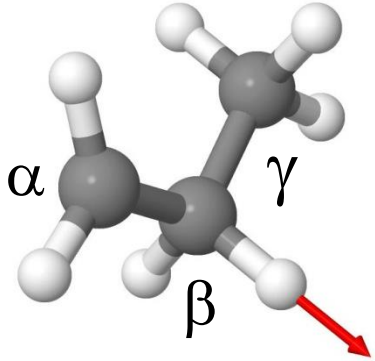

$$\begin{pmatrix}
\gamma\text{-}CH_3 & & & & & & \\
2954.2 & & & & & & \\
-19.8 & 2944.4 & & & & & \\
-19.8 & -19.9 & 2944.4 & & & & \\
4.4 & -7.8 & 4.6 & 2842.4 & & & \\
4.4 & 4.5 & -7.8 & -1.6 & 2842.4 & & \\
-0.2 & 1.5 & 1.5 & -4.1 & -4.1 & 3060.9 & \\
0.2 & 0.5 & 0.5 & 3.1 & 3.1 & -48.6 & 3061.6
\end{pmatrix}$$

β-CH_2

α-CH_2

Introduction to Local Mode Model Hamiltonian
Adding Anharmonicity

Initial Local Mode Picture

$$H^s = \sum_i^{N_s} \sum_j^{N_s} H_{ij}(a_i a_j^\dagger + h.c.)$$

$$H^s = \begin{pmatrix} 2954.2 & & & & & & \\ -19.8 & 2944.4 & & & & & \\ -19.8 & -19.9 & 2944.4 & & & & \\ 4.4 & -7.8 & 4.6 & 2842.4 & & & \\ 4.4 & 4.5 & -7.8 & -1.6 & 2842.4 & & \\ -0.2 & 1.5 & 1.5 & -4.1 & -4.1 & 3060.9 & \\ 0.2 & 0.5 & 0.5 & 3.1 & 3.1 & -48.6 & 3061.6 \end{pmatrix}$$

Add in select stretch-bend Fermi coupling terms, calculated ab initio, that are scaled by a single scaling factor

$$H^{sb} = \sum_i^{N_s} \sum_j^{N_b} \sum_k^{N_b} H_{ijk}(a_i a_j^\dagger a_k^\dagger + h.c.)$$

Only significant local coupling is between stretches and bends on the same CH_2/CH_3 group. We find this coupling to be similar for all systems.

Also add in bend anharmonicity, whose values are taken from perturbative studies of CH_2DCH_2D and CH_3CD_3 , to separate energies of bend overtones and combination states.

Introduction to Local Mode Model Hamiltonian

CH_3 Groups: Types Of Cubic Coupling

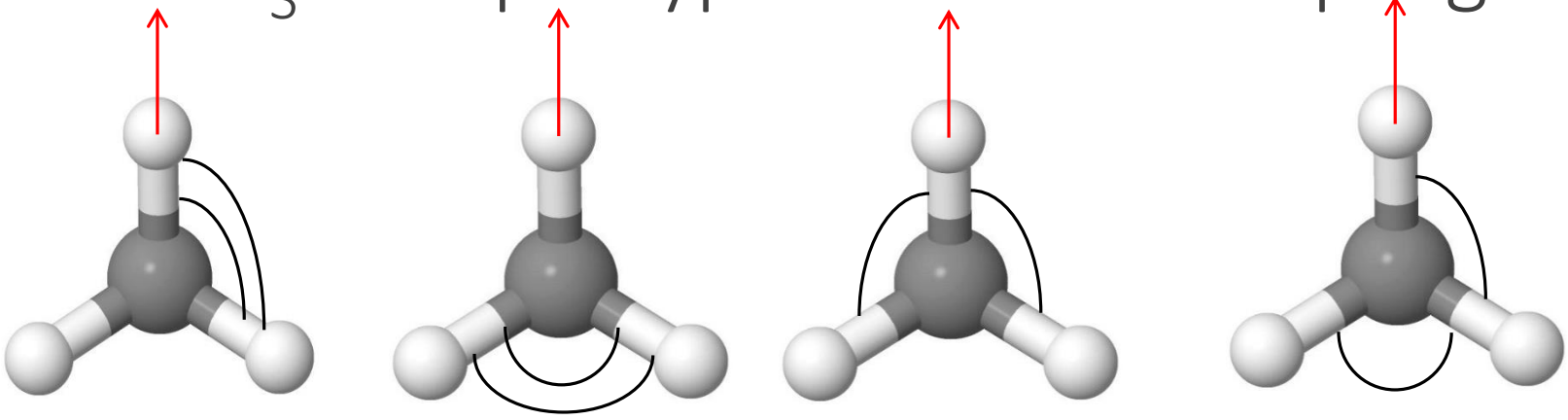

22.0 cm^{-1} α_1 2.5 cm^{-1} α_2 1.5 cm^{-1} γ_1 5.6 cm^{-1} γ_2

CH_3 Hamiltonian

$$
\begin{pmatrix}
2942.9 & & & & & & & & \\
-21.8 & 2948.1 & & & & & & & \\
-21.8 & -21.3 & 2948.1 & & & & & & \\
0.0 & 0.0 & 0.0 & 2852.2 & & & & & \\
0.0 & 0.0 & 0.0 & -4.5 & 2851.9 & & & & \\
0.0 & 0.0 & 0.0 & -4.5 & -4.5 & 2861.9 & & & \\
0.0 & 0.0 & 0.0 & -40.7 & -40.7 & 0.0 & 2861.6 & & \\
0.0 & 0.0 & 0.0 & -42.7 & 0.0 & -42.7 & -30.2 & 2866.6 & \\
0.0 & 0.0 & 0.0 & 0.0 & -42.7 & -42.7 & -30.2 & -28.8 & 2866.5
\end{pmatrix}
$$

Stretches

Scissor overtones

Scissor combinations

Introduction to Local Mode Model Hamiltonian

CH_3 Groups: Types Of Cubic Coupling

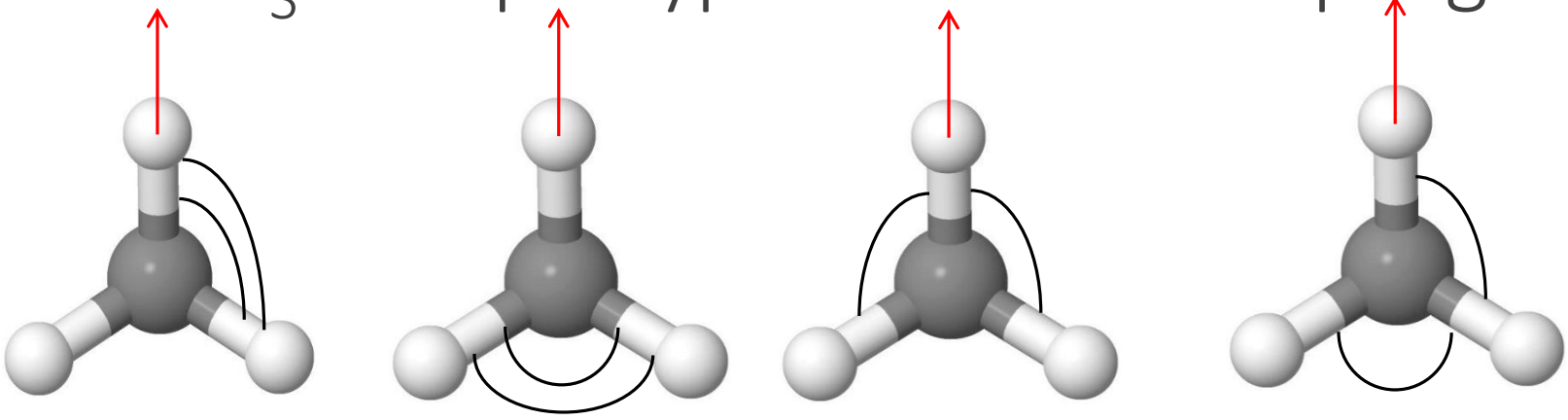

22.0 cm^{-1} α_1 2.5 cm^{-1} α_2 1.5 cm^{-1} γ_1 5.6 cm^{-1} γ_2

CH_3 Hamiltonian

Stretches

Scissor overtones

Scissor combinations

$$
\begin{pmatrix}
2942.9 & & & & & & & & \\
-21.8 & 2948.1 & & & & & & & \\
-21.8 & -21.3 & 2948.1 & & & & & & \\
22.0 & 22.0 & 2.5 & 2852.2 & & & & & \\
22.0 & 2.5 & 22.0 & -4.5 & 2851.9 & & & & \\
2.5 & 22.0 & 22.0 & -4.5 & -4.5 & 2861.9 & & & \\
1.5 & 5.6 & 5.6 & -40.7 & -40.7 & 0.0 & 2861.6 & & \\
5.6 & 1.5 & 5.6 & -42.7 & 0.0 & -42.7 & -30.2 & 2866.6 & \\
5.6 & 5.6 & 1.5 & 0.0 & -42.7 & -42.7 & -30.2 & -28.8 & 2866.5
\end{pmatrix}
$$

Introduction to Local Mode Model Hamiltonian
n-propyl Dipole Decompositions

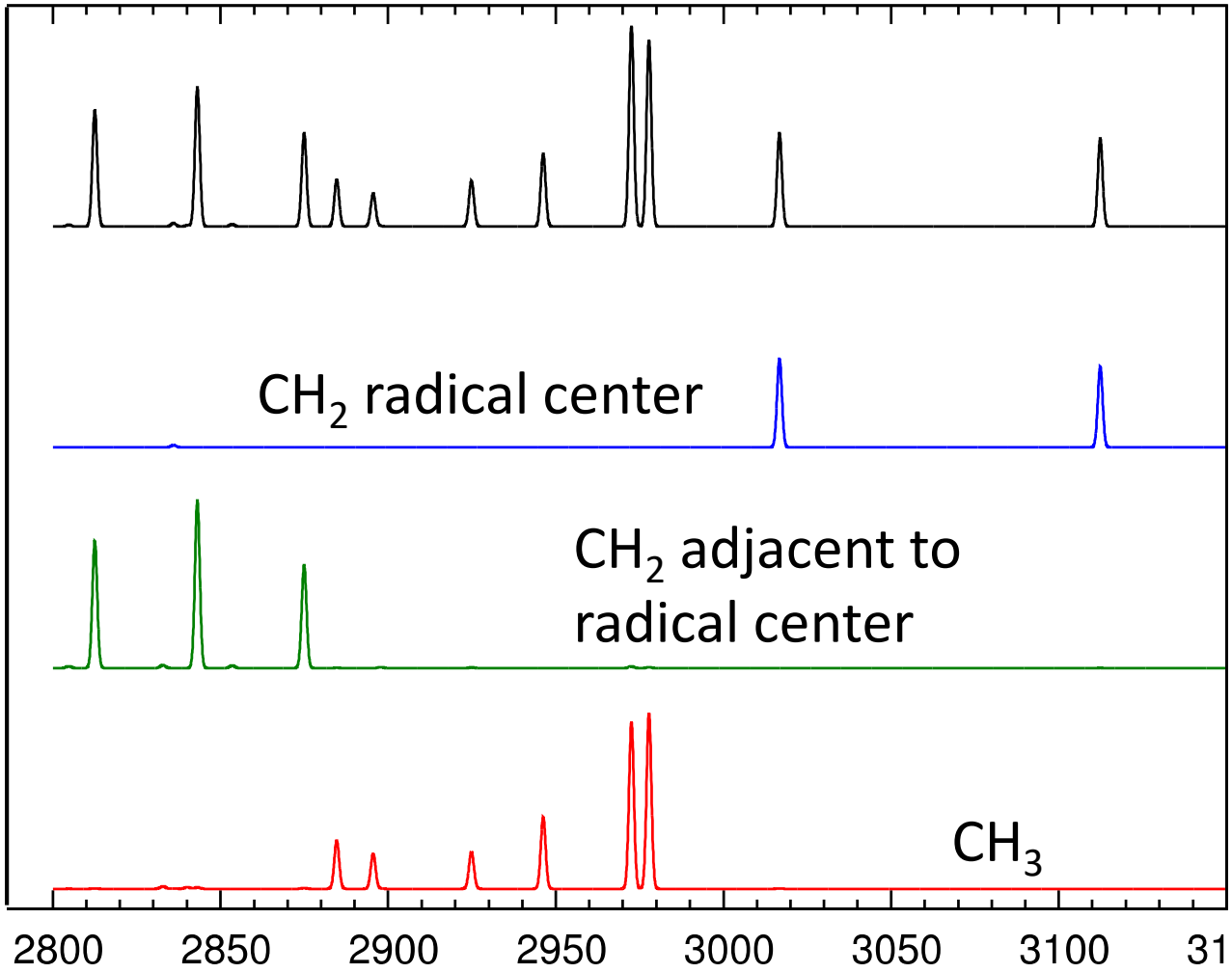

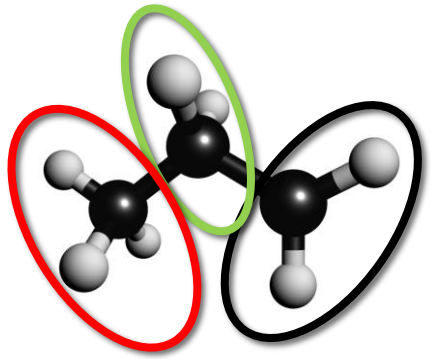

Introduction to Local Mode Model Hamiltonian
n-propyl Hamiltonian in normal coordinates

Stretches

$$
\begin{pmatrix}
2834.9 & & & & & & & & & & & & & & & & & & & & & & & & & & & & & \\
0.0 & 2837.6 & & & & & & & & & & & & & & & & & & & & & & & & & & & & \\
0.0 & 0.0 & 2903.8 & & & & & & & & & & & & & & & & & & & & & & & & & & & \\
0.0 & -0.3 & 0.0 & 2964.2 & & & & & & & & & & & & & & & & & & & & & & & & & & \\
0.2 & 0.0 & 0.0 & 0.0 & 2969.7 & & & & & & & & & & & & & & & & & & & & & & & & & \\
0.0 & 0.0 & -0.1 & 0.0 & -0.1 & 3005.4 & & & & & & & & & & & & & & & & & & & & & & & & \\
0.0 & 0.0 & 0.0 & 0.0 & 0.0 & 0.0 & 3106.6 & & & & & & & & & & & & & & & & & & & & & & & \\
0.4 & 0.0 & -35.9 & 0.0 & 3.3 & 1.4 & 0.1 & 2745.7 & & & & & & & & & & & & & & & & & & & & & & \\
0.4 & 0.0 & -8.8 & 0.0 & -2.0 & -6.4 & 0.1 & -1.3 & 2798.9 & & & & & & & & & & & & & & & & & & & & & \\
-0.9 & 0.0 & -2.9 & 0.0 & -0.1 & -3.2 & 0.0 & -0.4 & -0.3 & 2804.9 & & & & & & & & & & & & & & & & & & & & \\
0.0 & -1.4 & 0.0 & 13.8 & 0.0 & 0.0 & 0.0 & 0.0 & 0.0 & 0.0 & 2834.6 & & & & & & & & & & & & & & & & & & & \\
-0.8 & 0.0 & 0.1 & 0.0 & -12.5 & 1.8 & 0.1 & 0.5 & -0.4 & 0.0 & 0.0 & 2841.3 & & & & & & & & & & & & & & & & & & \\
5.7 & 0.0 & 1.6 & 0.0 & -0.1 & -23.5 & 0.2 & 0.6 & -1.4 & -0.7 & 0.0 & 0.5 & 2842.1 & & & & & & & & & & & & & & & & & \\
-16.7 & 0.0 & 0.2 & 0.0 & 0.6 & -16.3 & -0.4 & 0.3 & -1.0 & -0.7 & 0.0 & 0.3 & -2.9 & 2847.8 & & & & & & & & & & & & & & & & \\
-25.4 & 0.0 & -0.2 & 0.0 & 1.5 & 5.5 & -0.6 & -0.1 & 0.5 & -0.1 & 0.0 & -0.1 & 2.7 & -3.3 & 2851.9 & & & & & & & & & & & & & & & \\
0.0 & -0.1 & 0.0 & 0.6 & 0.0 & 0.0 & 0.0 & 0.0 & 0.0 & 0.0 & 0.1 & 0.0 & 0.0 & 0.0 & 0.0 & 2886.3 & & & & & & & & & & & & & & \\
0.0 & 0.0 & 0.0 & -0.4 & 0.0 & 0.0 & 0.0 & 0.0 & 0.0 & 0.0 & 0.1 & 0.0 & 0.0 & 0.0 & 0.0 & 0.0 & 2891.7 & & & & & & & & & & & & & \\
1.1 & 0.0 & -6.4 & 0.0 & -4.9 & -7.1 & 0.1 & -1.5 & -1.1 & -0.4 & 0.0 & -0.8 & -1.6 & -0.9 & 0.7 & 0.0 & 0.0 & 2891.2 & & & & & & & & & & & & \\
-2.7 & 0.0 & -0.8 & 0.0 & -0.9 & -3.6 & -0.1 & -0.1 & -0.3 & -0.2 & 0.0 & -0.2 & -0.7 & -1.0 & -0.5 & 0.0 & 0.0 & -0.4 & 2897.7 & & & & & & & & & & & \\
-0.8 & 0.0 & 20.9 & 0.0 & -11.8 & 0.0 & 0.0 & 6.1 & 1.1 & 0.4 & 0.0 & -1.9 & -0.3 & -0.1 & 0.0 & 0.0 & 0.0 & 1.2 & 0.1 & 2917.6 & & & & & & & & & & \\
0.0 & 1.5 & 0.0 & -14.2 & 0.0 & 0.0 & 0.0 & 0.0 & 0.0 & 0.0 & 2.4 & 0.0 & 0.0 & 0.0 & 0.0 & -0.1 & -0.1 & 0.0 & 0.0 & 0.0 & 2929.3 & & & & & & & & & \\
0.5 & 0.0 & 21.4 & 0.0 & 8.4 & -1.8 & -0.1 & 5.7 & 1.6 & 0.4 & 0.0 & 1.3 & -0.8 & -0.3 & 0.1 & 0.0 & 0.0 & 2.1 & 0.3 & -5.1 & 0.0 & 2930.6 & & & & & & & & \\
\end{pmatrix}
$$

Some large couplings boxed

Introduction to Local Mode Model Hamiltonian
i-propyl Dipole Decompositions

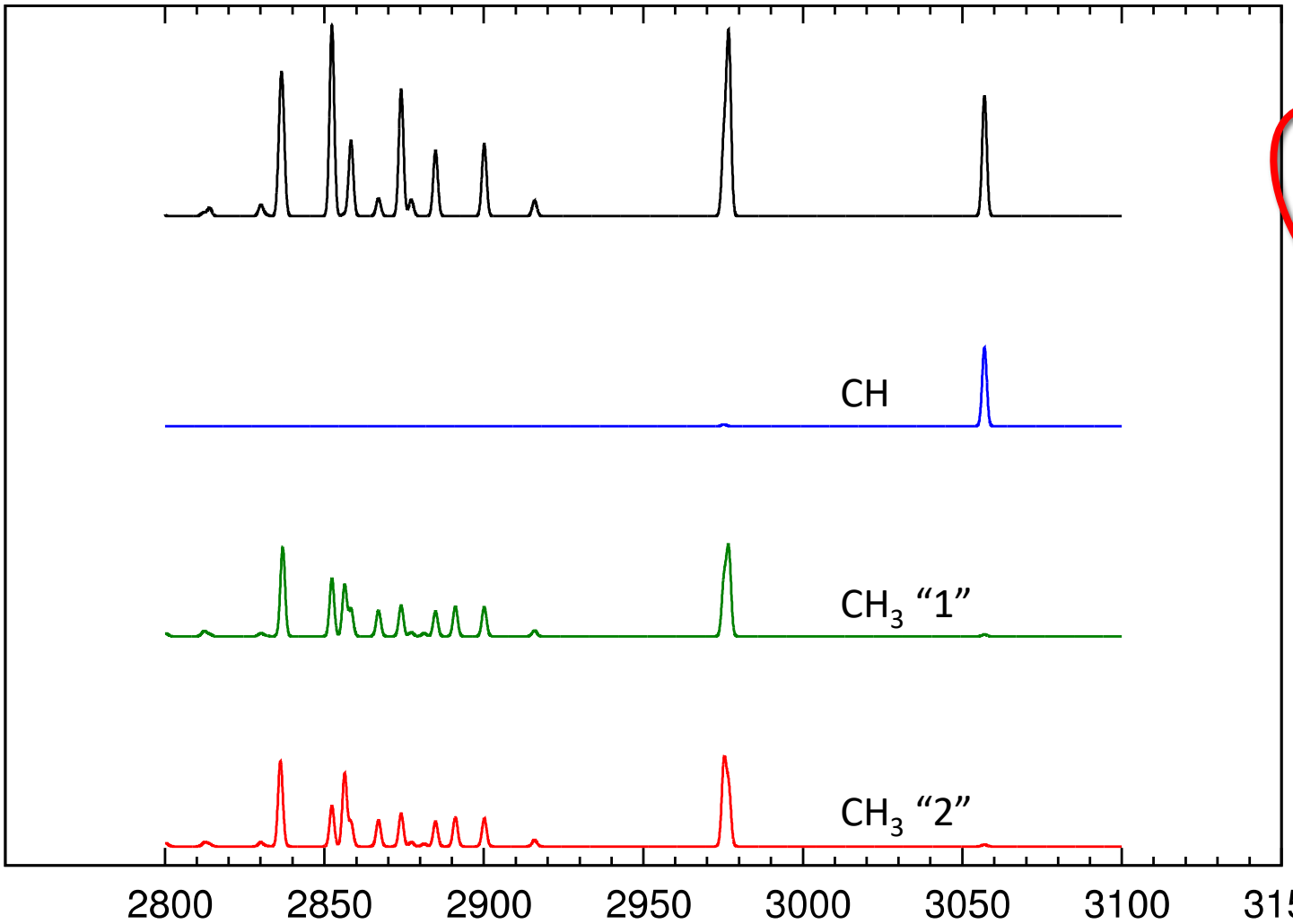

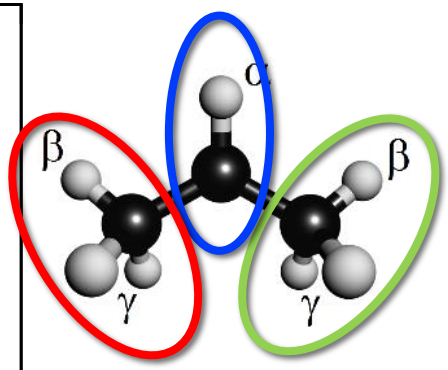

Introduction to Local Mode Model Hamiltonian
i-propyl Full Hamiltonian

CH stretches

Scissor overtones

CH_3 scissor combinations

$$
\begin{pmatrix}
2920.7 & & & & & & & & & & & & & & \\
-16.9 & 2920.7 & & & & & & & & & & & & & \\
4.1 & 4.1 & 2942.9 & & & & & & & & & & & & \\
-8.6 & 3.8 & -21.8 & 2948.1 & & & & & & & & & & & \\
3.8 & -8.6 & -21.8 & -21.3 & 2948.1 & & & & & & & & & & \\
22.0 & 22.0 & 0.0 & 0.0 & 0.0 & 2910.3 & & & & & & & & & \\
0.0 & 0.0 & 22.0 & 22.0 & 2.5 & 0.0 & 2852.2 & & & & & & & & \\
0.0 & 0.0 & 22.0 & 2.5 & 22.0 & 0.0 & -4.5 & 2851.9 & & & & & & & \\
0.0 & 0.0 & 2.5 & 22.0 & 22.0 & 0.0 & -4.5 & -4.5 & 2861.9 & & & & & & \\
0.0 & 0.0 & 1.5 & 5.6 & 5.6 & 0.0 & -40.7 & -40.7 & 0.0 & 2861.6 & & & & & \\
0.0 & 0.0 & 5.6 & 1.5 & 5.6 & 0.0 & -42.7 & 0.0 & -42.7 & -30.2 & 2866.6 & & & & \\
0.0 & 0.0 & 5.6 & 5.6 & 1.5 & 0.0 & 0.0 & -42.7 & -42.7 & -30.2 & -28.8 & 2866.5 & & & \\
0.0 & 0.0 & 0.0 & 0.0 & 0.0 & 3.5 & 3.5 & 0.0 & 0.0 & 2.5 & -8.4 & 0.0 & 2890.8 & & \\
0.0 & 0.0 & 0.0 & 0.0 & 0.0 & 3.5 & 0.0 & 3.5 & 0.0 & 2.5 & 0.0 & -8.4 & -28.8 & 2890.7 & \\
0.0 & 0.0 & 0.0 & 0.0 & 0.0 & -11.8 & 0.0 & 0.0 & -11.8 & 0.0 & 2.5 & 2.5 & -30.2 & -30.2 & 2895.7
\end{pmatrix}
$$

Combinations of CH_2 and CH_3 scissors

Only the CH local stretches have non-zero dipole derivatives in the model

Matrix Isolation Studies of Alkyl Radicals. The Characteristic Infrared Spectra of Primary Alkyl Radicals

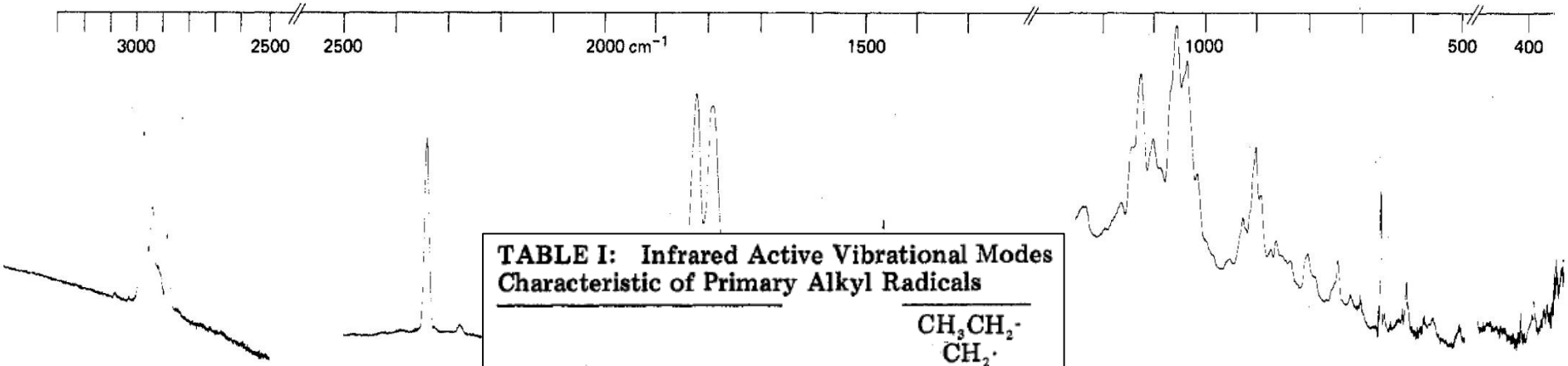

Figure 7. The infrared spectrum of dibutyr 1/500).

TABLE I: Infrared Active Vibrational Modes Characteristic of Primary Alkyl Radicals

	CH_3CH_2-$\dot{C}H_2$
CH stretching vibrations associated with the radical CH_2 group	3100 cm^{-1} 3017.5 cm^{-1}
Out-of-plane deformation of the radical center	530 cm^{-1}
Anomalous band observed in the CH stretching region	2812.5 cm^{-1}

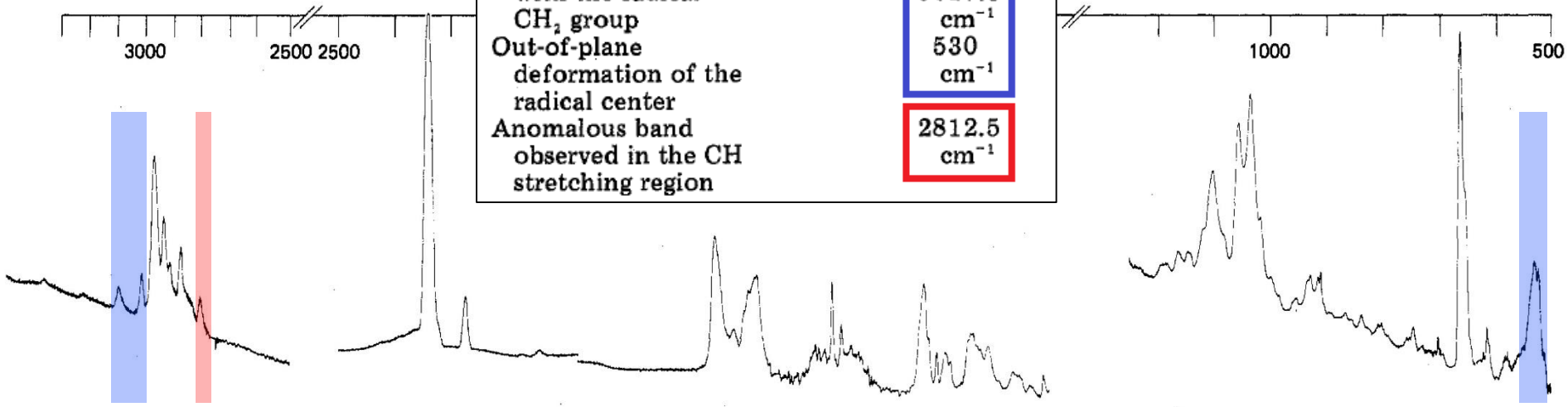

Figure 8. The infrared spectrum of butyryl peroxide in an argon matrix after irradiation with light $\lambda > 3000$ Å for $t = 1950$ min. The bands at 2340 cm^{-1} are due to CO_2. Those at ~ 1800 cm^{-1} are due to residual peroxide carbonyl absorption.

Electron Spin Resonance Studies of Conformations and Hindered Internal Rotation in Transient Free Radicals[1]

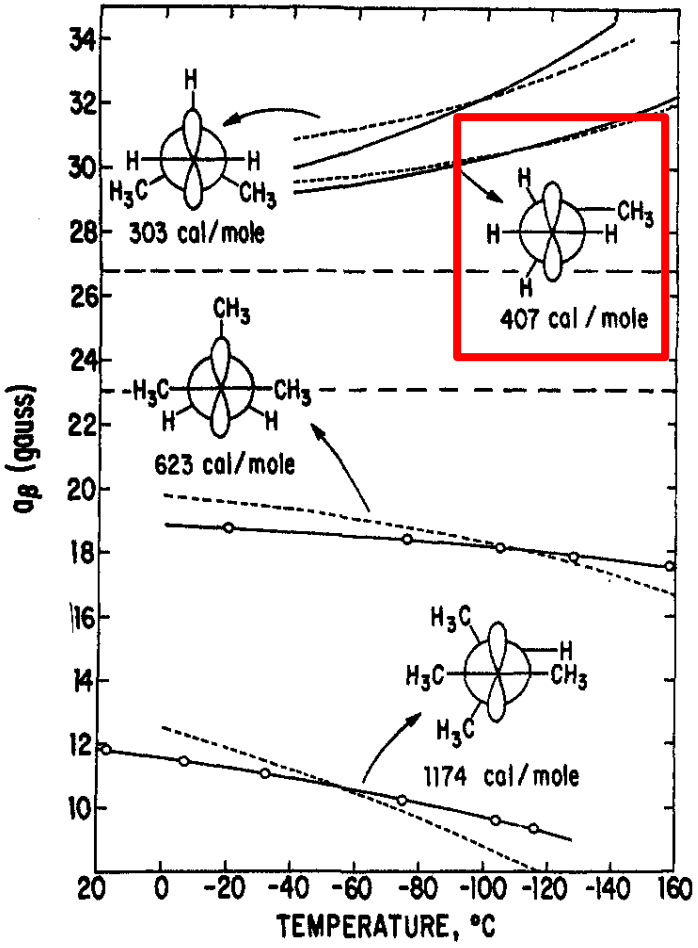

Figure 15. Experimental and calculated temperature dependences of β-coupling constants for isobutyl, *n*-propyl, *tert*-amyl, and dimethylisopropylcarbinyl radicals (the experimental curves for isobutyl and *n*-propyl are taken from ref 3a). The two horizontal lines indicate the temperature independent values of $a_\beta^{CH_3}$ for ethyl (upper) and *tert*-butyl (lower). The former represents the high-temperature limit of a_β for the two primary radicals while the latter is the same limit for the two tertiary radicals.

Temperature dependence of
β-proton hyperfine splittings

C_s minimum energy structure
0.407 kcal/mol barrier to internal rotation

The Journal of Physical Chemistry, Vol. 75, No. 22, 1971

Intricate Internal Rotation Surface and Fundamental Infrared Transitions of the *n*-Propyl Radical

Chenyang Li,[†] Jay Agarwal,[†] Chia-Hua Wu,[†,‡] Wesley D. Allen,[†,‡] and Henry F. Schaefer, III*,[†]

[†]Center for Computational Quantum Chemistry and [‡]Department of Chemistry, University of Georgia, Athens, Georgia 30602, United States

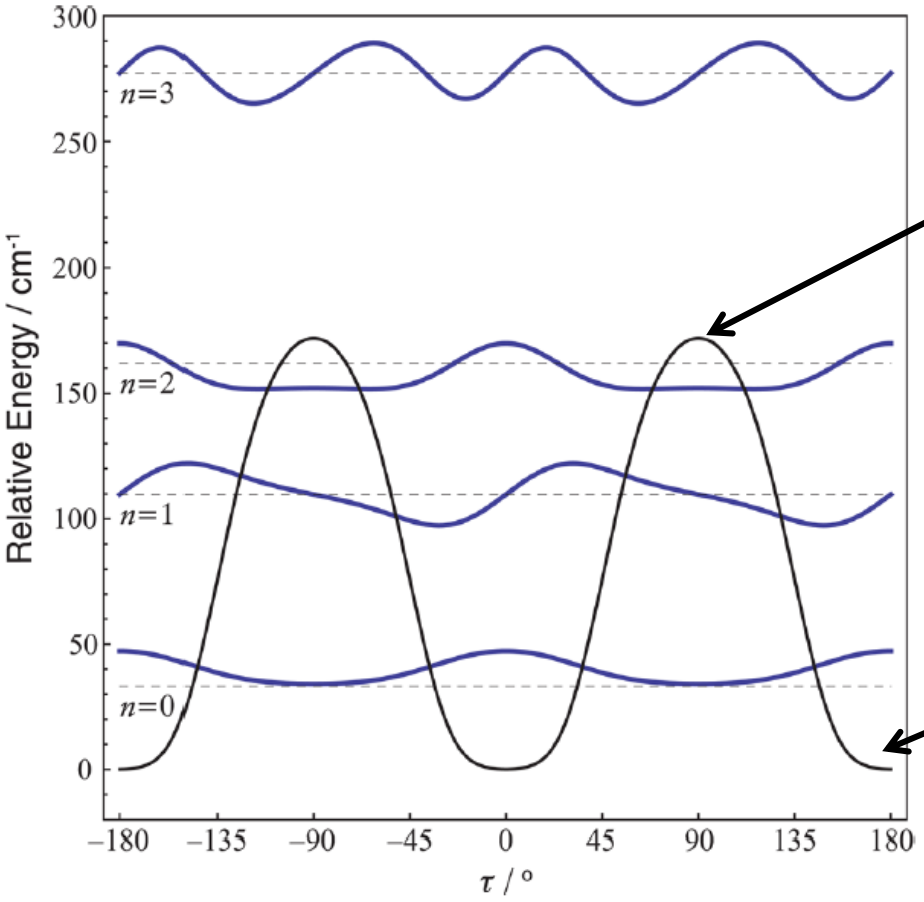

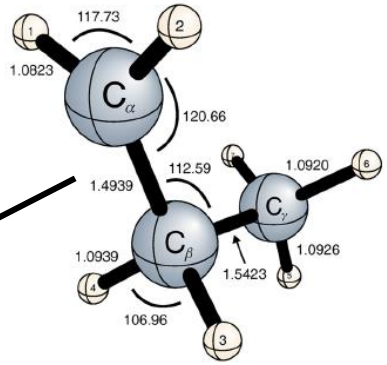

C_s symmetry

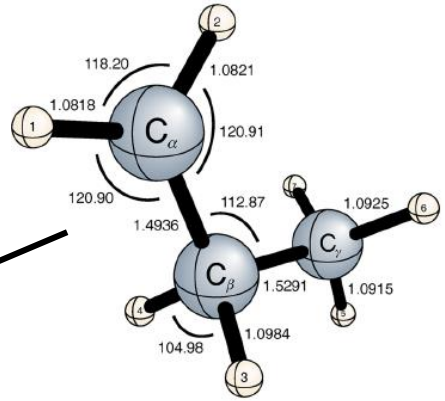

J. Phys. Chem. B., 2015, 119, 728-735

Our Current HENDI Setup

(**He**lium **N**ano**d**roplet **I**solation)

- Probe the vibrational spectra of molecules and complexes at 0.37 K

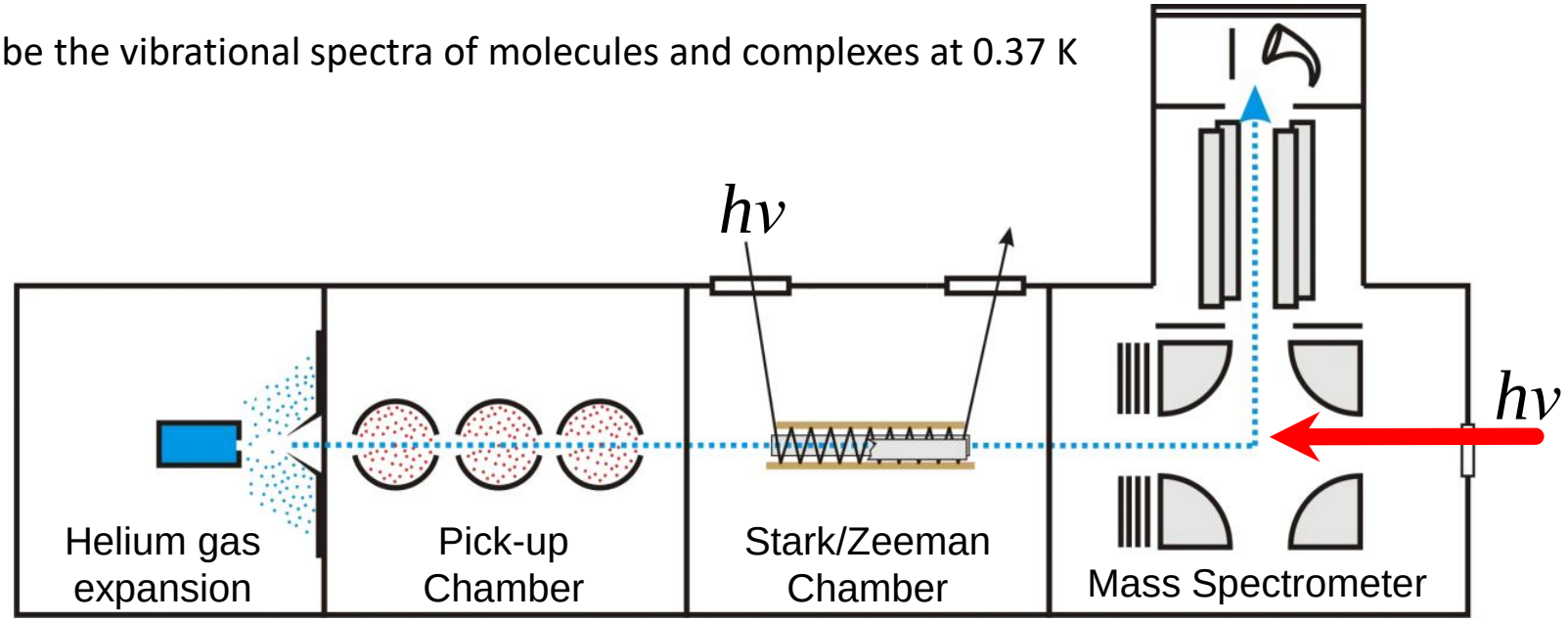

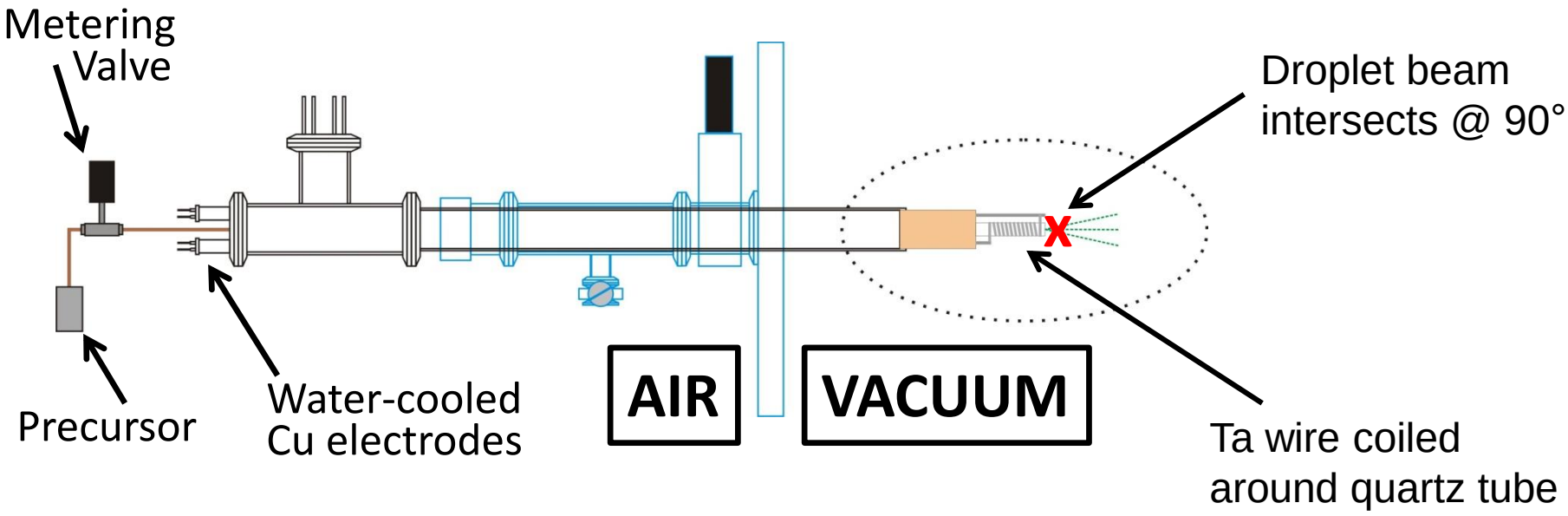

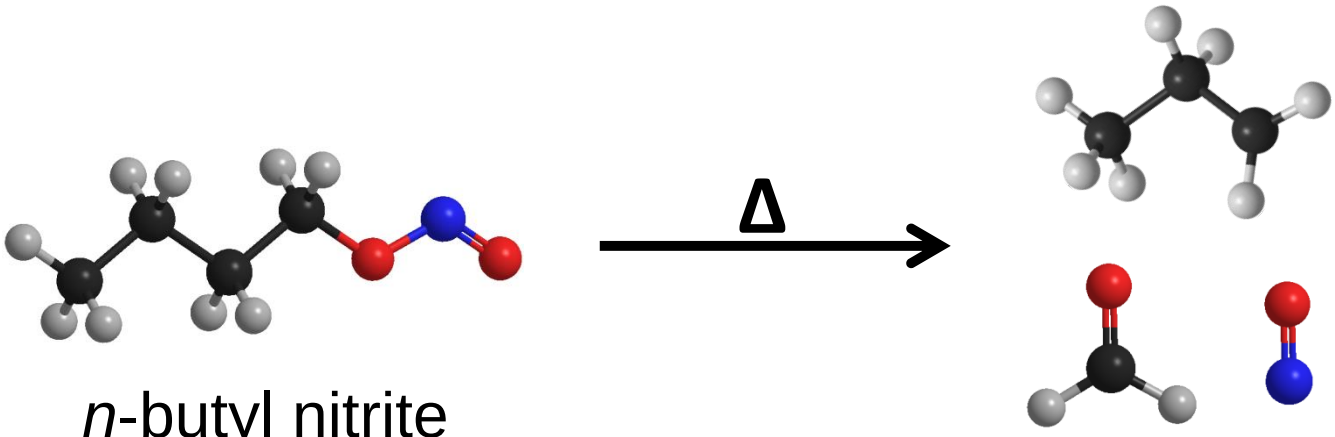

n-butyl nitrite

Mass Spectrometry

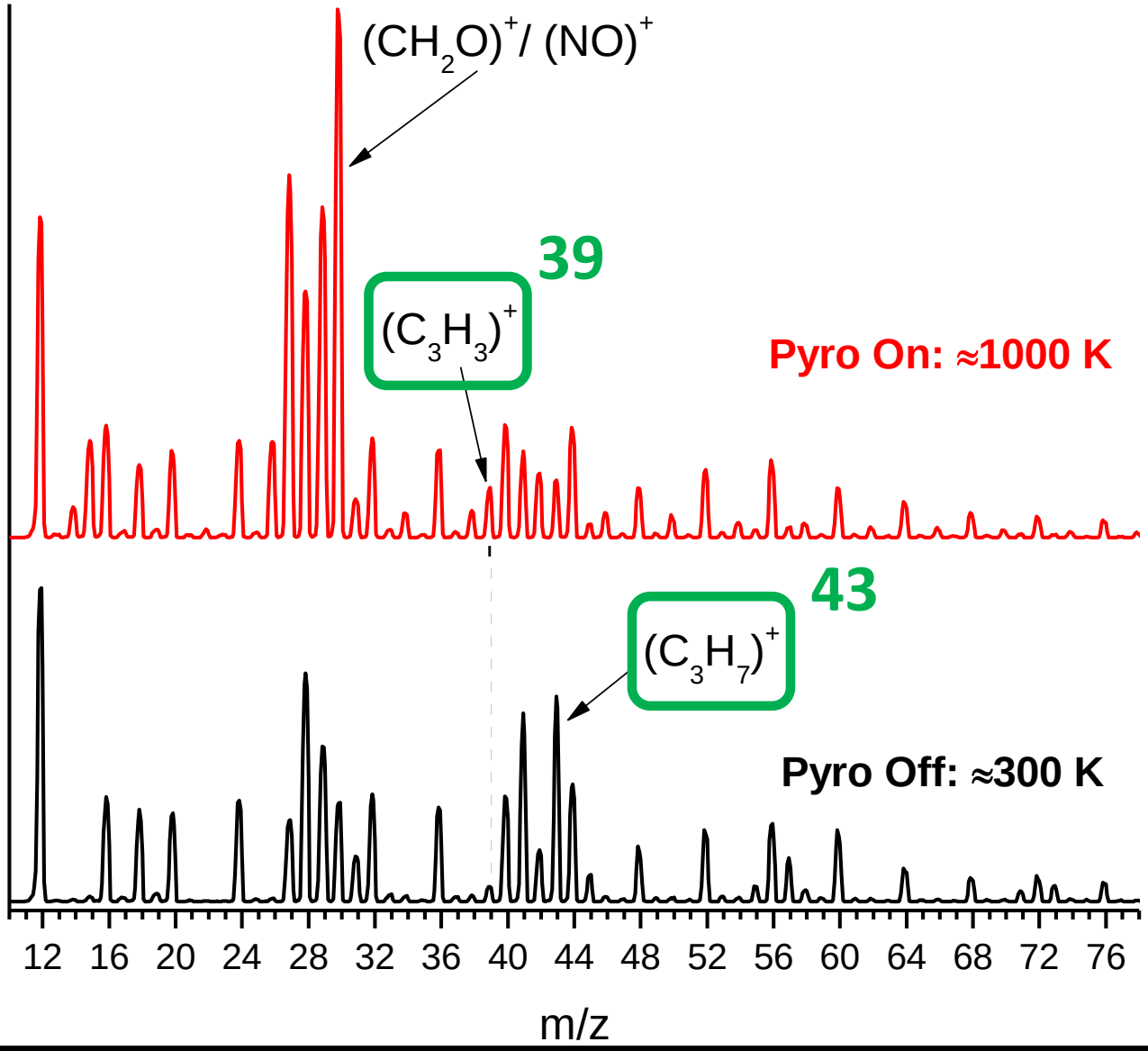

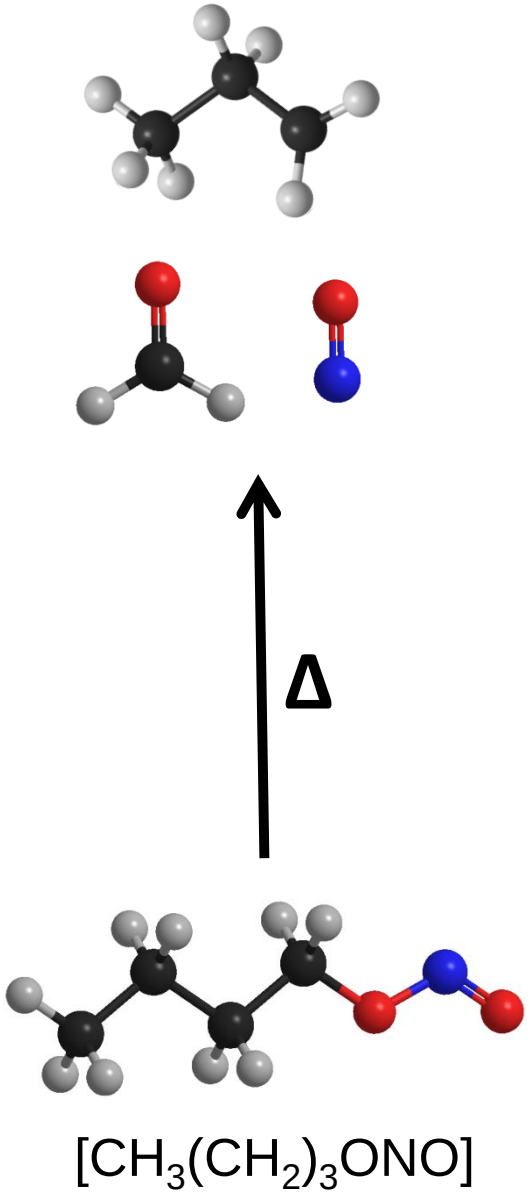

n-propyl Survey Scans

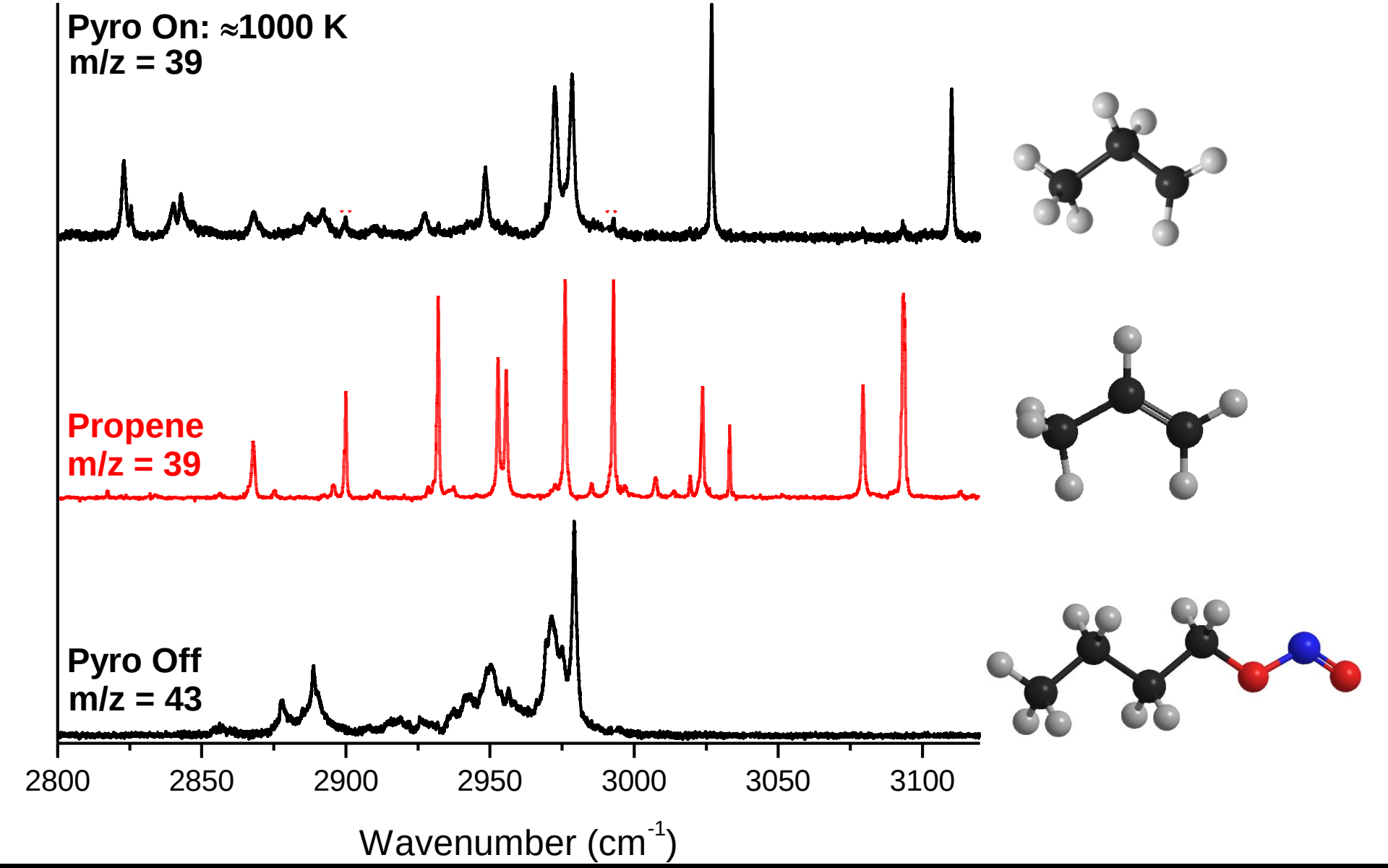

i-propyl Survey Scans

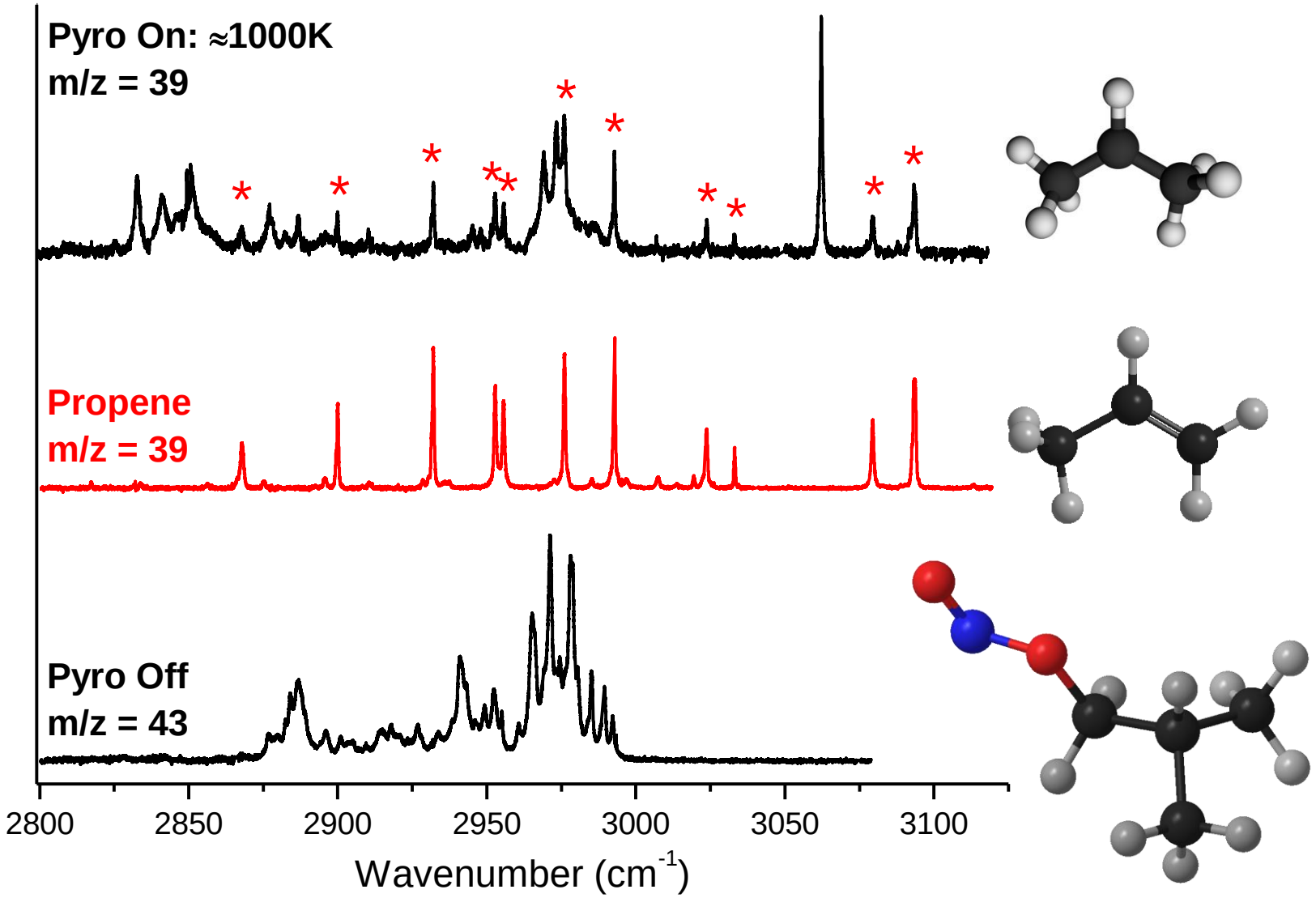

Lockheed-Martin Aculight ARGOS continuous-wave mid-infrared optical parametric oscillator lasers (cw mid-IR OPOs).

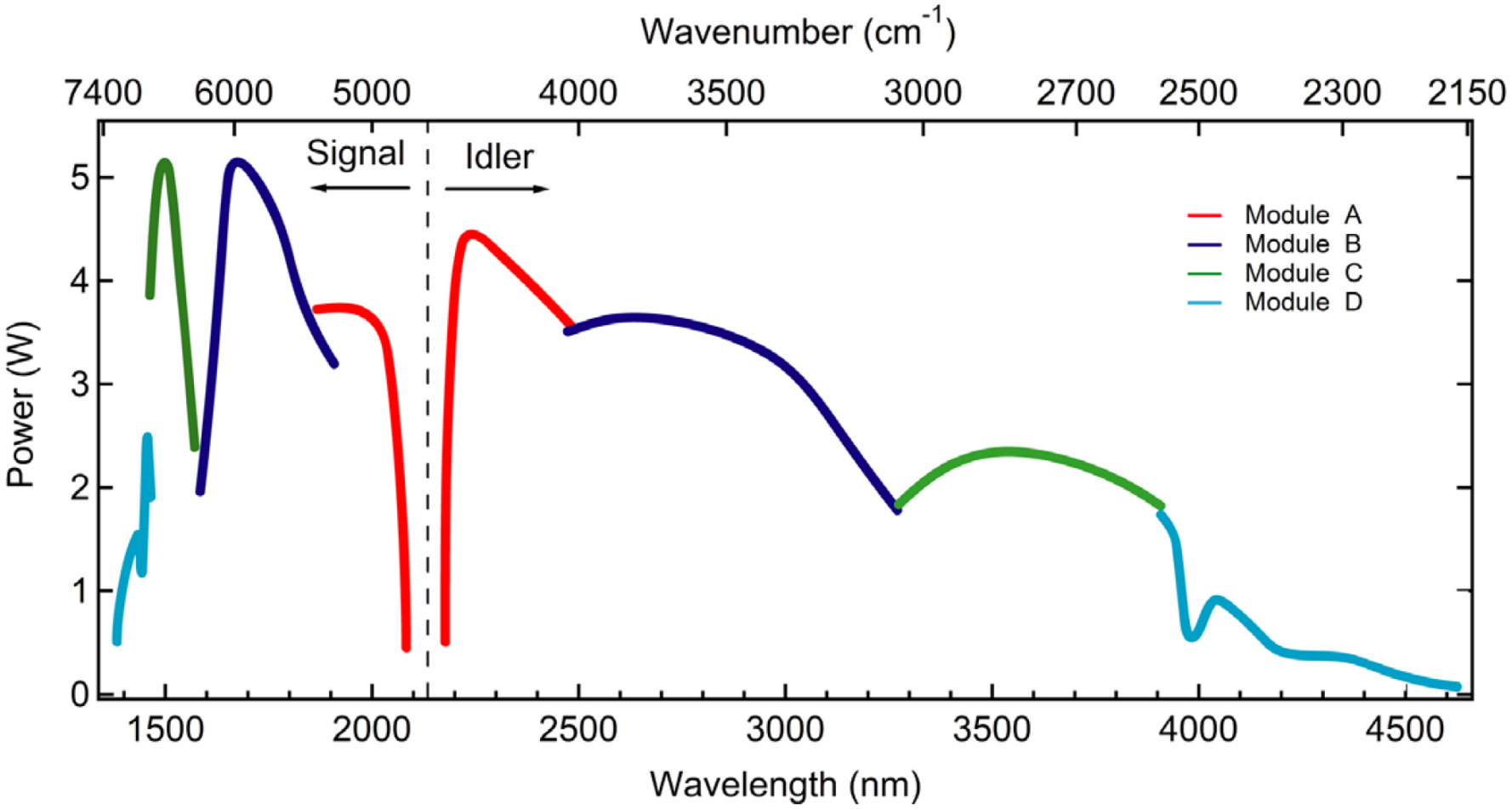

Typical Power vs. Wavelength for Model 2400-SF-15

(http://www.lockheedmartin.com/content/dam/lockheed/data/ms2/documents/aculight/Argos_Model_2400_SF_Series_Brochure.pdf)